

UCSF

UC San Francisco Electronic Theses and Dissertations

Title

Histoplasma capsulatum secretes cysteine-rich protein virulence factors to lyse host macrophages

Permalink

<https://escholarship.org/uc/item/8ms2408n>

Author

Azimova, Dinara

Publication Date

2021

Peer reviewed|Thesis/dissertation

Histoplasma capsulatum secretes cysteine-rich protein virulence factors to lyse host macrophages

by
Dinara Azimova

DISSERTATION

Submitted in partial satisfaction of the requirements for degree of
DOCTOR OF PHILOSOPHY

in

Biochemistry and Molecular Biology

in the

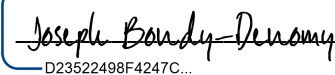
GRADUATE DIVISION

of the

UNIVERSITY OF CALIFORNIA, SAN FRANCISCO

Approved:

DocuSigned by:



D23522498F4247C...

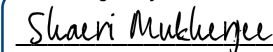
Joseph Bondy-Denomy

Chair



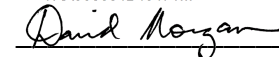
Anita Sil

DocuSigned by:



7AA908684B40471...

Shaeri Mukherjee



David O. Morgan, PhD

Committee Members

Copyright 2021
by
Dinara Azimova

This dissertation is dedicated to my parents Rushania Azimova and Rustam Azimov.

They have unconditionally supported me throughout my life and fostered my love for science.

Without their sacrifices I would not be who I am today.

Acknowledgements

This work took a village and would not have been possible without the contributions of many scientists who were all invested in trying to understand the central questions of this project. First, I would like to thank Anita Sil, my PhD advisor, whose tireless commitment to the field and the members of her lab knows no bounds. She is a leader in her field and her community. I would also like to thank all the members of the lab with whom I've overlapped. You have helped me grow into a stronger scientist and taught me how to be comfortable with tackling the unknown. I would particularly like to thank the previous and current members of the lab and collaborators who have deeply thought about Cbp1, especially Mark Voorhies, Bevin English, and Nadia Herrera who have brought our understanding of Cbp1 to where it is today. I would especially like to thank my lab twin Rosa Rodriguez, whose support and candid conversations about science, life, and the world have carried me through graduate school. I would like to thank the many people who I have had the privilege of knowing in the microbiology community at UCSF. Everyone's willingness to collaborate on projects and also to create a thriving, supportive community made this whole experience very fulfilling. I would like to thank my classmates in the Tetrad class of 2015 with whom I have grown throughout graduate school with and I'm excited to see what everyone will be doing in the future.

My journey through science has gone through many different fields and many people have taught me along the way. I'd like to thank all the members of the previous labs I have worked in - in the Nystul, the Kuriyan, and the Dernburg Labs. Thank you for teaching me different approaches to science. I would also like to thank my thesis committee members: Joe Bondy-Denomy, Shaeri Mukherjee, and Dave Morgan. Your advice is invaluable and has opened up new possibilities for this project.

I would like to thank my partner, Pedro Aguilar, who has supported me throughout this time with endless love and understanding. I could not have completed this journey without you.

You spent endless nights listening to me practice my presentations, editing my writing, making me tea while I freak out over my work, and for giving me supportive hugs when I needed them.

I inherited a lot of the respect and love for science from my parents. Science was the reason we were able to immigrate half-way around the world and get a new start at life. It was life-changing for me, and I know it was also life-changing for my parents. I'm forever thankful to my parents for supporting me throughout my educational career and for my love of science.

Contributions

The data presented in Chapter 2 of this dissertation has been prepared in the following manuscript:

Azimova, D.* Herrera, N.*, Duvenage, L., Voorhies, M., English, B., Hoving, J.C., Rosenberg, O., Sil, A. Cbp1, a rapidly evolving fungal virulence factor, forms an effector complex that drives macrophage lysis. *Submitted to PLoS Pathogens.*

The data in Chapters 3 and Chapters 4 of this dissertation are being prepared for the following manuscript.

Azimova, D., Voorhies, M, and Sil, A. *Histoplasma capsulatum* secretes cysteine-rich protein effectors into the cytosol of the host macrophage during infection. *In preparation.*

The primary author, Dinara Azimova conceived, designed and executed the experiments, collected and analyzed the data, and wrote this dissertation. This work was accomplished under the guidance of Dr. Anita Sil who supervised the research and provided the financial support.

***Histoplasma capsulatum* secretes cysteine-rich protein virulence factors to lyse host macrophages**

Dinara Azimova

Abstract

Intracellular pathogens secrete effectors to manipulate their host cells. *Histoplasma capsulatum* (*Hc*) is a fungal intracellular pathogen of humans that grows in a yeast form in the host. *Hc* yeasts are phagocytosed by macrophages, where fungal intracellular replication is followed by macrophage lysis. The most abundant virulence factor secreted by *Hc* yeast cells is Calcium Binding Protein 1 (Cbp1), which is absolutely required for macrophage lysis. In Chapter 2, we take an evolutionary, structural, and cell biological approach to understand Cbp1 function. We find that Cbp1 is present only in the genomes of closely related dimorphic fungal species of the *Ajellomycetaceae* family that lead primarily intracellular lifestyles in their mammalian hosts (*Histoplasma*, *Paracoccidioides*, and *Emergomyces*), but not conserved in the closely related extracellular fungal pathogen *Blastomyces dermatitidis*. We determine the *de novo* structures of Cbp1 from *Hc* H88 Cbp1 and the *Paracoccidioides americana* (Pb03) Cbp1, revealing a novel “binocular” fold, consisting of a helical dimer arrangement where two helices from each monomer contribute to a four-helix bundle. In contrast to Pb03 Cbp1, we show that *Emergomyces* Cbp1 orthologs are unable to stimulate macrophage lysis when expressed in the *Hc cbp1* mutant. Consistent with this result, we find that wild-type *E. africanus* yeast are able to grow within primary macrophages but are incapable of lysing them. Finally, we use subcellular fractionation of infected macrophages and indirect immunofluorescence to show that Cbp1 localizes to the macrophage cytosol during *Hc* infection, making this the first instance of a primary intracellular human fungal pathogen directing an effector into the cytosol of the host cell. We additionally show that Cbp1 forms a complex with Yps-3, another known *Hc* virulence factor. Taken together, these data imply that Cbp1 is a rapidly evolving fungal virulence factor that localizes to the cytosol to trigger host cell lysis.

We also show that Cbp1 is not the only virulence factor that enters the macrophage cytosol. In Chapter 3, we identify other virulence factors including a Cerato-platanin domain containing protein (*Scp1*) and Yps-3 that are also found in the macrophage cytosol and contribute to optimal lysis.

In Chapter 4, we identify a family of putative cysteine-knot containing proteins that are specifically expanded in *Hc* species using a new, unbiased algorithm known as KNOTTIN Finder. One putative cysteine-knot, Rockstar10, contributes to optimal lysis of macrophages during infection. Taken together, these investigations demonstrate that *Hc* relies on a strategy of secreting cysteine-rich proteins into the macrophage cytosol in order to potentiate the lysis of its host cell to further dissemination.

Table of Contents

Chapter 1: Background

Intracellular pathogens	1
Phytopathogenic fungi secrete cysteine-rich protein effectors	1
Thermally dimorphic fungal pathogens cause disease in humans	2
<i>Histoplasma capsulatum</i> (Hc) epidemiology and pathogenesis	3
<i>Histoplasma capsulatum</i> virulence factors	5
<i>Histoplasma capsulatum</i> knottins	6

Chapter 2: Cbp1, a rapidly evolving fungal virulence factor, forms an effector complex that drives macrophage lysis

Introduction	8
Cbp1 is conserved amongst the Ajellomycetaceae with the exception of Blastomyces species	10
<i>De novo</i> structures of Cbp1 homologs	14
Emergomyces Cbp1 homologs cannot complement the Hc cbp1 mutant	20
<i>E. africanus</i> yeast are unable to cause macrophage lysis despite replicating intracellularly	23
Hc and Pb03 Cbp1 enters the cytosol during macrophage infection	24
Hc Cbp1 forms a complex with Yps-3, another known Hc virulence factor that is also in the macrophage cytosol	28
Discussion and future directions	31

Chapter 3: Multiple *Histoplasma capsulatum* cysteine-rich protein effectors enter the macrophage cytosol and are required for lysis

Enrichment of expression of secreted and cysteine rich proteins in the yeast phase of <i>Histoplasma capsulatum</i>	35
Identification of Hc proteins in the macrophage cytosol during infection	38

Hc Secreted Cysteine-rich Protein-1 (Scp1) is required for optimal macrophage lysis	43
The <i>Hc</i> -containing phagosome is not permeabilized	45
Discussion and future directions	47
Chapter 4: Histoplasma species have an expanded family of putative cystine-knot genes which contain a virulence factor, Knot-1	
KNOTTIN Finder	50
Deletion of Rockstar10, but not other knottins, generates a lysis defective mutant	55
Rockstar10 does not contribute to the Integrated Stress Response	60
Discussion and future direction	62
Chapter 5: Materials and Methods	64
References	85

List of Figures

Figure 2.1: Cbp1 is conserved amongst closely related thermally dimorphic fungi that are intracellular pathogens of humans	13
Figure 2.2: Complete alignment of all Cbp1 homologs detected in Ajellomycetaceae genomes	14
Figure 2.3: InstantBlue™ stained SDS-PAGE gel of Cbp1 homologs purified directly from culture supernatants	15
Figure 2.4: <i>De novo</i> crystal structures of H88 and Pb03 Cbp1 reveal a novel “binocular” fold	16
Figure 2.5: Comparisons of the previously published G186AR NMR structure with the H88 and Pb03 Cbp1 crystal structure	18
Figure 2.6: <i>Emergomyces</i> species contain Cbp1 homologs in their genomes that can be expressed and secreted by the <i>Hc</i> G217B strain but are insufficient to confer macrophage lysis	21
Figure 2.7: Generation of chimeric <i>Hc-E. crescens</i> and Pb03- <i>E. crescens</i> alleles	23
Figure 2.8: <i>E. africanus</i> yeast are unable to lyse macrophages actively	24
Figure 2.9: <i>Hc</i> and <i>Pb03</i> Cbp1 exit the <i>Hc</i> -containing phagosome and enter the macrophage cytosol during infection	26
Figure 2.10: Controls for fractionation to assess rupture of small membranous compartments or <i>Hc</i> -containing phagosome	27
Figure 2.11: BMDM infections with <i>Hc</i> strains expressing tagged versions of <i>Hc</i> or Pb03 Cbp1	28
Figure 2.12: <i>Hc</i> G217B Cbp1 forms a complex with Yps-3, another abundant <i>Hc</i> virulence factor	30
Figure 2.13: Generation of the <i>YPS-3</i> deletion mutant in <i>Hc</i> G217B using CRISPR-Cas9	31

Figure 3.1: There signal-peptide containing transcripts are enriched in both yeast and hyphal extremes, but cystine-rich transcripts are only enriched in the yeast phase	36
Figure 3.2: Candidate list of putative secreted cysteine-rich protein effectors found in the <i>Histoplasma capsulatum</i> G217B genome	38
Figure 3.3: Scp1 is a yeast expressed protein that is necessary for optimal lysis of macrophages during infection	45
Figure 3.4: The <i>Hc</i> -containing phagosome is not permeable to the CCF4-AM probe	47
Figure 4.1: KNOTTIN Finder is a naïve algorithm to search for fungi1-like putative knottins in genomes	52
Figure 4.2: Heatmap showing the number of knottins in the genomes of selected fungi	54
Figure 4.3: Probcons alignments of Rockstar1, Rockstar6, Rockstar10, and <i>Hc</i> AVR9 homolog clades	56
Figure 4.4: Generation of knottin disruption and deletion mutant alleles using CRISPR-Cas9	57
Figure 4.5: The knottin Rockstar10, but not Rockstar1, Rockstar6, or the AVR9 homolog, disruption and deletion mutants have a defect in macrophage lysis	59
Figure 4.6: Rockstar10 is able to enter the macrophage cytosol during infection but does not contribute to the induction of the Integrated Stress Response	61

List of Tables

Table 3.1: <i>Histoplasma capsulatum</i> proteins identified in the host macrophage cytosol by mass spectrometry	40
Table 4.1: List of putative knottin hits generated by the KNOTTIN Finder algorithm in the <i>Hc</i> G217B genome	51
Table 4.2: List of sgRNA protospacers and their corresponding PAM sites used to generate knottin CRISPR mutants in <i>Hc</i> G217B	58
Table 5.1: List of primers used in this work	76

Chapter 1: Background

Intracellular pathogens

Intracellular pathogens contend with the need to co-opt their host cells to fashion a replicative niche and the need to manipulate host-cell survival, sometimes destroying their host cell at the appropriate time to promote exit and further dissemination. To shape their host environment, intracellular pathogens secrete a number of diverse molecules to help the pathogen evade detection by the immune system, scavenge nutrients, and assist in replication and dissemination throughout their host. Bacteria, viruses, parasites, and fungi all secrete effectors, many of which are proteins that are capable of manipulating the biology of the host cell (Alto & Orth, 2012; Hakimi & Bougdour, 2015; Ham et al., 2011; Mitchell et al., 2016; Pradhan et al., 2021). Pathogens that reside in nutritionally limiting phagosomal compartments that are normally slated for degradation must be particularly adept at remodeling this niche to make it compatible with microbial replication (Asrat et al., 2014; Fredlund & Enninga, 2014; Personnic et al., 2016). In the case of human pathogenic fungi, we understand much less about secreted effectors of virulence (Brown, Denning, Gow, et al., 2012; Brown, Denning, & Levitz, 2012; Chu et al., 2006). Phytopathogenic fungi have the most well studied examples of effector proteins (Lo Presti et al., 2015; Stergiopoulos & de Wit, 2009).

Phytopathogenic fungi secrete cysteine-rich protein effectors

Phytopathogenic fungi, or plant-disease causing fungi, annually damage up to 30% of crops worldwide and threaten the food security of the world (Avery et al., 2019). Many phytopathogenic fungi deliver proteinaceous effectors through a specialized cell appendage known as an appressorium to affect their host plant cell both intracellularly and extracellularly (He et al., 2020; Pradhan et al., 2021). These protein effectors play many roles, including dampening the host cell immunity, changing the host cell metabolism, and scavenging nutrients for the invading fungus (Dodds & Rathjen, 2010; Pradhan et al., 2021). The defining characteristics of these effectors are that they are typically on the smaller end (less than 300 amino acids), are

expressed primarily during host-colonization, and are cysteine-rich (Lo Presti et al., 2015). These cysteines form stabilizing disulfide bridges to help the effectors deal with the harsher environments of the host plant cell. The effectors typically act by binding to host cell proteins and altering their function. Large repertoires of plant fungal effectors have been characterized and classified but less is known overall for intracellular human fungal pathogen effectors. The same characteristics that have come to define phytopathogenic fungal effectors seem to be similar for human pathogenic fungal effectors as more are being discovered. Hence, it is useful to think about phytopathogenic fungal effectors as models for what human fungal pathogens effectors could be doing.

Thermally dimorphic fungal pathogens cause disease in humans

Many human fungal pathogens are opportunistic and only cause diseases such as *Aspergillosis*, *Candidiasis*, *Cryptococcosis*, and *Mucormycosis* in immune compromised individuals (Brown, Denning, Gow, et al., 2012; Brown, Denning, & Levitz, 2012). With the growing rise of immunocompromised individuals around the world due to pandemics like HIV/AIDS and a global aging population, many more humans are now at risk for lethal and invasive fungal infections (Brown, Denning, Gow, et al., 2012; Brown, Denning, & Levitz, 2012; Lockhart & Guarner, 2019; Reid et al., 2020; Suleyman & Alangaden, 2016). Additionally, rampant use of antifungals has led to outbreaks of antifungal-resistant nosocomial infections as with *Candida auris* (Du et al., 2020). Amongst the species of fungi that causes disease in humans, the thermal dimorphic fungi stand out, as the majority of them are primary fungal pathogens, meaning they can cause disease even in immunocompetent hosts (Sil & Andrianopoulos, 2014). The name of this fungal group comes from the ability of these fungi to change their cell morphology and their expression profiles depending on the temperature of their environment (Beyhan & Sil, 2019; Lockhart et al., 2021). Thermal dimorphism exists in multiple phyla of fungi including the Ascomycota, Basidiomycota, and Zygomycota, suggesting it could have evolutionarily arisen multiple times (Sil & Andrianopoulos, 2014). The major human disease-causing fungi belong to

the order of Onygenales and include the following species: *Histoplasma*, *Paracoccidioides*, *Emergomyces*, *Coccidioides* and *Blastomyces* (Govender & Grayson, 2019; Holbrook & Rappleye, 2008; Lockhart et al., 2021; McBride et al., 2019; Sil, 2019; Sil & Andrianopoulos, 2014). Each has specialized cell forms with differential expression profiles to be able to invade and colonize their host cells (Sil & Andrianopoulos, 2014).

The phylogeny of *Histoplasma* species has recently undergone a restructuring due to improvements in sequencing technology (Lockhart et al., 2021; Sepulveda et al., 2017). Previously, the major clade division was between the strains found in the Americas versus *Histoplasma duboisii* (later referred to as H88 and H143), the African-associated species which has a slightly different disease presentation with more skin lesions. New phylogenetic information has delineated the North (later referred to as G217B) and Central American (later referred to as G186AR/G184AR) clades into four further clades but the disease presentation is the same amongst these species and the new naming scheme is currently considered invalid because it does not follow the International Code of Botanical Nomenclature (Lockhart et al., 2021).

***Histoplasma capsulatum* (Hc) epidemiology and pathogenesis**

Hc is the causative agent of histoplasmosis and causes high morbidity and mortality even in immunocompetent humans (Arauz & Papineni, 2021; Chu et al., 2006; Kauffman, 2007; Woods, 2016). This fungus is found world-wide, and in the Central and Eastern United States *Histoplasma* species are commonly found in the moist soil near the Ohio and Mississippi River Valleys (Benedict & Mody, 2016; Lockhart et al., 2021; Maiga et al., 2018). *Hc* is a thermally dimorphic fungus that grows in a multicellular filamentous form in the soil that produces spores known as conidia in two different sizes; macroconidia (8-15 µm) and microconidia (2-5 µm) (Arauz & Papineni, 2021; Garfoot & Rappleye, 2016; Holbrook & Rappleye, 2008; Maresca & Kobayashi, 1989; Wheat et al., 2016). Filamentous fragments and conidia can be inhaled by a mammalian host, where host temperature induces a transition to a pathogenic yeast form. Microconidia are

small enough to reach the terminal bronchioles and alveoli where they are believed to transition into their yeast form and become phagocytosed by macrophages. Changing the temperature at which the fungus is grown in the laboratory is sufficient to induce either the hyphal growth phase at room-temperature or the yeast growth at 37°C. The two different phases have differential expression profiles that equip each phase with the tools necessary to survive in each environment (Gilmore et al., 2015). *Hc* yeast are phagocytosed by resident alveolar macrophages in the lungs, where they replicate within a modified phagosomal compartment (Howard, 1964, 1965; Newman et al., 1990; Newman et al., 2006; Shen & Rappleye, 2017; Strasser et al., 1999) . Once *Hc* replicates to high levels, the host cells lyse, thereby releasing yeast cells and facilitating further spread of the fungus to neighboring macrophages.

Hc is most common cause of endemic mycosis in North and Central America but is often misdiagnosed or confused for other community acquired pneumonias (Arauz & Papineni, 2021; Wheat et al., 2016). Most humans infected with *Hc* are asymptomatic or experience very limited symptoms that resolve after several weeks. In about 10% of cases, people develop pulmonary symptoms with a fever, dry cough, chest pain, and shortness of breath that could progress to acute respiratory distress syndrome (Arauz & Papineni, 2021; Benedict & Mody, 2016; Wheat et al., 2016). Disseminated histoplasmosis occurs typically in people who are severely immunocompromised, such as in patients with advanced AIDS. Disseminated histoplasmosis typically comes with more severe symptoms which could include gastrointestinal symptoms, skin and oral lesions, and central nervous symptoms (Arauz & Papineni, 2021; Chu et al., 2006). Histoplasmosis could occur from a brand new infection or could re-occur in a patient who has recently become immunocompromised with the likely reservoir coming from nodules in the lungs, much like *Mycobacterium tuberculosis*(Lockhart & Guarner, 2019).

***Histoplasma capsulatum* virulence factors**

The yeast form of *Hc* turns on a transcriptional program managed by a network of temperature responsive transcription factors known as the Required for Yeast Phase (RYPS1-4)

that together upregulate the production of effectors that help the fungus combat the macrophage's antimicrobial pathways (Beyhan & Sil, 2019; Nguyen & Sil, 2008; Shen & Rappleye, 2017; Webster & Sil, 2008). To avoid immune system detection, some but not all species of *Hc* yeast are coated with α -glucan, a polysaccharide that masks the underlying immunogenic β -glucan which is detectable by the pathogen recognition receptor Dectin-1 (Rappleye et al., 2007; Rappleye et al., 2004). Additionally, *Hc* secretes a yeast-phase specific glucanase, Eng1 to trim any revealed β -glucan chains (Garfoot et al., 2017). Beyond preventing recognition by the immune system, the *Hc* yeast also have to counteract the host defense mechanisms such as reactive oxygen species (ROS). *Hc* yeast use an extracellular superoxide dismutase, Sod3, and two catalases, the extracellular CatB and the intracellular CatP, to fight off ROS (Holbrook et al., 2013; Youseff et al., 2012). *Hc* also has to contend with nutritional limitation that is imposed on the yeast when they reside in a phagosomal compartment where there is a lack of essential metals like iron, zinc, and copper. To circumvent the iron restrictions, *Hc* secretes siderophores which can uptake ferric iron directly or secretes γ -glutamyl transferase enzyme Ggt1 that generates cysteinylglycine, a ferric reductant (Burt et al., 1981; Howard et al., 2000; Zarnowski et al., 2008). For both copper and zinc, *Hc* relies on transporters to bring in extracellular metal ions (Dade et al., 2016; Shen et al., 2018). Additionally, *Hc* synthesizes its own vitamins like riboflavin to overcome other nutritional limitations of the anti-microbial phagosomal compartment (Garfoot et al., 2014). Other interesting effectors of *Hc* include cysteine-rich secreted proteins whose function is still not fully understood but when they are knocked-out or knocked-down produce yeast that fail to thrive in macrophages or in a mouse host, including Yps-3 and Cbp1 which are discussed in greater detail in Chapter 2 (Batanghari et al., 1998; Bohse & Woods, 2007b; English et al., 2017; Isaac et al., 2015; Keath & Abidi, 1994; Weaver et al., 1996). Beyond these effectors, *Hc* secretes a large quantity of extracellular vesicles of varying sizes which are filled with RNA,

glycans, pigments and other unexpected proteins that could modulate the host response to *Hc* by moonlighting and disrupting the macrophage processes (Alves et al., 2019; Baltazar et al., 2018; Holbrook et al., 2011; Nosanchuk et al., 2008; Rodrigues et al., 2008; Zamith-Miranda et al., 2021).

Histoplasma capsulatum knottins

One interesting class of effectors from fungi that are newly recognized are the fungal knottins (de Guillen et al., 2019; van den Hooven et al., 1999; van den Hooven et al., 2001; Vervoort et al., 1997). The *Hc* G217B transcriptome was recently reannotated based on RNAseq and ribosomal profiling data and one interesting group of genes that emerged was a family of yeast phase specific, small, secreted proteins that resembled cystine-knot miniproteins (Gilmore et al., 2015; Postic et al., 2018). Cystine-knot proteins or “knottins” are small cystine-rich proteins in which three of the disulfide bridges are interwoven in such a way that they resemble a knot. The knottin fold is highly stable and resistant to temperature, proteolysis, pH changes, and mechanical stress (Postic et al., 2018). The loops are typically of varying lengths and dictate the function of the protein making the knottin fold a great scaffold for protein engineering and drug design (Ackerman et al., 2014; Moore & Cochran, 2012; Moore, 2012). Knottins are found across all the kingdoms of life and have a variety of different functions ranging from protease inhibitors, toxins, antimicrobial peptides, to human neuropeptides (Ackerman et al., 2014; Cheek et al., 2006). The founding member of the first established fungal family known as fungi1 is the AVR9 elicitor of the fungal tomato blight pathogen *Cladosporium fulvum* (Postic et al., 2018; van den Hooven et al., 1999; van den Hooven et al., 2001; Vervoort et al., 1997). The original family of knottins discovered in the G217B *Hc* genome contained 12 genes with the cysteine spacing (C₁-X₃₋₄-C₂-X₅-C₃-X₃₋₆-C₄-X₂-C₅-X₆₋₁₂-C₆) that resemble the AVR9-based fungi1 family knottins (Gilmore et al., 2015). This relation was also confirmed with a Hidden Markov Model (HMM) search. As the putative knottin proteins in *Hc* are small, cysteine-rich, yeast phase expressed,

and contain a signal peptide, they are excellent candidates for being *Hc* virulence factors during macrophage infection.

Chapter 2: Cbp1, a rapidly evolving fungal virulence factor, forms an effector complex that drives macrophage lysis

Introduction

One of the most abundant yeast-phase proteins secreted by *Hc* into culture supernatants is a small 7.8 kDa protein known as Calcium binding protein 1 (Cbp1) (Batanghari et al., 1998; Batanghari & Goldman, 1997; Kugler et al., 2000; Sebghati et al., 2000). As resolved previously by an NMR structure and other biochemical analyses, native Cbp1 is a dimer with three intramolecular disulfide bridges that make it highly stable (Beck et al., 2009; Beck et al., 2008). The mature secreted form of Cbp1 is 78 amino acids in length, has no known domains, and, prior to this work, had only one known homolog in the closely related fungus *Paracoccidioides*. Interestingly, Cbp1 is a critical virulence factor that is required for virulence of *Hc in vitro* and *in vivo* (English et al., 2017; Isaac et al., 2015; Sebghati et al., 2000). *Hc* that lacks Cbp1 is able to grow to high levels within the macrophage but is unable to lyse either primary murine bone marrow derived macrophages (BMDMs) or primary alveolar macrophages (English et al., 2017; Isaac et al., 2015). These data suggest that Cbp1 is a protein effector used by *Hc* to actively lyse macrophages. Cbp1 is also critical for virulence in an *in vivo* mouse model of *Hc* infection (Isaac et al., 2015). Recent work from our lab has demonstrated that Cbp1 actively triggers apoptosis of macrophages through the integrated stress response (ISR), a cascade that is triggered in the cytosol of infected macrophages. The secretion of a functional Cbp1 is absolutely required for this stress response to be initiated in infected macrophages (English et al., 2017). Additionally, we have previously shown that the *Paracoccidioides americana* (*Pb03*) homolog of Cbp1 is capable of fully restoring lytic capability when expressed in a *Hc cbp1* mutant background (English et al., 2017), suggesting that *Hc* is not the only species that could be using Cbp1 to elicit host cell death. How Cbp1 triggers the ISR and macrophage death is still not fully understood.

Another known secreted effector of *Hc* is the Yeast phase specific 3 (Yps-3) protein (Bohse & Woods, 2005, 2007a, 2007b). Like Cbp1, Yps-3 is a secreted factor that is only

produced by the pathogenic yeast phase of the fungus and has been previously shown to be important for virulence in a murine model of Histoplasmosis using an RNA interference strain with reduced expression of *YPS3* (Bohse & Woods, 2007b). Yps-3 is thought to coat the surface of the yeast cell by binding to chitin (Bohse & Woods, 2005). Neither Cbp1 nor Yps-3 has been shown to interact with any other fungal proteins.

In this study, we used evolutionary, structural, and cellular approaches to study the *Hc* Cbp1 and its homologs. We found new, previously unannotated Cbp1 homologs in the genomes of *Paracoccidioides*, and *Emergomyces* species. *Emergomyces* are newly emerging human fungal pathogens that are responsible for a rising incidence of mycoses in immunocompromised humans worldwide (Dukik et al., 2017; Govender & Grayson, 2019; Samaddar & Sharma, 2021; Schwartz et al., 2019). In contrast, despite its close evolutionary relationship to *Hc*, the extracellular pathogen *Blastomyces* does not harbor a Cbp1 homolog. We determined a new structure of both *Hc* and *Pb* homologs of Cbp1, thereby revealing a novel protein fold. To perform a functional analysis of Cbp1 homologs, we expressed Cbp1 from *Pb03* and *Emergomyces* species in the *Hc cbp1* mutant and assessed the ability of each homolog to complement the host lysis defect. Despite the conservation of Cbp1 homologs in the genomes of *Emergomyces* species, these proteins were unlike the *Pb03* Cbp1 in that they could not restore lysis during *Hc* infection. For the first time, we assessed the interaction between BMDMs and wild-type *E. africanus* and discovered that this fungus is capable of robust intracellular replication within BMDMs without any evidence of host-cell lysis, consistent with the inability of *Emergomyces* Cbp1 to complement the *Hc* mutant. Finally, to determine the site of action of *Hc* Cbp1, we discovered that it enters the macrophage cytosol from the *Hc*-containing phagosome, making it the first example of an effector from an intracellular fungal pathogen of humans that accesses the host cell cytosol. Biochemical analyses revealed that Cbp1 forms a complex with Yps-3 and coupled with our observation that *yps3Δ* mutants cannot achieve maximal lysis of macrophages, suggested the formation of a cytosolic effector complex that mediates host-cell death. Given that

Cbp1 1) is unique to the Ajellomycetaceae, 2) shows significant sequence divergence between homologs, and 3) mediates differential lysis between intracellular pathogens, we conclude that the virulence factor Cbp1 is a rapidly evolving protein that is critical for macrophage manipulation by *Hc*.

Cbp1 is conserved amongst the Ajellomycetaceae with the exception of Blastomyces species

Cbp1 is a secreted virulence factor that is required for *Hc* to cause host cell death during intracellular infection of macrophages (Batanghari et al., 1998; English et al., 2017; Isaac et al., 2015; Sebghati et al., 2000). Cbp1 homologs are not broadly present in the fungal kingdom (English et al., 2017). Due to its critical role during intracellular infection, we hypothesized that Cbp1-dependent virulence strategies could be conserved amongst closely related thermally dimorphic fungal species in the Ajellomycetaceae family that are human intracellular pathogens. To identify all putative Cbp1 homologs, we expanded the Cbp1 alignment previously published in (English et al., 2017) by building a Hidden Markov Model (HMM) to search through the annotated protein sets generated from all the additional published genomes of *Emergomyces*, *Blastomyces*, and *Paracoccidioides* species deposited in GenBank. We detected five new Cbp1 *Emergomyces* and two new *Paracoccidioides* homologs which were previously unannotated. To identify the *Emergomyces* homologs, we first defined a syntenic region based on the previously established *Hc* and *Pb* homologs. When we interrogated the corresponding syntenic region in *Emergomyces* species, we uncovered three new *Emergomyces* homologs. All three share the conserved two intron structure found in the *Hc* and *Pb* *CBP1* genes (Batanghari et al., 1998; English et al., 2017). In the case of *E. pasteuriana*, we discovered two Cbp1 homologs (*E. pasteuriana_1* and *E. pasteuriana_2*). One homolog was in the syntenic region and maintained the two-intron structure whereas the other was located in a different genomic region and had a three-intron gene structure. Using the *E. pasteuriana* homologs as templates, we searched through the unannotated *E. orientalis* genome and found two additional homologs (*E. orientalis_1*, *E. orientalis_2*). As with *E.*

pasteuriana, one homolog was syntenic with a two-intron structure and one was orthologous to the three-intron *E. pasteuriana_2* Cbp1. In contrast, we found that Cbp1 was not present in any of the *Blastomyces* genomes. Unlike the other three major members of this fungal family, *Blastomyces* leads a largely extracellular lifestyle *in vivo* (Dukik et al., 2017; McBride et al., 2019; Sil & Andrianopoulos, 2014), suggesting that Cbp1 could be a virulence factor that represents a specialized adaptation to an intracellular lifestyle inside of a mammalian host.

We aligned the new Cbp1 homologs to the Cbp1 consensus sequence generated by the HMM (Figure 2.1.A) along with the previously characterized *Hc* and *Pb03* Cbp1 homologs, which have been previously shown to be necessary for macrophage lysis (English et al., 2017; Isaac et al., 2015; Sebghati et al., 2000). The entire protein alignment of all known Cbp1 homologs can be found in Figure 2.2. The 5' portion of the Cbp1 coding sequence, which contains the putative signal peptide necessary for extracellular secretion of the protein, is well conserved amongst all the homologs. However, the residues flanking the putative cleavage site of the signal sequence, as based upon *Hc* G217B Cbp1, are poorly conserved. The N-terminus of the mature protein is fairly well conserved whereas the latter half of the predicted coding sequence is highly conserved, especially the six cysteines that confer stability to the *Hc* Cbp1 homolog by forming three intramolecular disulfide bridges (Beck et al., 2009; Beck et al., 2008).

When comparing the sequences of the Cbp1 homologs on a primary amino acid level relative to the sequence of G217B Cbp1, it is clear that these sequences diverge rapidly. We see that the Cbp1 sequences within each genus *Histoplasma*, *Paracoccidioides*, and *Emergomyces* are much closer to each other than they are to homologs from a different species. The percent identity between G217B and G186AR/H88 Cbp1 are high, both at about 91.8% identity (Figure 2.1.A). The next closest sequence is that of *Pb03* and other *Paracoccidioides* species which range between 52-55% identical (Figure 2.1.A and Figure 2.2). *Emergomyces* Cbp1 homologs are even less identical, ranging between 38-53% (Figure 2.1.A). Using Phylogenetic Analysis by Maximum Likelihood (PAML) (Yang, 2007) over the alignment of the 11 orthologs found in the syntenic

region of the G217B *Hc* Cbp1, we find that there is significant support for a positive selection model (M8/M7) of Cbp1 in these genomes with a $p = 7.918e-06$ [cite]. The dN/dS values show positive selection (>95% probability) for the following 5 residues in the alignment: 35, 36, 38, 52, and 69 (dN/dS = 3.379, 3.429, 3.475, 3.481, 3.389) all of which are in the mature form of the protein. These data suggest that even though Cbp1 was gained recently amongst the fungi of Ajellomycetacea, it diverged rapidly between the various species in this family and remains under positive selection.

The most parsimonious explanation for the emergence of Cbp1 in this fungal family is that Cbp1 evolved in an early common ancestor and was then subsequently lost from the *Blastomyces* ancestral species as it diverged away from the other members of Ajellomycetaceae (Figure 2.1.B). Similarly, the duplication of the Cbp1 gene in *E. pasteuriana* and *E. orientalis* may have occurred in a common ancestor of the *E. orientalis*, *E. pasteuriana*, and *E. africanus* species. We note that this implies either subsequent loss of the Cbp1 paralog in *E. africanus* or omission of this gene from the *E. africanus* assembly (GCA_001660665.1), which is highly fragmented and 3MB smaller than the other *Emergomycetes* genomes. Taken together, these data suggest that Cbp1 is a rapidly evolving protein.

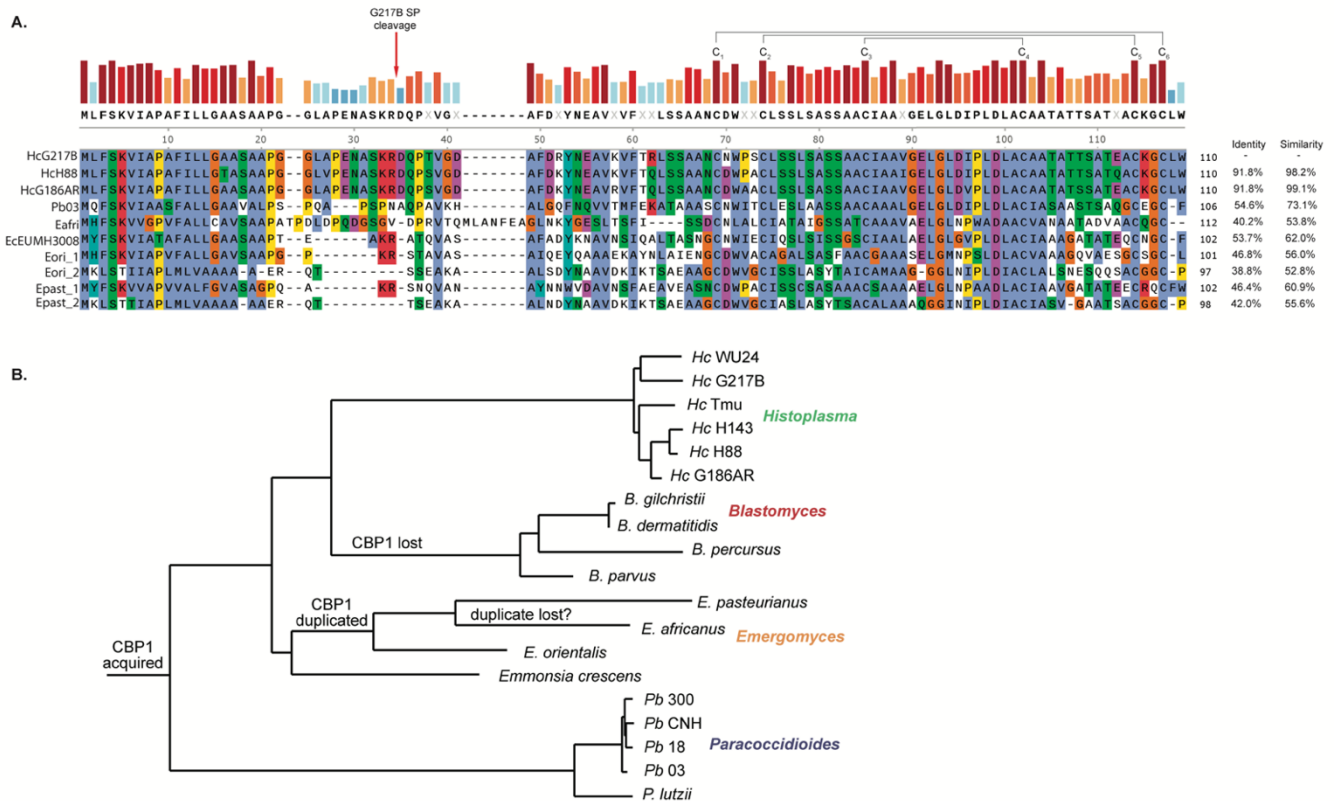


Figure 2.1: Cbp1 is conserved amongst closely related thermally dimorphic fungi that are intracellular pathogens of humans.

(A) Protein alignments of *Hc* G217B Cbp1 and closely related homologs. The site of signal peptide cleavage in the *Hc* G217B protein as well as the six cysteine residues that form intramolecular disulfide bonds are highlighted in the figure. The sequences of three *Hc* homologs (G217B, H88, G186AR), one *Pb* homolog (Pb03), one *E. africanus* homolog, one *E. crescens* homolog, two *E. orientalis* homologs, and two *E. pasteurianus* homologs are shown. The percentages of identity and similarity of each homolog relative to the *Hc* G217B Cbp1 are listed.

(B) Species tree that tracks the acquisition and loss events of Cbp1 in of Ajellomycetaceae species that are human fungal pathogens.

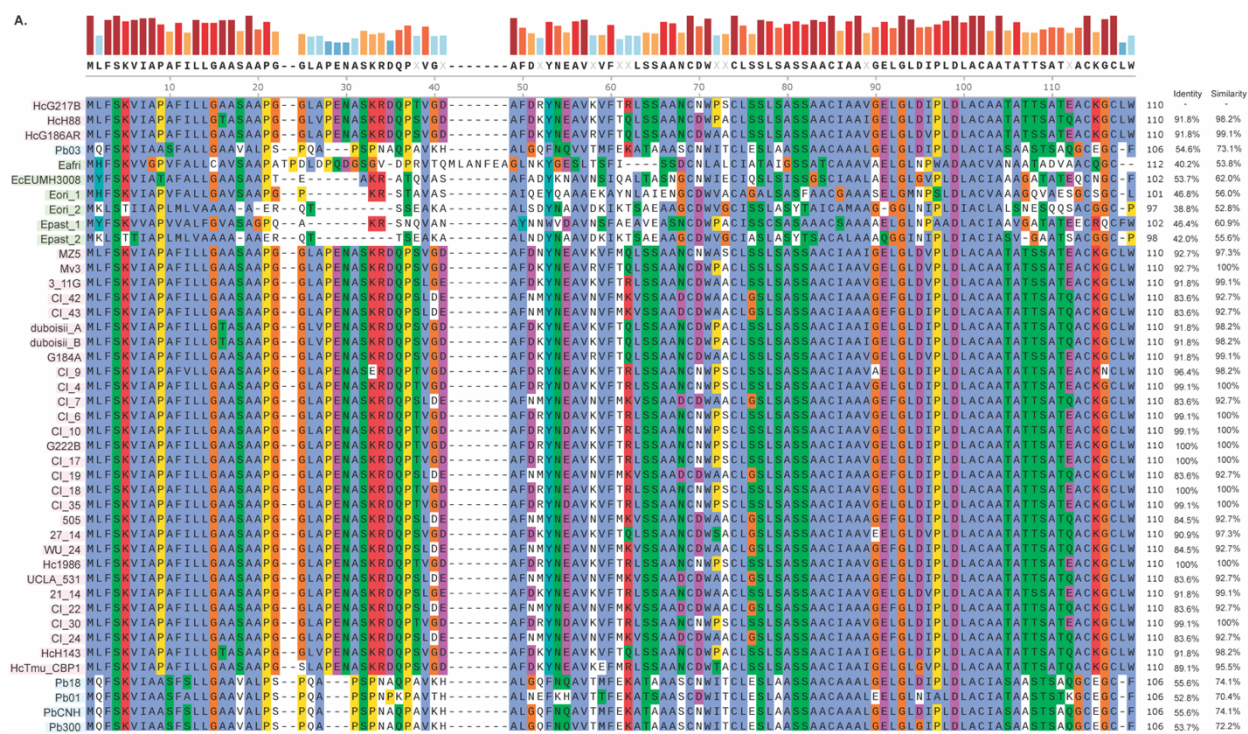


Figure 2.2: Complete alignment of all Cbp1 homologs detected in Ajellomycetaceae genomes. (A) Protein sequence of *Hc* G217B Cbp1 and alignment of all identified homologs is shown. *Histoplasma* genome abbreviations are highlighted with pink, *Paracoccidioides* genomes with blue, and *Emeryomyces* genomes with green.

De novo structures of Hc H88 and Pb03 Cbp1 reveal a novel helical “binocular” fold

To determine if there is any structural conservation between these homologs and the previously published G186AR NMR Cbp1 structure (Beck et al., 2009), we decided to purify and solve the structure of a subset of homologs. Since Cbp1 makes up the vast majority of the *Hc* secretome (Holbrook et al., 2011), we purified the protein directly from culture supernatants. We concentrated *Hc* culture supernatants and then purified Cbp1 by selecting first for charge and then size, thereby achieving purification with minimal perturbation of the native protein. We used this approach to purify *Hc* G217B, G186AR, H88, Pb03, *E. crescens*, and *E. africanus* Cbp1 homologs expressed in *Hc* (Figure 2.3). All of the Cbp1 homologs were purified as dimers according to a sizing column. We were able to generate crystals for *Hc* H88 and Pb03 Cbp1 homologs that were able to diffract to 1.5 and 1.2 angstroms respectively (Figure 2.4.A) The other

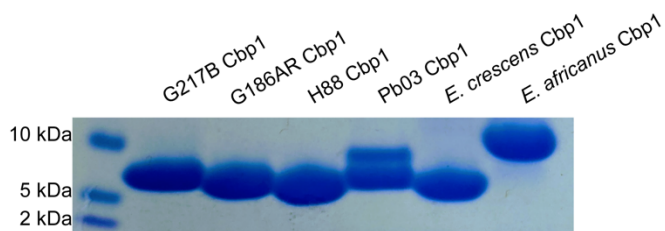


Figure 2.3: InstantBlue™ stained SDS-PAGE gel of Cbp1 homologs purified directly from culture supernatants. Cbp1 was purified from supernatants of the indicated strains (*Hc* G217B; *Hc* G186AR; *Hc* H88; *Hc* G217B *ura5 cbp1* carrying either Pb03 Cbp1, *E. crescens*, or *E. africanus* Cbp1). Purified proteins were subjected to SDS-PAGE and InstantBlue staining.

Cbp1 crystals were unable to diffract well or had internal twinning defects, as in the case of G217B, and hence we were unsolvable. For the *Pb03* homolog, we were able to phase the data by soaking the crystals in a platinum compound and gathering a parallel dataset. For the *Hc H88* homologs, we were able to phase the data by using molecular replacement based on the *Pb03* structure.

For *Pb03* Cbp1, the quaternary structure contained a single dimer, whereas H88 formed a dimer of dimers (Figure 2.4.A-B). The two dimers of the H88 Cbp1 structure were highly similar in their 3D structure when aligned as the RMSD value was 0.668 (Figure 2.4.B). These structures had no significant structural homology to any known proteins according to DALI(Holm, 2020) or VAST(Madej et al., 2014) searches but are highly similar to each other as can be seen when the dimers of *Pb03* and *H88* are aligned (Figure 2.4.C). The Cbp1 structures displayed an alpha-helical dimer arrangement with an intermolecular four-helix bundle fold at the core formed from the 3rd and 4th helices of each monomer, creating a binocular shape, and thus we dubbed this new arrangement as a “binocular” fold. The bundle formed by two of the three C-terminal helices of each monomer contains a number of aliphatic residues (Ile55, Pro56, Leu59, Ala63) that create a greasy patch that forms a platform for the longer N-terminal helices (Figure 2.5.CC). The N-terminal helices from both monomers interact with each other in an anti-parallel manner and their register relative to each other seems to be determined by the N-terminal residues packing against the aliphatic patch right underneath them. For both the H88

and Pb03 structure, the interfaces where the N-terminus of one monomer interacts with the C-terminal tail of the other monomer are not symmetric (Figure 2.4.E). In the Pb03 structure, the

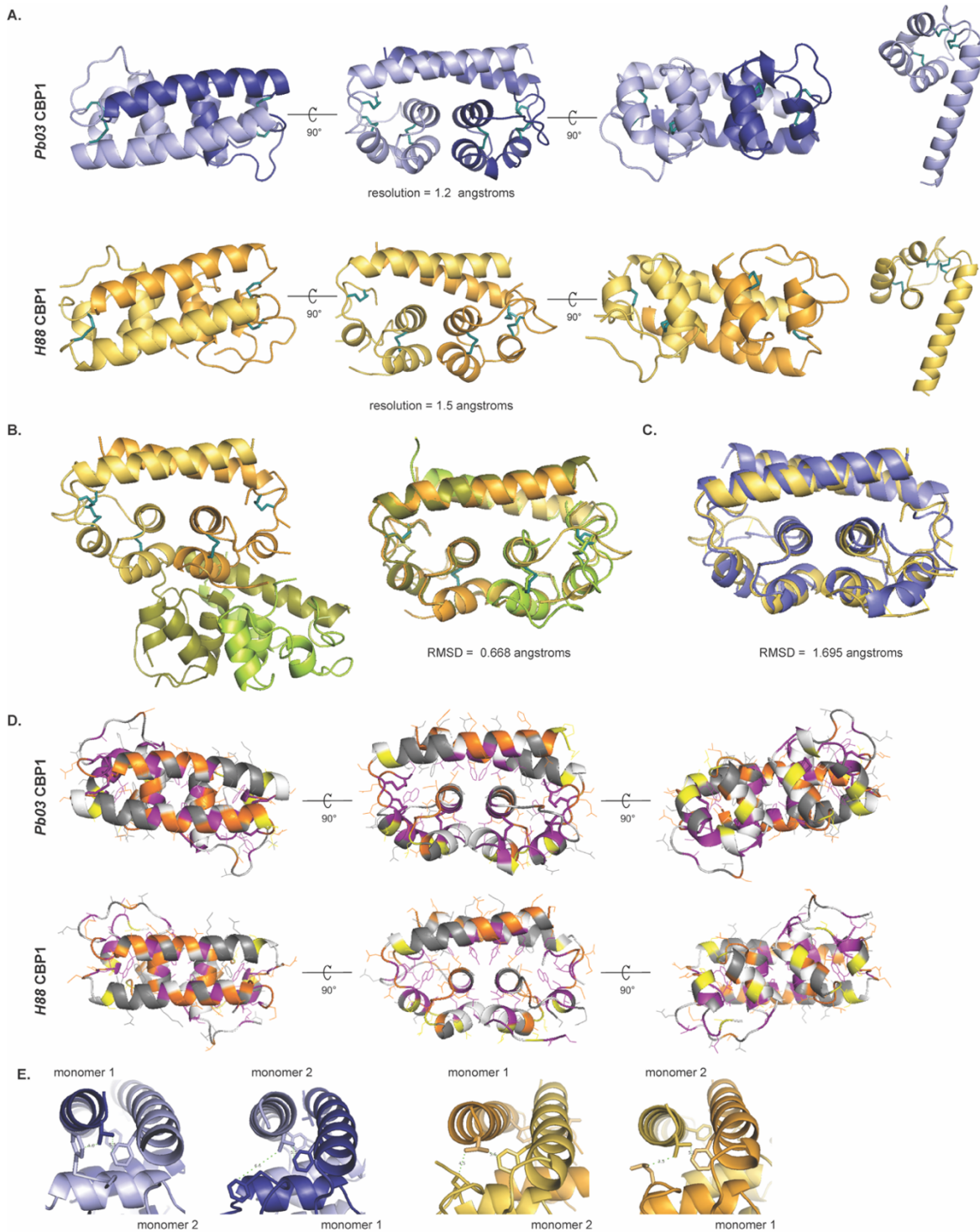


Figure 2.4: *De novo* crystal structures of H88 and Pb03 Cbp1 reveal a novel “binocular” fold. (A) Structures of *Pb03* and *H88* Cbp1 as determined by crystallographic methods are shown in native dimer form and as a monomer.

(B) Quaternary structure of the H88 Cbp1 shows a dimer of dimers that interact through the C-terminal helical bundles. The two dimers in the H88 quaternary structure are aligned and the RMSD score was determined to be 0.668 angstroms.

(C) Structural alignments of *Pb03* and *H88* Cbp1 structures reveal a highly similar fold with an RMSD value of 1.695 angstroms.

(D) Purple residues were previously determined to be required for secretion (English et al., 2017) and are predicted to face inwards based on the structure. Orange residues were previously determined to be required for lysis whereas yellow residues contribute to lysis (English et al., 2017); these residues are predicted to be on the surface of the protein facing outwards.

(E) Zoom-in of the non-symmetrical interaction between the N-terminal helix Val5 of monomer 1 with the C-terminal tail of monomer 2 through coordination of Val5 with Phe19 and Phe77(*Pb03*)/Leu77(*H88*) of the opposite monomer.

last residue of the N-terminal helix, Val5 of monomer 1, is coordinated between Phe19 from the other monomer's N-helix and Phe77 of the other monomer's C-terminal tail, effectively tucking the tail of the protein against the N-terminal helix. In contrast, on the other dimer interface, monomer 1 Phe77 is turned away and not coordinating the other Val5 from monomer 2. The Phe77 residue immediately follows the last disulfide bridge in *Pb03* is not a conserved aromatic in all the Cbp1 homologs (Figure 2.1). In *Hc* species, the last disulfide is followed with a Leu and Trp in the *H88* structure where it visibly cannot tuck the C-terminal tail in the same manner as *Pb03* Cbp1. The *Emergomyces* orthologs differ even further; *E. africanus* has no residues following the last disulfide, *E. orientalis* has a single Leu, *E. pasteurianus_1* has two aromatics a Phe and a Trp, and *E.pasterurianus_2* and *E. orientalis_2* have a Pro. The three disulfide bonds present in each monomer orient the alpha helices so that the aromatic residues (Phe12, Phe19, Trp30) are packed in the interior of the protein, creating the hydrophobic core (Figure 2.5.C). Despite the fact that the *Pb03* and *H88* structures are similar when they are aligned with an RMSD = 1.6 angstroms (Figure 2.4.C), an emerging property that differs between the two is the distribution of charge over the surface of the protein at a neutral pH (Figure 2.5.D)(Baker et al., 2001; Dolinsky et al., 2004). Whereas the *Pb03* structure has a clear positive charge at the C-terminal pole of the protein and is partially negative at interface of the N-terminal helices, the *H88* structure is not as clearly polarized. There is a groove of strong positive charge on the side of the

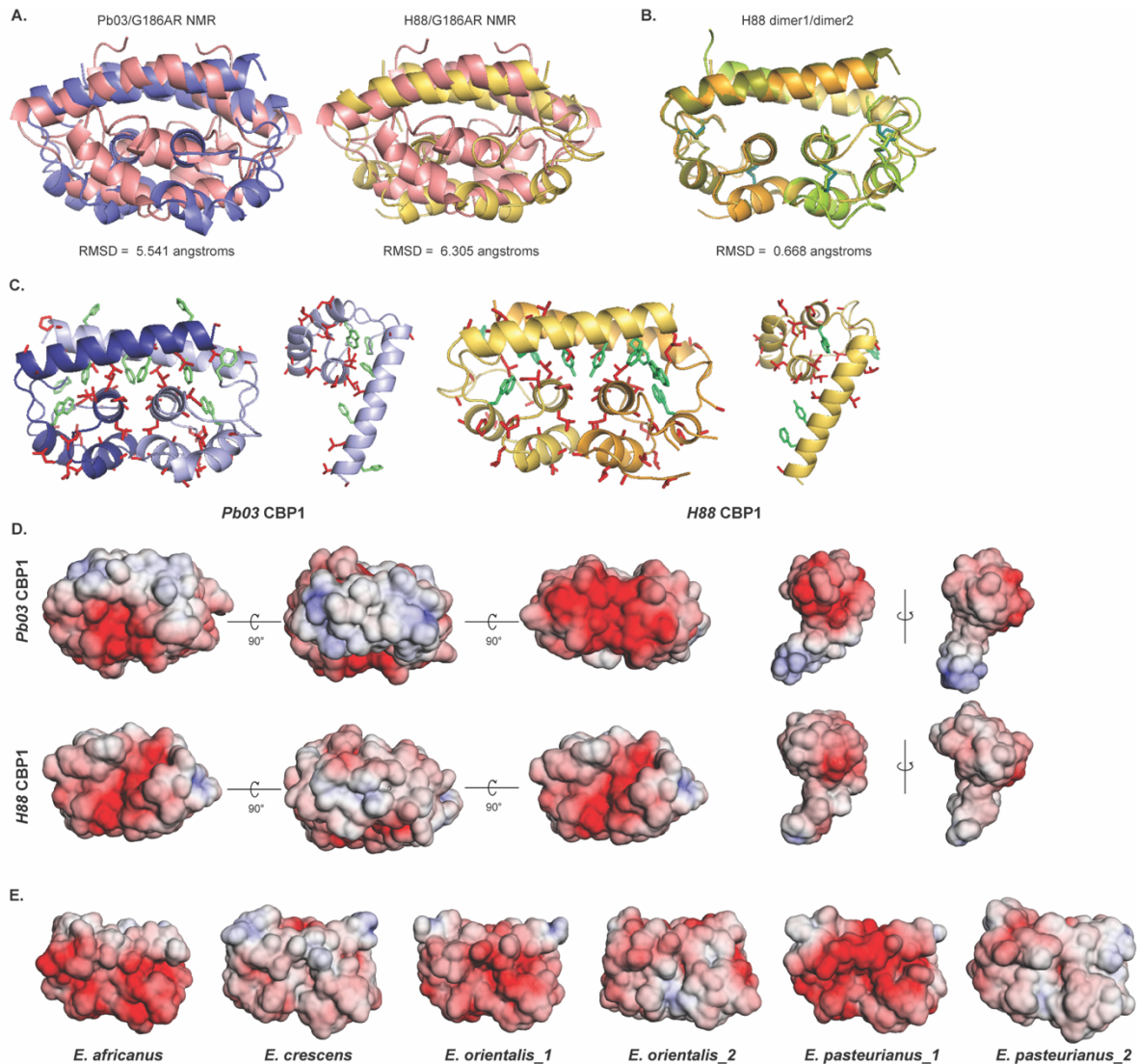


Figure 2.5: Comparisons of the previously published G186AR NMR structure with the H88 and Pb03 Cbp1 crystal structure.

(A) Alignment of the Pb03 and H88 crystal structures with the G186AR NMR structure shows major differences in the arrangement of the helices. The RMSD scores from the alignments of G186AR to Pb03 and H88 are 5.541 and 6.305 respectively.

(B) Overlay of the two H88 dimers present in the quaternary structure shows they are highly similar with an RMSD score of 0.668 angstroms.

(C) Highlight of the aromatic (colored mint green) and aliphatic (colored red) residues to showcase the greasy patch formed by the C-terminal helices of each monomer and the aromatic residues packing into the hydrophobic core.

(D) Charge distribution over the surface of the protein structures shows major differences in the positive charge at neutral pH. Positive charge is indicated on surface with red, negative charge with blue, and neutral with white. The Pb03 dimer has a positive charge patch at the bottom of the C-terminal helical bundles, whereas the H88 dimer is only partially positive there. The H88 dimer has a positive groove that runs along the side of the protein. Only the Pb03 structure has a

partial negative charge over the N-terminal helices. The electrostatic surfaces were determined using the APBS/PDB2PQR software (Baker et al., 2001; Dolinsky et al., 2004).

(E) The tertiary structures of *Emergomyces homologs* were modelled on top of the H88 Cbp1 backbone using MODELLER (Webb & Sali, 2016, 2021) and the surface charge distribution was determined using the APBS/PDB2PQR software.

H88 protein, but there is not as much positive charge at the C-terminus nor much negative charge at the N-terminus. These contrasts are also clearly visible in the individual monomer charge distribution (Figure 2.5.D).

Interestingly, the previously published *Hc* G186R NMR Cbp1 structure (Beck et al., 2009) is distinct from the crystal structures determined here. The RMSD values when the new structures were aligned against the G186AR NMR structure were approximately 5.5 and 6.5 angstroms for Pb03 and H88 Cbp1 respectively (Figure 2.5.A). The orientation of the three C-terminal alpha-helices is now perpendicular to the N-terminal helices whereas in the NMR structure it was parallel; the N-terminal helices are now more linear and align in a different register relative to each other; and in the NMR structure, the two monomers are intercalated, whereas in the crystal structures this is not the case. Multi-wavelength anomalous diffraction (MAD) screens for the presence of any coordinated ions showed that no metal ions, including calcium ions, were present within these structures.

In prior work, we used alanine scanning to identify Cbp1 residues that are critical for function (English et al., 2017) (Figure 2.4.D). The alanine scan identified residues that, when mutated to alanine, resulted in Cbp1 variants which were 1) incapable of being secreted, 2) capable of being secreted but only caused partial macrophage lysis, or 3) capable of being secreted but completely deficient in macrophage lysis capability. Notably, when we modeled these residues on the crystal structure, we found that the residues that were required for Cbp1 protein secretion were all facing inwards away from the protein surface, suggesting they are important for proper folding (Figure 2.4.D). This observation was consistent with a role in proper packing of the hydrophobic core. The majority of the residues that were necessary or contributed to Cbp1 lytic capability had side chains that are oriented out towards the external surface and

were preferentially located in the N-terminal helix, suggesting that those residues create surfaces that are necessary for Cbp1 function. Thus, the alanine scan data is highly consistent with the newly determined crystal structures of *Hc* Cbp1 and its homologs.

Emergomyces Cbp1 homologs cannot complement the Hc cbp1 mutant

To further probe the function of the newly identified Cbp1 homologs, we expressed them in *Hc* to determine whether they could complement the *cbp1* mutant. The *Hc* (G217B) *cbp1* mutant is unable to lyse macrophages after intracellular infection (English et al., 2017; Isaac et al., 2015). A second phenotype of the *Hc cbp1* mutant is a delay in intracellular growth after macrophage infection, although ultimately the *cbp1* mutant reaches high levels of intracellular fungal burden equivalent to or exceeding that of wild-type *Hc* (English et al., 2017; Isaac et al., 2015). We have previously shown that expression of the *Paracoccidioides americana* (*Pb03*) Cbp1 homolog in the *Hc* (G217B) *cbp1* mutant can restore macrophage lysis (English et al., 2017). We expressed five of the newly detected *Emergomyces* Cbp1 homologs (*E. africanus*, *E. orientalis_1*, *E. crescens*, *E. pasteuriana_1* and *E. pasteuriana_2* Cbp1) in the *Hc* G217B *cbp1* background to see if these homologs can complement either the ability of *Hc* to lyse macrophages or grow intracellularly without any delay. To monitor for production and secretion of each of the *Emergomyces* homologs, we subjected concentrated culture supernatants from multiple isolates expressing each of the Cbp1 homologs to SDS-PAGE followed by staining with InstantBlue™ stain to monitor for the presence of a prominent Cbp1 band. We found that all five homologs were capable of being secreted from *Hc* under the control of the *Emergomyces* native signal peptide (Figure 2.6.A). Their identity was also confirmed with mass spectrometry of chymotrypsin or trypsin digested peptides from SDS-PAGE gel bands.

To determine if expression of any of these homologs could complement the phenotypes of the *Hc* G217B *cbp1* mutant, we infected primary murine bone marrow-derived macrophages (BMDMs) with our cohort of heterologous expression strains and monitored for the release of lactate dehydrogenase into the supernatant as a measure of host cell lysis. The *Hc cbp1* mutant

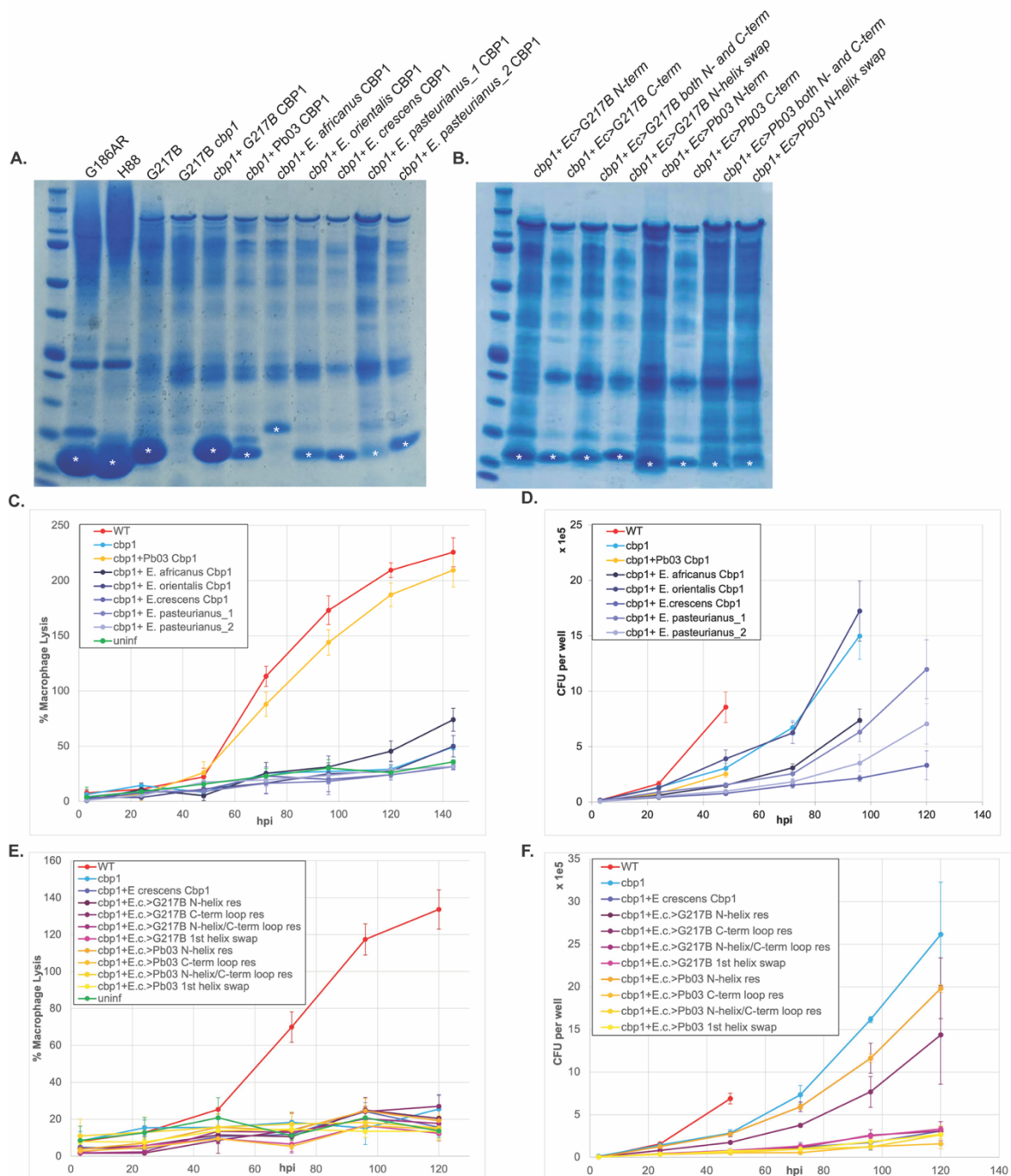


Figure 2.6: *Emergomyces* species contain Cbp1 homologs in their genomes that can be expressed and secreted by the Hc G217B strain but are insufficient to confer macrophage lysis. (A) InstantBlue™ stained SDS-PAGE gel of culture supernatants of G186AR Hc, H88 Hc, G217B Hc, G217B Hc *cbp1* mutant, and Hc (G217B) *cbp1* mutant expressing the G127B, *P. americana* (Pb03), *E. crescens*, *E. orientalis*, *E. pasteurianus_1*, *E. pasteurianus_2*, *E. africanus* Cbp1. White asterisk denotes the bands that were excised for mass spectrometric analysis. (B) InstantBlue™ stained SDS-PAGE gel of culture supernatants of G217B Hc *cbp1* mutant expressing the chimeric constructs that convert key residues from *E. crescens* Cbp1 into their

counterpart residue from G217B or Pb03 Cbp1 in the N-terminus, the C-terminal loops, both the N-terminus and C-terminal loops, and a 1st helix swap.

(C) *Hc cbp1* mutant isolates expressing the *Emergomyces* Cbp1 homologs were used to infect BMDMs at an MOI of 1 as described in the Methods. “WT” indicates the *Hc* G217B *cbp1* mutant carrying the *Hc* G217B *CBP1* on a plasmid. LDH release was used to quantify percent host cell lysis.

(D) Intracellular growth of *Hc cbp1* mutant isolates expressing the *Emergomyces* Cbp1 homologs was determined from BMDM infection as described in the Methods. “WT” indicates the *Hc* G217B *ura5* mutant carrying the *URA5* gene on a plasmid. At 48 hpi, CFU counts were terminated for the WT *Hc* infection because the extent of host-cell lysis made it difficult to distinguish between intracellular and extracellular growth of *Hc*.

(E) *Hc cbp1* mutant isolates expressing *E. crescens* chimeric Cbp1 homologs were used to infect BMDMs and LDH release was quantified.

(F) Intracellular growth of *Hc cbp1* mutant isolates expressing the *E. crescens* chimeric Cbp1 homologs was determined from BMDM infection as described in the Methods. “WT” indicates the *Hc* G217B *ura5* mutant carrying the *URA5* gene on a plasmid. At 48 hpi, CFU counts were terminated for the WT *Hc* infection because the extent of host-cell lysis made it difficult to distinguish between intracellular and extracellular growth of *Hc*.

fails to lyse BMDMs and also exhibits an intracellular growth delay before it undergoes replication during infection. The *Pb03* homolog was able to fully restore the lytic capability of the *cbp1* mutant (Figure 2.6.C) but did not complement the growth delay as measured by intracellular CFU counts (Figure 2.6.D). Surprisingly, none of the *Emergomyces* Cbp1 homologs were able to restore the ability of the *Hc* G217B *cbp1* mutant to lyse macrophages (Figure 2.6.C) or grow intracellularly without a delay (Figure 2.6.D).

To assess which molecular differences between Cbp1 homologs might correlate with differences in function, we created a series of chimeric Cbp1 protein constructs (Figure 2.7.A-B). Of the *Emergomyces* Cbp1 homologs, we chose *E. crescens* Cbp1 as a template because it had the highest percent identity to *Hc* G217B Cbp1. Based on the alanine scan data described above, we identified key amino acids in *Hc* G217B Cbp1 that are required for macrophage lysis (English et al., 2017) (Figure 2.7.A). A subset of the analogous amino acids in *E. crescens* Cbp1 were changed to the corresponding G217B *Hc* or *Pb03* Cbp1 residues. These residues were selected based on the following criteria: whether their sidechains were facing the external surface, whether they were necessary for lysis based on the alanine scan data, and whether there was a significant change in either polarity, charge, or size as compared to *Hc* G217B Cbp1. Four chimeric

constructs were ultimately generated that either exchanged the 1) entire N-terminal helix, 2) only the residues necessary for lysis in the N-terminal helix, 3) the residues necessary for lysis in the loops and helices of the C-terminal helical bundle, or 4) a combination of constructs 2 and 3 (Figure 2.7.A). These chimeric Cbp1 proteins were expressed in the *Hc* G217B cbp1 mutant background. We found that the chimeric proteins were expressed and secreted (Figure 2.6.B), suggesting that they were properly folded, but none could restore macrophage lytic capability (Figure 2.6.E) or ameliorate the intracellular growth delay (Figure 2.6.F).

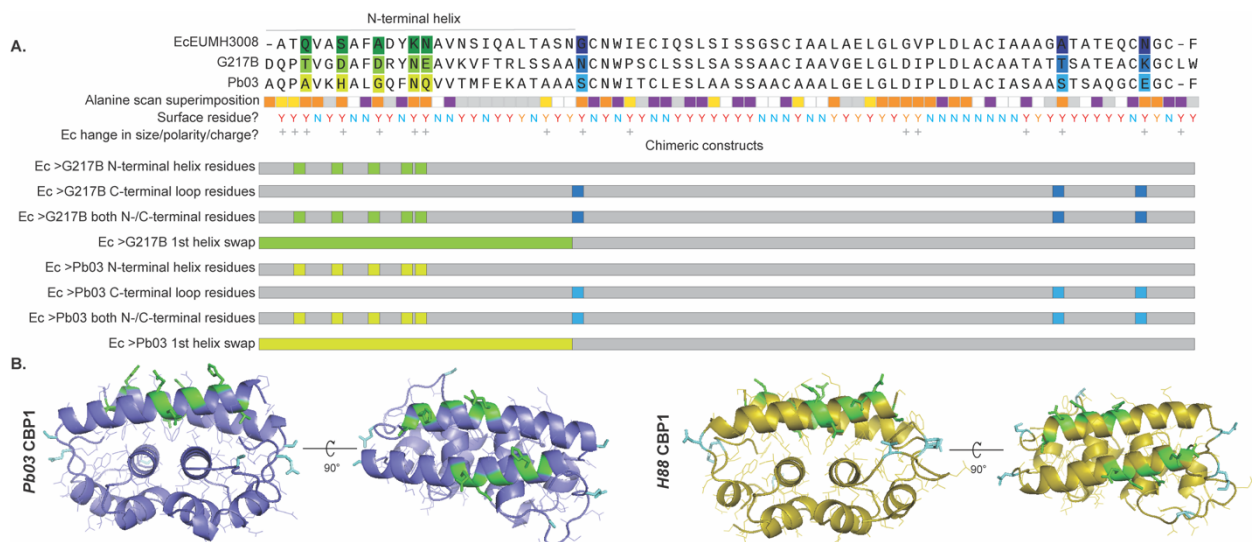


Figure 2.7: Generation of chimeric *Hc-E. crescens* and Pb03-*E. crescens* alleles. (A) Illustration of residue changes made to *E. crescens* Cbp1 to make chimeras with either G217B or Pb03 Cbp1. The protein alignments were compared to the alanine scan of G217B to determine differential residues necessary for lysis. Based on the H88 and Pb03 Cbp1 structures, we determined which residues were oriented outwards on the surface. The differential residues were also checked for whether they had major differences in the characteristics of the side chain of the residue in terms of size, polarity, or charge. The proposed chimeric constructs are illustrated. The green colored residues represent residues in the N-terminal helix whereas the teal residues represent residues in the C-terminal loops. (B) The selected differential residues that were mutated in the N-terminal helix and C-terminal loops are highlighted in green and teal respectively in the Pb03 and H88 structures.

***E. africanus* yeast are unable to cause macrophage lysis despite replicating intracellularly**

To determine if the lack of lysis caused by *Emergomyces* Cbp1 homologs is reflective of the *Emergomyces* natural infection of primary macrophages, we infected BMDMs with

Emergomyces africanus wildtype yeast at an MOI of 1. We monitored for lysis as we did with *Hc*, by measuring the release of Lactate-dehydrogenase into the culture supernatants. We saw that the infected macrophages did not lyse over the course of infection (Figure 2.8.A). Despite this lack of lysis, we still see the intracellular replication of *E. africanus* intracellularly of macrophages, as the cells become full of yeast over the course of an infection (Figure 2.8.B). This behavior is strikingly similar to how the *Hc cbp1* mutant is able to grow intracellularly to a high fungal burden but cannot actively lyse out of their host cells (Isaac et al., 2015). This suggests that the lack of lysis we see in the *Hc* expressing the *Emergomyces* homologs is biologically relevant to the natural *E. africanus* infection. *E. africanus* and other *Emergomyces* species are still capable of causing systemic disease in humans (Govender & Grayson, 2019; Samaddar & Sharma, 2021) suggesting that *Emergomyces* species rely on other virulence factors since their Cbp1 homolog does not function to help the yeast actively lyse out of macrophages like it does for *Hc* infection.

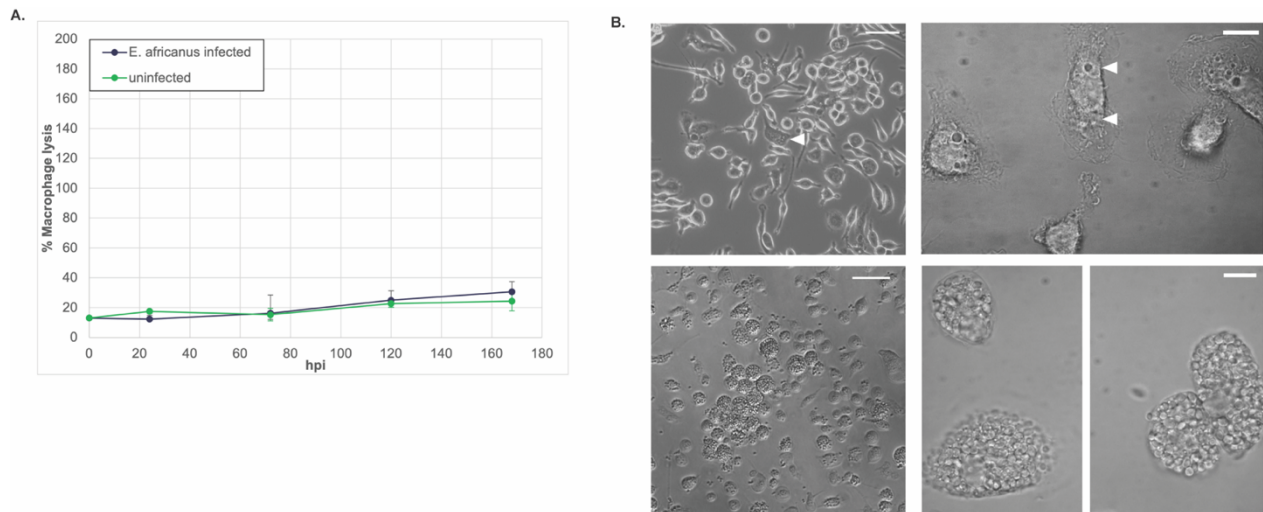


Figure 2.8: *E. africanus* yeast are unable to lyse macrophages actively.

(A) Lactate dehydrogenase release from Bone Marrow Derived Macrophages infected with wildtype *E.africanus* at an MOI of 1 as described in the Methods.

(B) DIC images of BMDMs infected with wildtype *E. africanus* at an MOI of 1. The top row of DIC images were taken one day post-infection and the images in the bottom row are taken five days post infection.

***Hc* and *Pb03 Cbp1* enters the cytosol during macrophage infection**

To further probe the mechanism of Cbp1 function, we investigated its subcellular localization during *Hc* infection. Once *Hc* is phagocytosed by macrophages, it begins to replicate

intracellularly within a modified phagosomal compartment that is prevented from fusing with degradative lysosomes and maintains a neutral pH (Eissenberg et al., 1993; Strasser et al., 1999; Taylor et al., 1989). We have previously shown that *Hc* infection triggers a cytosolic stress response inside of macrophages known as the Integrated Stress Response (ISR) that is dependent on Cbp1 (English et al., 2017). As in the case of *Hc*-infection, if the cytosolic stress remains unresolved, the macrophage undergoes apoptotic cell death. Since Cbp1 seems to be a crucial secreted virulence factor and is required to cause a host cell cytosolic response, we hypothesized that Cbp1 gains access to the macrophage cytosol during infection. It has been reported in the literature that a Cbp1-GFP fusion localizes to the *Hc*-containing phagosome (Kugler et al., 2000), but localization of the native Cbp1 during infection has not been determined. Additionally, it is unknown whether the Cbp1-GFP fusion is functional. Almost all attempts at tagging *Hc* Cbp1 render it non-functional, and peptide antibodies generated against Cbp1 recognize only the denatured form of the protein, making it difficult to localize the protein during infection by indirect immunofluorescence. We fractionated infected macrophages to test whether Cbp1 accumulates in the macrophage cytosol. We separated the cytosolic fraction from the membrane fraction and validated the integrity of the cytosolic fraction (by probing with alpha-tubulin) and the membrane fraction (by probing with calnexin, an ER membrane protein). Cbp1 localized exclusively to the cytosolic fraction, suggesting it exits the *Hc*-containing phagosome during infection (Figure 2.9). To ensure that small endosomal compartments weren't ruptured during the fractionation process, we probed for LAMP1 and found it solely in the membrane fraction (Figure 2.10). Additionally, we checked that the *Hc* yeast themselves are not rupturing during the fractionation protocol by confirming that the *Hc* transcription factor *RYP1* is present only in the fraction that contains whole *Hc* yeast, which are separated from the lysates along with the nuclear fraction prior to ultracentrifugation (Figure 2.10). This is the first instance of an effector of an intracellular human fungal pathogen being able to enter the cytosol of the host cell. Using a N-terminal FLAG-tagged Pb03 Cbp1 homolog that retains its lytic capability during infection

(Figure 2.11), we confirmed the cytosolic localization of *Pb03* Cbp1 via the fractionation approach (Figure 2.9). Interestingly, the analogous tagged version of *Hc* G217B Cbp1 is non-functional but nonetheless localizes to the macrophage cytosol during infection, suggesting cytosolic localization alone is not sufficient to cause lysis of the host macrophage (Figure 2.9, Figure 2.11.B). The functional *Pb03*-3XFLAG Cbp1 homolog appears in a punctate pattern throughout the infected macrophage cytosol and occasionally overlaps with *Hc*-containing phagosome, suggesting it could be accumulating and aggregating in the cytosol during infection (Figure 2.9B).

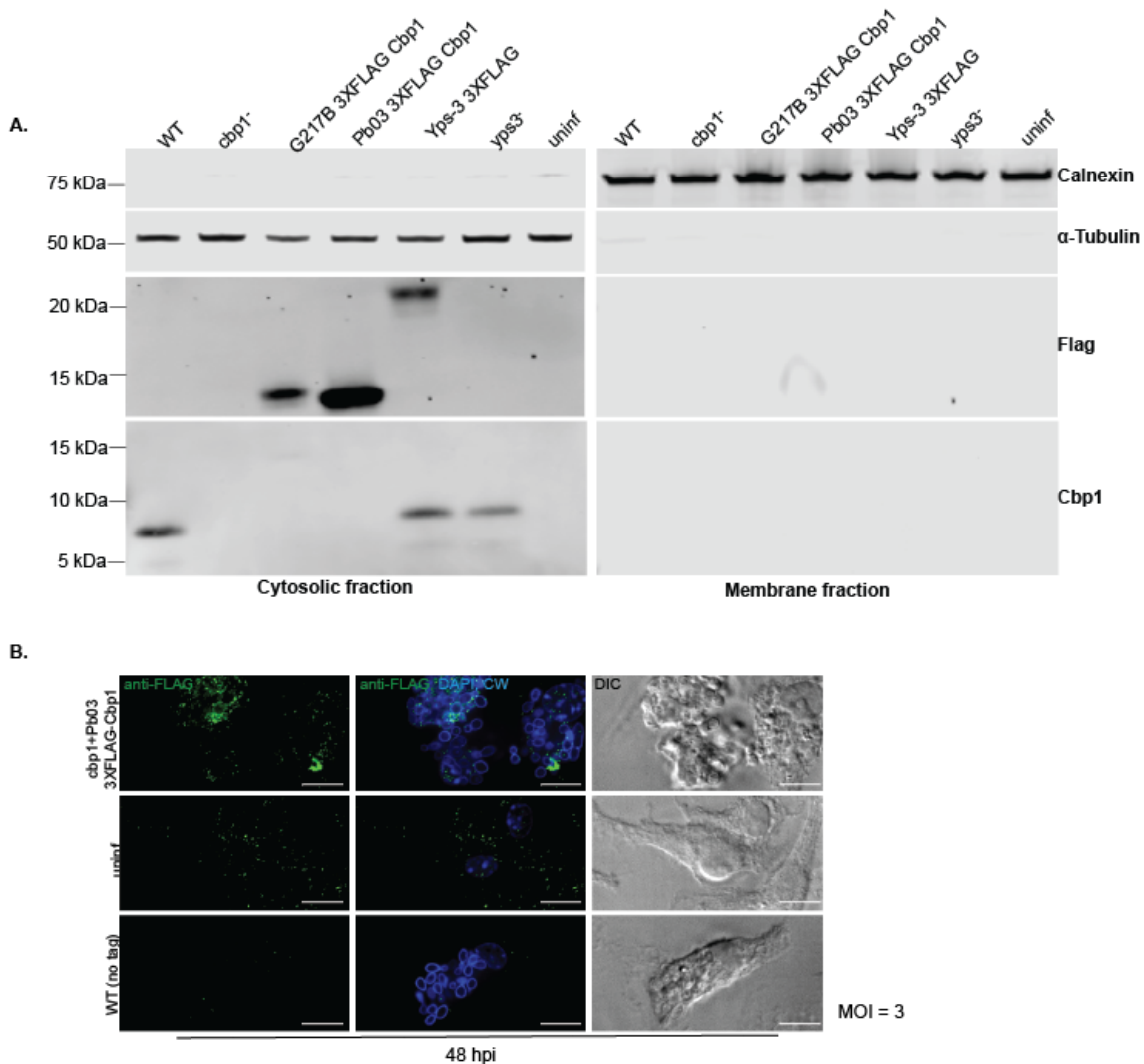


Figure 2.9: *Hc* and *Pb03* Cbp1 exit the *Hc*-containing phagosome and enter the macrophage cytosol during infection.

(A) BMDMs were mock-infected (uninf) or infected with either the “WT” strain (G217B *Hc ura5*⁻ carrying the vector control expressing the URA5 gene), the *cbp1* mutant *Hc* (G217B *Hc ura5*⁻ *cbp1*⁻) carrying either the control vector or G217B Cbp1 with 3 FLAG (G217B Cbp1 3XFLAG),

Pb03 Cbp1 with 3XFLAG (Pb03 Cbp1 3XFLAG), WT G217B *ura5⁻* carrying Yps-3 3XFLAG (Yps-3 3XFLAG), or the *yps3* mutant (G217B *Hc ura5⁻ yps3⁻*). Macrophage lysates were subjected to fractionation to separate cytosolic and membrane fractions, followed by SDS-PAGE and Western blotting using anti-Calnexin (marking the endoplasmic reticulum), anti- α -Tubulin (marking the cytosol), anti-FLAG or anti-Cbp1 antibodies.

(B) BMDMs were either mock-infected or infected with G217B *Hc ura5⁻ cbp1⁻* expressing the WT Cbp1(WT) or the *cbp1* mutant carrying the Pb03 Cbp1 tagged with 3XFLAG. Cells were fixed and subjected to indirect immunofluorescence with the FLAG antibody. Scale bar represents 10 μ m.

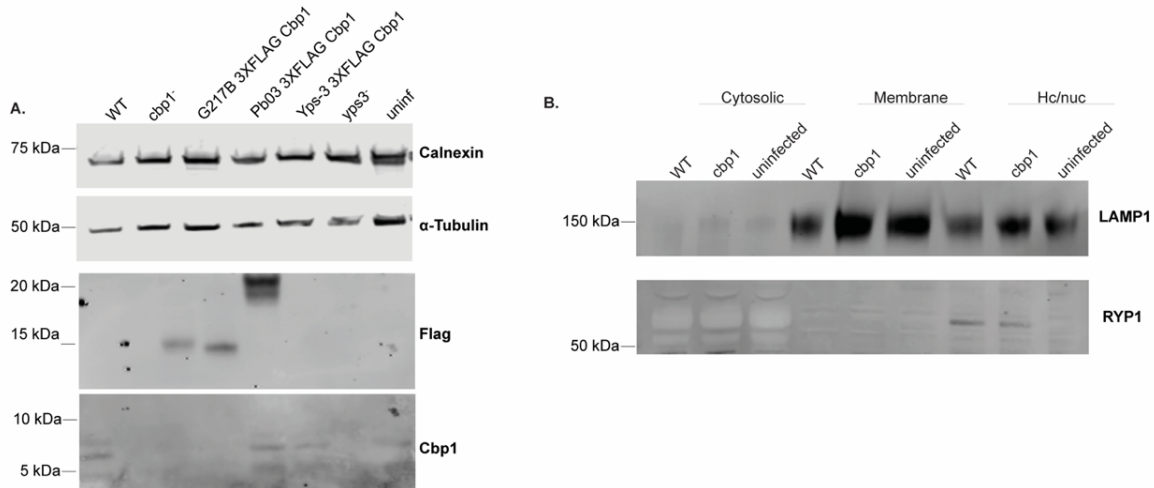


Figure 2.10: Controls for fractionation to assess rupture of small membranous compartments or *Hc*-containing phagosome.

(A) BMDMs were mock-infected (uninf) or infected with either the “WT” strain (G217B *Hc ura5⁻* carrying the vector control expressing the URA5 gene), the *cbp1* mutant *Hc* (G217B *Hc ura5⁻ cbp1⁻*) carrying either the control vector or G217B Cbp1 with 3 FLAG, Pb03 Cbp1 with 3XFLAG, WT G217B *ura5⁻* carrying Yps-3 3XFLAG, or the *yps3* mutant (G217B *Hc ura5⁻ yps3⁻*). Macrophage lysates were subjected to fractionation to separate cytosolic and membrane fractions, followed by SDS-PAGE and Western blotting using anti-Calnexin (marking the endoplasmic reticulum), anti- α -Tubulin (marking the cytosol), anti-FLAG or anti-Cbp1 antibodies. Shown here is the *Hc* and nuclear fraction that is separated with a low-speed spin prior to ultracentrifugation contains both cytosolic and membrane components.

(B) The cytosolic, membrane, and *Hc* and nuclear fraction (containing both cytosolic and membrane components that pellet with a low-speed spin prior to ultracentrifugation) were subjected to SDS-PAGE and Western blotting using anti-LAMP1 (marking the late endosomes and lysosomes) or anti-Ryp1 (an *Hc* transcription factor that is not released from the *Hc* cells, indicating that they are intact).

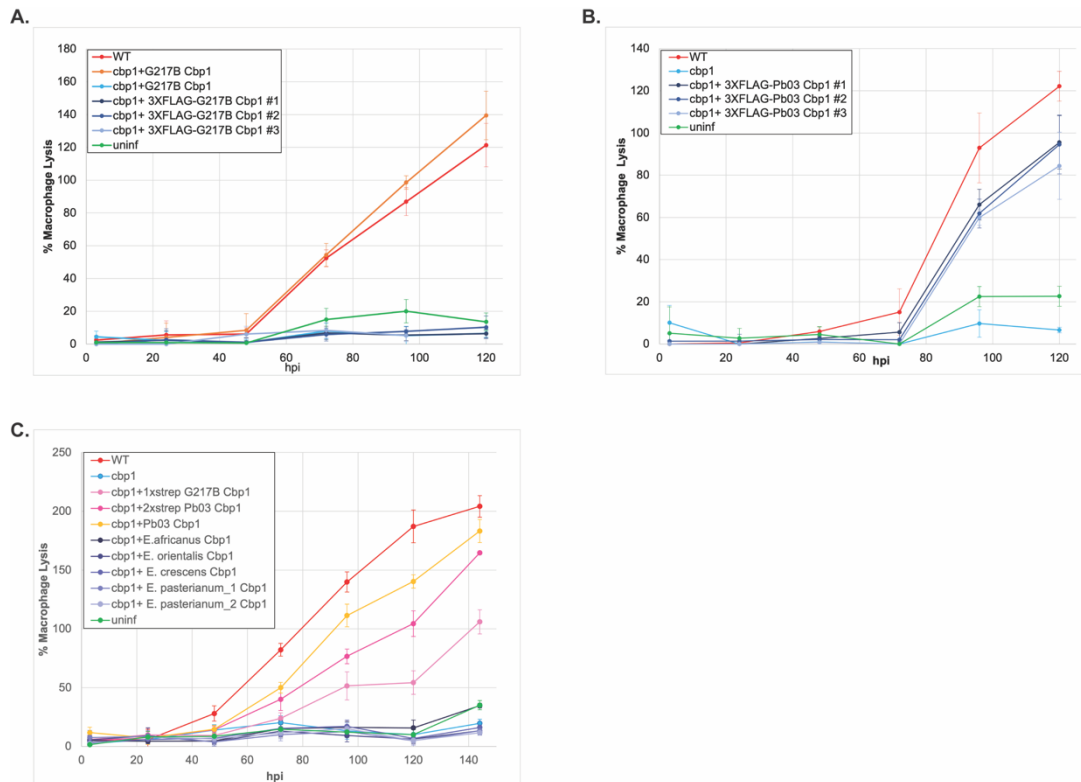


Figure 2.11: BMDM infections with *Hc* strains expressing tagged versions of *Hc* or Pb03 Cbp1. (A) BMDMs were mock-infected (uninfl) or infected with a wildtype G217B *ura5⁻* carrying the control URA5 vector, and the *cbp1* mutant strain carrying untagged G217B Cbp1 or infected with 3 independent transformants of the *cbp1* mutant strain carrying G217B Cbp1 tagged with 3XFLAG. LDH release was monitored over time. (B) BMDMs were mock-infected (uninfl) or infected with 3 independent transformants of the *cbp1* mutant strain carrying Pb03 Cbp1 tagged with 3XFLAG. LDH release was monitored over time. (C) BMDMs were mock-infected (uninfl) or infected with the *Hc cbp1* mutant carrying G217B Cbp1 or Pb03 Cbp1 tagged with 1XStrep or 2XStrep respectively. Other strains included *Hc cbp1* mutant transformed with a variety of *Emergomyces/Emmonsia* Cbp1 alleles. LDH release was monitored over time.

Hc Cbp1 forms a complex with Yps-3, another known Hc virulence factor that is also in the macrophage cytosol

To see if Cbp1 acts alone or as a part of complex of fungal proteins, we isolated 1xstrep-tagged G217B Cbp1 (Figure 2.10.C) from *Hc* culture supernatants and determined which *Hc* proteins associate with Cbp1 by mass spectrometry (Figure 2.12.A). The 1xstrep-tagged G217B *cbp1* allele retains partial lytic function during macrophage infection (Figure 2.11.C). In the

elutions of the 1xstrep *Hc G217B Cbp1* pulldown we observed a prominent band around 17-20 kDa that was absent in the control pull down of 2xstrep-eGFP. The identity of this band was later confirmed by mass spectrometry as Yps-3. Conversely, Cbp1 co-purified with a reverse pulldown of Yps-3-1xstrep from *Hc* culture supernatants (Figure 2.12.A). Additionally, our fractionation experiments demonstrated that, like Cbp1, Yps-3 is able to enter the macrophage cytosol during *Hc* infection (Figure 2.9.A).

To determine if Yps-3 and Cbp1 form a complex, we purified C-terminally tagged Yps3-6xhis from culture supernatants using a cobalt resin and observed that Cbp1 co-purifies with Yps-3 (Figure 2.12). To isolate pure Yps3-6xhis, we used a cation exchange column, but a large portion of Yps-3 was present in the flow through of the cation exchange column along with Cbp1. To confirm that the proteins are truly in a complex, we passed the flow through over a sizing column and discovered that Yps-3 and Cbp1 were present in the same fractions, suggesting they remained in a tight complex (Figure 2.12.B). Additionally, we mixed purified Yps3-6xhis and G217B Cbp1 in molar ratios of 1:1, 1:2, 2:1, 5:1 and pulled down on the 6xHis tag with a Ni-NTA resin. We found that the molar ratio of 1:2 Cbp1:Yps-3 yielded the most robust interaction of the two proteins (Figure 2.12.E).

Previously Yps-3 RNAi knockdown had shown no yeast phenotype in a macrophage cell line (Bohse & Woods, 2007b). To further characterize the role of Yps-3 in macrophage infection, we generated CRISPR deletion mutant of *YPS-3* (Figure 2.13) (Joehnk, in preparation; Kujoth et al., 2020). We found that a *yps-3* Δ mutant has a partial lysis defect in BMDMs (Figure 2.12.D) despite the presence of Cbp1 in the cytosol of macrophages (Figure 2.9.A). These data indicate that Yps-3 is required for robust lysis of infected macrophages.

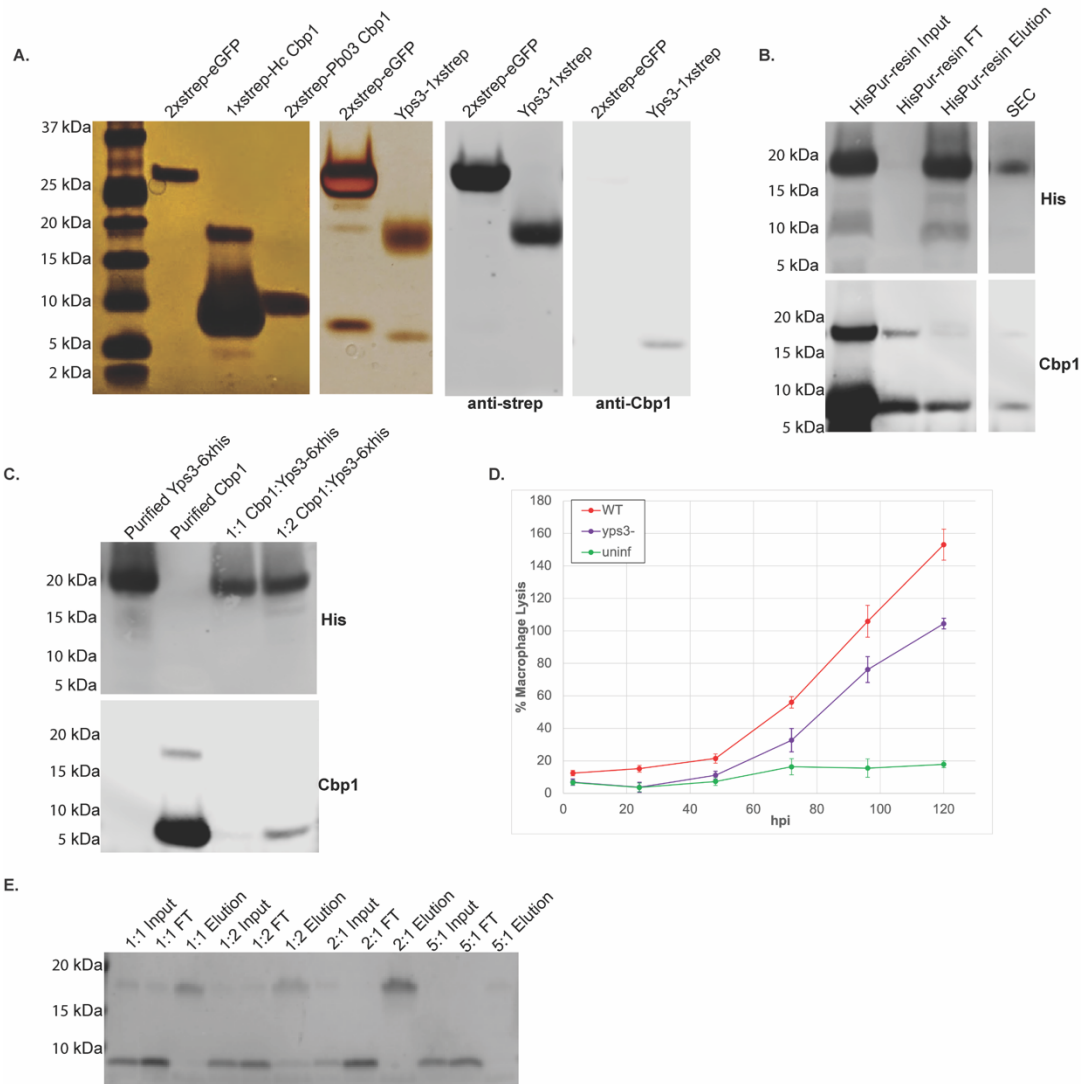


Figure 2.12: Hc G217B Cbp1 forms a complex with Yps-3, another abundant Hc virulence factor. (A) *Hc* culture supernatants from the G217B *ura5⁻* *Hc* carrying a 2xstrep tagged enhanced GFP driven by the Cbp1 promoter (2xstrep-eGFP), the G217B *ura5⁻* *cbp1⁻* carrying a plasmid with the Cbp1 promoter driving either a 1xstrep tagged G217B *Hc* Cbp1 and 2xstrep *Pb03* Cbp1, and the G217B *ura5⁻* strain carrying a 2xstrep tagged Yps-3 driven by the Cbp1 promoter, were subjected to strep affinity purification. Eluates were analyzed by SDS-PAGE followed by silver staining. (B) *Hc* culture supernatant from the Yps-3-6XHis strain was subjected to SDS-PAGE followed by Western blotting with either anti-His or anti-Cbp1 antibodies. The left-hand panel shows input, flow-through (FT) and elution from the HisPur resin whereas the right-hand panel shows fractions from the Size Exchange Column (SEC). (C) Purified Yps3-6XHis and purified G217B Cbp1 were either subjected separately to SDS-PAGE and Western blotting (lanes 1 and 2) or mixed first at defined molar ratios and then isolated by Ni-NTA pulldown of Yps-3-6XHis (lanes 3 and 4). (D) BMDMs were either mock-infected (uninf) or infected at an MOI = 1 with G217B *ura5⁻* (WT) or G217B *ura5⁻* *yps-3 Δ* , each transformed with a *URA5* vector. LDH release was calculated at different timepoints post-infection.

(E) Purified Cbp1:Yps-3-6xhis were mixed in the following molar ratios: 1:1, 1:2, 2:1, and 5:1 and then Yps-3-6xhis was pulled down with Ni-NTA beads to determine if it co-purified with Cbp1.

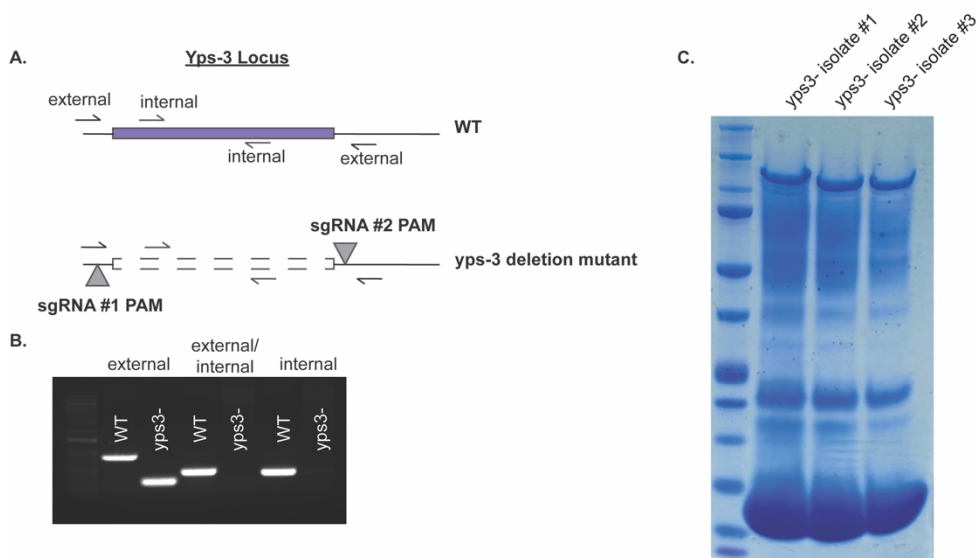


Figure 2.13: Generation of the *YPS-3* deletion mutant in *Hc* G217B using CRISPR-Cas9.

(A) Schematic of CRISPR sgRNA guide target sites (triangles) for the *Yps-3* locus and the location of internal and external primers that were used to probe for the deletion of the locus in panel B. Purple box indicates the *YPS-3* coding sequence.

(B) PCR of *YPS-3* locus from genomic DNA from WT *Hc* and *yps-3*Δ mutant utilizing the external or internal primers designated in A.

(C) InstantBlue™ stained SDS-PAGE gel of concentrated supernatants from three independent *yps-3*Δ mutants.

Discussion and future directions

Macrophages are innate immune cells that are critical for the early detection and killing of infectious microbes. *Hc* is an intracellular pathogen that evades macrophage anti-microbial mechanisms, thereby surviving and replicating within a modified phagosomal compartment. Here we focus on a secreted *Hc* effector, Cbp1, that is critical for manipulating the macrophage response. Cbp1 is absolutely required for macrophage lysis during *Hc* infection. Using cutting-edge bioinformatics tools, we identified all existing Cbp1 homologs in the fungal kingdom and interrogated these proteins for their ability to trigger macrophage lysis when expressed in a *Hc cbp1* mutant. These experiments revealed that only *Hc* and *Pb* carry “lytic” Cbp1 alleles, whereas

closely related *Emergomyces* Cbp1 variants cannot promote macrophage lysis during *Hc* infection. Interestingly, we solve the crystal structure of *Hc* and *Pb* Cbp1 proteins, revealing a novel fold in this rapidly evolving lysis factor.

Our previous work revealed that *Hc* Cbp1 is absolutely required for triggering an Integrated Stress Response (ISR) in the macrophage cytosol during *Hc* infection. When we mutagenized Cbp1 to yield alleles that were partially lytic or completely defective for lysis, we observed little or no ISR induction, respectively, indicating a correlation between the ability of Cbp1 to trigger the ISR and lyse macrophages (English et al., 2017). Here we show for the first time that *Hc* Cbp1 accesses the macrophage cytosol during infection, suggesting that the site of action of Cbp1 is in the cytosol of the host cell. Additionally, we show that Cbp1 binds another known *Hc* virulence factor, Yps-3, which we detect in both the *Hc*-containing phagosome and the macrophage cytosol. Previous work in the literature showed that Yps-3 localizes to the *Hc* cell wall and is released into culture supernatant. RNA interference strains targeting Yps-3 were used to show a role for Yps-3 in organ colonization in the mouse model of infection but no defect in macrophage lysis was observed at the single timepoint examined (Bohse & Woods, 2007b). Interestingly, we show here that deletion of Yps-3 results in diminished host-cell lysis, suggesting that Yps-3 could help potentiate the function of Cbp1.

How Cbp1 and Yps-3 effectors transit from the phagosome to the macrophage cytosol is not yet clear. Perhaps the *Hc*-containing phagosome is leaky, thereby allowing small fungal proteins to access the cytosol. Alternatively, *Hc* is known to secrete copious amounts of extracellular vesicles that contain varied cargo of *Hc* proteins. These virulence factors could enter the cytosol because exosomes, or even multi-vesicular bodies, fuse with the phagosome membrane and releasing their contents directly into the cytosol. Once in the reducing environment of the host cytosol, perhaps Cbp1 changes its conformation and triggers the ISR. We observed that a tagged allele of the *Pb03* Cbp1 (*Pb03-3XFLAG* Cbp1) was distributed throughout the cytosol in a punctate pattern. We speculate that Cbp1 could be aggregating in the cytosol and

triggering cellular stress, and future work will focus on the mechanism of action of the Cbp1-Yps-3 complex in triggering host-cell death.

We observed that Cbp1 appears to be a rapidly evolving lysis factor that is undergoing positive selection. Since Cbp1 is present in all of the genomes of the Ajellomycetaceae human fungal pathogens except *Blastomyces* species, it is likely that Cbp1 arose at the base of the Ajellomycetaceae tree and was subsequently lost only in *Blastomyces*. Notably, *Blastomyces* yeast cells are largely extracellular during infection of mammals, in contrast to *Histoplasma* and other Ajellomycetaceae, suggesting that Cbp1 could be an adaptation to an intracellular lifecycle. Interestingly, despite its lack of Cbp1, *Blastomyces* has retained a Yps-3 homolog, *Blastomyces* Adhesin 1 (Bad1). Bad1 mediates binding of *Blastomyces* to host cells and plays an immunoregulatory role during infection (Beaussart et al., 2015; Brandhorst et al., 2003; Finkel-Jimenez et al., 2002; McBride et al., 2019; Rooney & Klein, 2004). In the case of *Hc*, it is possible that Yps-3 acts with Cbp1 to promote macrophage lysis as well as playing a Cbp1-independent role during infection.

Hc Cbp1 is critical for macrophage lysis and dissemination (English et al., 2017; Isaac et al., 2015). *Pb18* Cbp1, is highly expressed in *Paracoccidioides Pb18* yeast cells (da Silva et al., 2016) and *Pb03* Cbp1 is capable of triggering host-cell lysis when expressed in the *Hc G217B cbp1* mutant background, but whether any *Paracoccidioides* species utilize Cbp1 during infection is yet to be determined. In contrast, *Emergomyces* species have Cbp1 in their genomes but heterologous expression of these Cbp1 alleles in *Hc* suggests that they are non-lytic. This observation correlates with the natural infection of primary BMDMs by *E. africanus*, characterized here for the first time. We observed that *E. africanus* undergoes intracellular replication within macrophages but is unable to lyse them, much like the *Hc G217B cbp1* mutant. It is unclear whether the absence of a lytic Cbp1 affects *Emergomyces* pathogenesis, but notably *Emergomyces* species are pathogens of immunocompromised people whereas *Hc* is a primary pathogen that can infect healthy individuals. Nonetheless, *Emergomyces* species can

disseminate and cause disease in their hosts despite the likelihood that their Cbp1 proteins are non-lytic.

The analysis of *Hc* H88 and *Pb03* Cbp1 protein structures revealed a novel fold that was dissimilar to the previously published NMR G186AR Cbp1 structure. Our protein purification strategy was non-denaturing, which contrasts to the methodology used for the NMR structure. It is possible that Cbp1 can fold differently depending on its environment; for example, perhaps the reducing environment of the macrophage cytosol triggers a conformational change in Cbp1 protein. When we compared the two new structures of *Pb03* and H88 Cbp1, we found that charge was not distributed similarly across the proteins. The bottom of the C-terminal helices that form the core four-helix bundle of the *Pb03* Cbp1 are much more positive relative to the *Hc* H88 Cbp1 homolog. Interestingly, only the *Pb03* and not H88 structures show partially negative N-terminal helices. In addition, when we overlaid the previously published alanine scan of G217B Cbp1 over the two new structures, we found that the majority of the residues necessary for optimal lysis are distributed in the N-terminal helix, suggesting that this region of the protein mediates host-cell death. However, when we swapped the 1st helix of the non-lytic *E. crescens* Cbp1 allele with the corresponding helix from either *G217B* or *Pb03* Cbp1, the resulting chimeric protein was not lytic, suggesting that other regions of the protein may affect folding and/or function. Nonetheless, the concordance between the alanine scan phenotypes and the location of the residues in the crystal structure gives strong support to our analysis of the Cbp1 fold and indicates that this structural analysis of Cbp1 is a critical step in understanding how intracellular fungal pathogens manipulate host cell viability.

Chapter 3: Multiple *Histoplasma capsulatum* cysteine-rich protein effectors enter the macrophage cytosol and are required for lysis

Enrichment of expression of secreted and cysteine rich proteins in the yeast phase of Histoplasma capsulatum

First, we identified all the transcripts that contained a signal peptide and determined if they showed growth phase-specific enrichment. We used previously published transcriptomics data from (Gilmore et al., 2015) and (Rodriguez et al., 2019) in which yeast to hyphal (Y/H) expression profiles were compared. In (Gilmore et al., 2021) the yeast cells were grown at 37°C for three 2-day passages and the hyphae were grown at RT for 4-6 weeks. In (Rodriguez et al., 2019) the day 0 profile of yeast cultures was compared to hyphal cultures that were transitioned to room temperature (RT) over the course of 8 days. Therefore, the hyphae in (Rodriguez et al., 2019) are newly transitioned from yeast-phase cells whereas the hyphae in (Gilmore et al., 2015) are in stationary phase, so they have slightly different expression profiles. To determine which transcripts had signal peptides that would direct the protein into the secretory pathway, we used the Phobius (Kall et al., 2007) prediction algorithm to identify putative signal peptides. When overlaying the two distributions on a spectrum of yeast to hyphae enrichment (Y/H), we found that both transcriptomics datasets show an enrichment in signal peptide-containing transcripts at both the yeast and hyphal extremes, suggesting that both phases use secreted protein effectors to modify their respective environments (Figure 3.1). This can also be seen in a corresponding quantile-quantile (Q-Q) plot, which shows the percentile value in both distributions graphed against each other. If an enrichment in gene expression is more probable in one distribution over the other, they will fall off the line with a slope of 1. As can be seen in both transcriptomics sets, both tail ends of the Y/H distribution fall off the line, suggesting that transcripts with a signal peptide are more likely to be at either end of the Y/H distribution.

Additionally, we wanted to determine if transcripts that are cysteine-rich, with 4 or more cysteines, are also enriched in either hyphal or yeast phases. This time, both Y/H transcriptional

profiles indicated there was a slight enrichment in the yeast phase for cysteine-rich proteins and a slight depletion in the hyphal phase (Figure 3.1). This effect was much less pronounced than the signal-peptide containing distributions but present none the less.

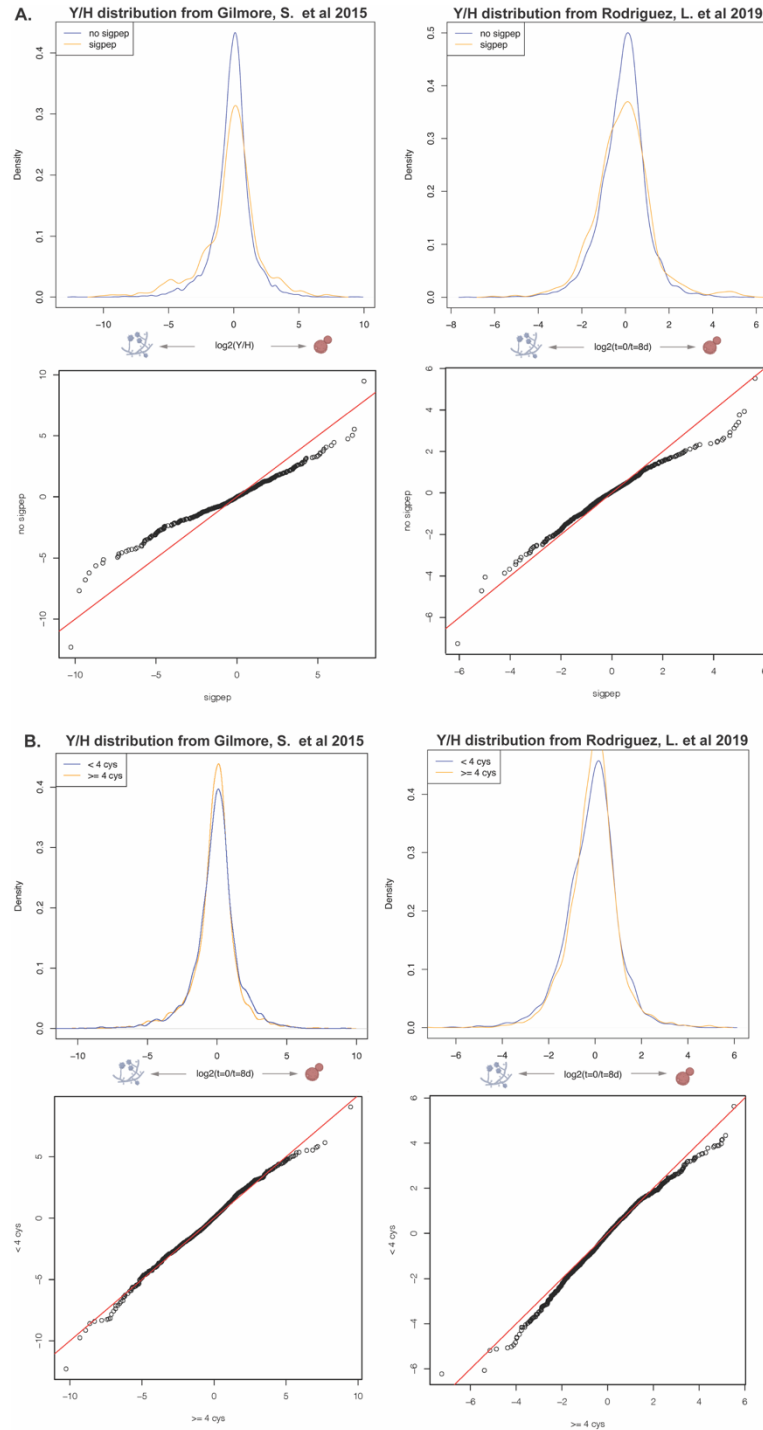


Figure 3.1: There signal-peptide containing transcripts are enriched in both yeast and hyphal extremes, but cystine-rich transcripts are only enriched in the yeast phase.

(A) Overlaid kernel density estimates of signal peptide-containing or no signal-peptide transcripts as predicted by Phobius and the corresponding Q-Q plot in both (Gilmore et al., 2015) and (Rodriguez et al., 2019) Y/H comparisons.

(B) Overlaid kernel density estimates of 4 or more cysteine containing and less than 4 cysteine containing transcripts and the corresponding Q-Q plot in both (Gilmore et al., 2015) and (Rodriguez et al., 2019) Y/H comparisons.

To identify a candidate list of putative secreted effectors specifically in the yeast phase, one approach we used was to look through all the genes that had the following characteristics: (1) had 4 or more cysteines, (2) had less than 400 amino acids, (3) contained a Phobius predicted signal peptide and (4) had upstream RYP binding events (Beyhan et al., 2013; Nguyen & Sil, 2008; Webster & Sil, 2008). The RYPs comprise a transcription factor network that regulates the switch to yeast phase morphology and is required for virulence in a host. This narrowed down the list to 51 genes, the vast majority of which were highly yeast expressed (Figure 3.2). Included in this list were previously identified yeast specific virulence factors such as Cbp1, Yps-3, Yps-21, SOD3, and CTR3 ((Abidi et al., 1998; Batanghari et al., 1998; English et al., 2017; Isaac et al., 2015; Keath & Abidi, 1994; Sebghati et al., 2000). Some of these virulence factors like SOD3 and CTR3 are proteins that enable *Hc* yeast survival within a limiting phagolysosomal environment. Other factors include proteins that enable *Hc* to be able to optimally kill macrophages *in vitro* or *in vivo* such as Cbp1 and Yps-3. The genes of unknown function are candidate virulence factors that can be explored in the future.

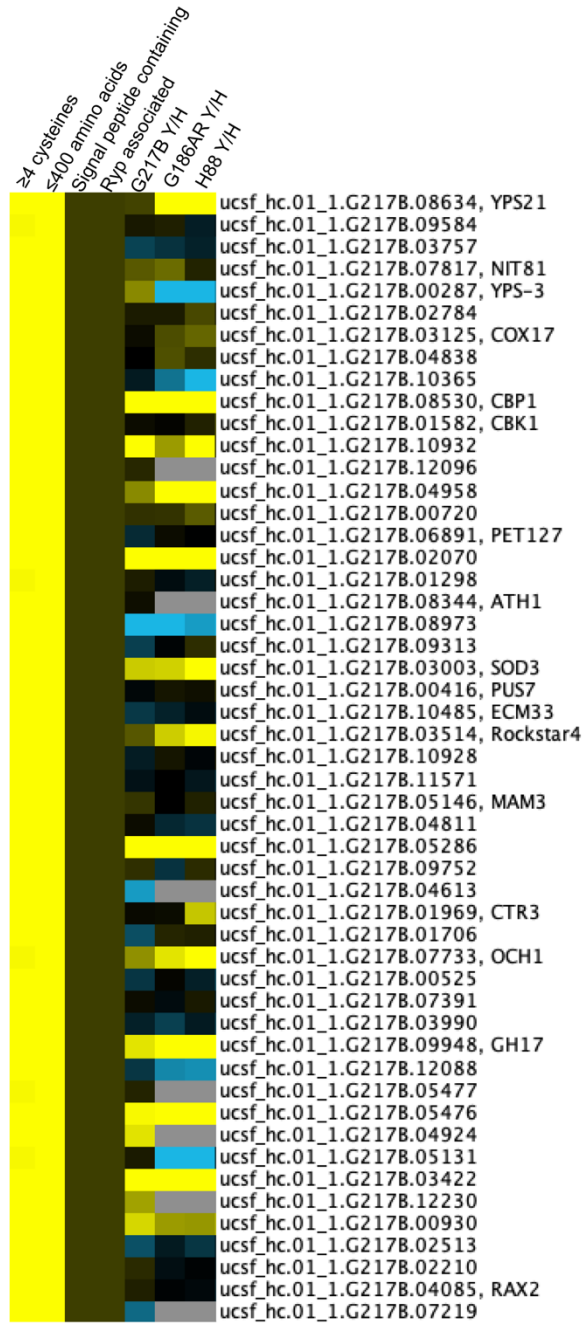


Figure 3.2: Candidate list of putative secreted cysteine-rich protein effectors found in the *Histoplasma capsulatum* G217B genome. The Y/H expression of each of these genes in G217B, G186AR, and H88 is displayed along with the transcript and any previously annotated gene names.

Identification of Hc proteins in the macrophage cytosol during infection

To take a more unbiased approach to find yeast-phase specific effectors that *Hc* uses during macrophage infection, we used the fractionation as described in Chapter 2 of this

dissertation work to identify any proteins that enter the macrophage cytosol directly. We have previously shown that two important *Hc* virulence factors, Cbp1 and Yps-3, are present in the macrophage cytosol during infection, but we wanted to see if there were any other *Hc* proteins present there. Additionally, we wanted to determine if the presence of any of these proteins in the macrophage is dependent on Cbp1, a critical virulence factor that is absolutely required for macrophage cell death.

We submitted three biological replicates of the cytosol fractionation for MS analysis to identify any *Hc* proteins in the mouse macrophage cytosol and identified 79 *Hc* proteins present there (Table 3.1). The identification of *Hc* proteins is difficult because they are vastly outnumbered by mouse protein, hence few proteins consistently appeared across all the replicates. Their absence from other replicates is not necessarily indicative that those proteins were absent from those samples, as those peptides might just have not flown well or perhaps their signal was obscured by mouse peptides. There was not a significant difference between WT *Hc*-infected macrophages versus *cbp1* mutant *Hc*-infected macrophages; besides Cbp1 no other proteins were present in all three replicates of one condition and absent in all the other ones. The proteins that tended to have a high peptide count would appear in both WT and *cbp1* mutant infected conditions, suggesting that Cbp1 is not required for other *Hc* proteins to access the cytosol. Interestingly only 15 out of 79 (19%) of all the *Hc* proteins identified did not contain a signal peptide by Phobius prediction, suggesting they were not secreted through the canonical secretory pathway. As *Hc* has previously been reported to secrete extracellular vesicles (EVs) we decided to cross reference our list of identified *Hc* proteins with proteins previously established to be in EVs (Albuquerque et al., 2008; Baltazar et al., 2018; Zamith-Miranda et al., 2021). We found that 31/79 (39.2%) were previously also reported to be associated with EVs, suggesting that there are potentially multiple routes that *Hc* uses to get effectors into the host cytosol. This analysis did not identify proteins that remain in the *Hc*-containing phagosome as that lipid-rich membrane fraction is difficult to directly analyze with mass spectrometry.

Table 3.1: *Histoplasma capsulatum* proteins identified in the host macrophage cytosol by mass spectrometry. The proteins are listed under their gene name identifier. The distribution amongst the replicates of WT *Hc* or *cbp1* mutant *Hc* cytosolic fractions is listed as a value out of 3 replicates in each condition. Phobius was used to determine whether the gene has a canonical signal peptide (Y= Yes, N=No). Association with *Hc* EVs was cross referenced with (Albuquerque et al., 2008). Annotations were determined based on annotations from the BROAD and pFAM motifs.

Gene	Replicates (WT, <i>cbp1</i> -)	SP-containing	Previously associated with EVs	Annotation	Function
ucsf_hc.01_1.G217B.10586	1/3, 1/3	N	Y	2-methylcitrate synthase	Acyltransferase
ucsf_hc.01_1.G217B.06907	1/3, 0/3	Y	N	Aspartate transaminase	Amino acid metabolism
ucsf_hc.01_1.G217B.11386	1/3, 0/3	Y	Y	Ketol-acid reductoisomerase	Amino acid metabolism
ucsf_hc.01_1.G217B.10755	1/3, 0/3	N	Y	Cobalamin-independent methionine synthase MetH/D	Amino acid metabolism
HISTO_GL.Contig296.Fgenesh_histo.85.final_new	1/3, 0/3	N	N	Alanine aminotransferase	Amino acid metabolism
ucsf_hc.01_1.G217B.01586	1/3, 0/3	N	N	Aspartate aminotransferase	Amino acid metabolism
HISTO_DM.Contig936.Fgenesh_histo.8.final_new	1/3, 0/3	N	N	Alanine-glyoxylate aminotransferase	Amino acid metabolism
ucsf_hc.01_1.G217B.07797	0/3, 1/3	N	Y	3-methylcrotonyl-CoA carboxylase biotin-containing subunit	Amino acid metabolism
HISTO_ZZ.Contig127b.Fgenesh_histo.66.final_new	0/3, 1/3	N	Y	SodB, Ortholog of Sc SOD2, Mn superoxide dismutase	Antioxidant defense
ucsf_hc.01_1.G217B.02730	1/3, 0/3	N	Y	TSA1, thiol-spec antioxidant	Antioxidant defense
ucsf_hc.01_1.G217B.05310	3/3, 1/3	N	Y	ATP synthase beta subunit	ATP synthesis
ucsf_hc.01_1.G217B.04564	1/3, 0/3	Y	Y	ATP synthase alpha subunit	ATP synthesis
ucsf_hc.01_1.G217B.07602	0/3, 2/3	N	N	Vacuolar ATP synthase subunit D	ATP synthesis
ucsf_hc.01_1.G217B.02919	1/3, 0/3	Y	N	SLDB, spindle assembly checkpoint protein	Cell cycle
ucsf_hc.01_1.G217B.04721	1/3, 1/3	Y	Y	Crf1, extracellular cell wall glucanase	Cell wall architecture
ucsf_hc.01_1.G217B.10365	1/3, 0/3	Y	Y	H antigen, beta-glucosidase	Cell wall architecture
ucsf_hc.01_1.G217B.05064	1/3, 1/3	Y	N	Heat shock 70 kDa protein C precursor, dnaK-type molecular chaperone bipA	Chaperones
ucsf_hc.01_1.G217B.08997	1/3, 0/3	N	N	Hsp98/Hsp104/CipA, heat shock protein	Chaperones
ucsf_hc.01_1.G217B.05246	1/3, 0/3	N	Y	TUB1, tubulin alpha-1 chain	Cytoskeleton
ucsf_hc.01_1.G217B.05625	0/3, 1/3	N	Y	CDC10, septin	Cytoskeleton
HISTO_ZL.Contig1161d.Fgenesh_histo.38.final_new	1/3, 0/3	N	Y	Enolase	Glycolysis

Gene	Replicates (WT, cbp1-)	SP-containing	Previously associated with EVs	Annotation	Function
ucsf_hc.01_1.G217B.02885	2/3, 1/3	N	Y	GAPDH, glyceraldehyde dehydrogenase	Glycolysis
ucsf_hc.01_1.G217B.03343	2/3, 1/3	N	N	Ras family protein	GTPases
HISTO_DM.Contig93.eannot.1687.final_new	1/3, 0/3	N	N	CpcB, G-protein complex beta subunit	GTPases
ucsf_hc.01_1.G217B.05255	3/3, 0/3	N	Y	Ypt3/Rab1a, GTP-binding protein	GTPases
ucsf_hc.01_1.G217B.07685	1/3, 0/3	N	N	GPA1, guanine nucleotide-binding protein alpha subunit	GTPases
ucsf_hc.01_1.G217B.11913	0/3, 1/3	N	N	PAP2 domain-containing protein	Kinase/Phosphatase
ucsf_hc.01_1.G217B.05159	2/3, 1/3	N	N	CDC2, cyclin-dependent protein kinase	Kinase/Phosphatase
ucsf_hc.01_1.G217B.07867	1/3, 1/3	N	N	CNA1, calcineurin A subunit	Kinase/Phosphatase
ucsf_hc.01_1.G217B.09077	0/3, 1/3	N	N	Leucine carboxyl methyltransferase, C3HC4 type (RING finger) zinc finger containing protein	Kinase/Phosphatase
ucsf_hc.01_1.G217B.07995	2/3, 0/3	N	Y	Nucleoside diphosphate kinase	Kinase/Phosphatase
ucsf_hc.01_1.G217B.04838	1/3, 0/3	Y	N	AcuF, phosphoenolpyruvate carboxykinase	Kinase/Phosphatase
ucsf_hc.01_1.G217B.02879	1/3, 0/3	N	N	Heat shock transcription factor	Nuclear proteins/Transcription factors
ucsf_hc.01_1.G217B.09828	0/3, 1/3	N	N	ATP-dependent helicase NAM7	Nuclear proteins/Transcription factors
ucsf_hc.01_1.G217B.07486	0/3, 1/3	N	N	RAD5, DNA repair protein	Nuclear proteins/Transcription factors
HISTO_FE.Contig19.fgenes_plus.1.final_new	0/3, 1/3	N	N	PCNA, proliferating cell nuclear antigen	Nuclear proteins/Transcription factors
ucsf_hc.01_1.G217B.02604	0/3, 2/3	N	N	SUB2, ATP dependent RNA helicase	Nuclear proteins/Transcription factors
ucsf_hc.01_1.G217B.09475	0/3, 2/3	N	Y	AP-1 complex subunit beta-1	Nuclear proteins/Transcription factors
ucsf_hc.01_1.G217B.01972	0/3, 1/3	N	Y	AldA, aldehyde dehydrogenase	Oxidation
ucsf_hc.01_1.G217B.06842	0/3, 1/3	N	N	MPD1, mannitol-1 dehydrogenase	Oxidation
HISTO_ZZ.Contig127a.Fgenes_histo.78.final_new	1/3, 0/3	Y	N	FAD binding protein, isoamyl alcohol oxidase	Oxidation
ucsf_hc.01_1.G217B.11651	0/3, 1/3	N	N	Allergen Asp F3 like, peroxisomal matrix protein	Peroxisome
ucsf_hc.01_1.G217B.05577	1/3, 0/3	N	N	Rhomboid family protein	Protease
ucsf_hc.01_1.G217B.07243	0/3, 1/3	Y	N	Peptidase S41 family protein	Protease

Gene	Replicates (WT, cbp1-)	SP-containing	Previously associated with EVs	Annotation	Function
ucsf_hc.01_1.G217B.01451	1/3, 1/3	N	Y	Protein disulfide-isomerase	Protein folding
ucsf_hc.01_1.G217B.04283	0/3, 1/3	Y	Y	FK506-binding protein	Protein folding
ucsf_hc.01_1.G217B.11298	0/3, 1/3	N	Y	Peptidyl-prolyl cis-trans isomerase	Protein folding
ucsf_hc.01_1.G217B.09428	1/3, 0/3	N	N	L-PSP endoribonuclease family protein (Hmf1)	Protein synthesis
ucsf_hc.01_1.G217B.09863	1/3, 0/3	N	Y	Eukaryotic translation initiation factor 5A-2	Protein synthesis
ucsf_hc.01_1.G217B.06860	0/3, 1/3	N	Y	Eukaryotic translation initiation factor 3	Protein synthesis
ucsf_hc.01_1.G217B.09596	2/3, 1/3	N	N	TIF1 eukaryotic translation initiation factor eIF4A	Protein synthesis
ucsf_hc.01_1.G217B.11693	1/3, 0/3	N	N	SEN1 tRNA-splicing endonuclease, DEAD-box type RNA helicase	Protein synthesis
ucsf_hc.01_1.G217B.09672	1/3, 0/3	N	N	DED1, ATP-depend RNA helicase DED1	Protein synthesis
ucsf_hc.01_1.G217B.12225	1/3, 0/3	N	N	Eukaryotic translation elongation factor Eef1 subunit beta	Protein synthesis
ucsf_hc.01_1.G217B.08224	0/3, 1/3	N	Y	26S proteasome regulatory subunit	Proteasome
ucsf_hc.01_1.G217B.09722	0/3, 1/3	N	N	26S protease regulatory subunit S10b	Proteasome
ucsf_hc.01_1.G217B.04935	1/3, 0/3	N	N	UFD4, ubiquitin fusion degradation protein	Proteasome
ucsf_hc.01_1.G217B.01095	2/3, 2/3	N	N	UBA1, ubiquitin-enzyme E1	Proteasome
ucsf_hc.01_1.G217B.03940	2/3, 1/3	N	N	RPL12, 60S ribosomal protein L12	Ribosomal proteins
ucsf_hc.01_1.G217B.07552	0/3, 1/3	N	N	Ebp2, rRNA processing protein	Ribosomal proteins
ucsf_hc.01_1.G217B.11813	2/3, 1/3	N	N	RLI1, ATP-binding cassette sub-family E member 1	Ribosomal proteins
ucsf_hc.01_1.G217B.00287	1/3, 2/3	Y	N	Yps-3, yeast phase-specific protein	Secreted virulence factors
ucsf_hc.01_1.G217B.08530	3/3, 0/3	Y	N	CBP1, calcium-binding protein	Secreted virulence factors
ucsf_hc.01_1.G217B.05131	1/3, 1/3	Y	N	Aspf13-like, allergenic ceratoplatenin containing protein	Secreted virulence factors
ucsf_hc.01_1.G217B.03683	1/3, 0/3	Y	Y	Aspf4-like, A. fumigatus allergen	Secreted virulence factors

Gene	Replicates (WT, cbp1-)	SP-containing	Previously associated with EVs	Annotation	Function
ucsf_hc.01_1.G217B.06993	1/3, 0/3	N	Y	Acetyl-CoA acetyltransferase	Short-chain fatty acid metabolism
ucsf_hc.01_1.G217B.01710	1/3, 0/3	N	N	Electron transfer flavoprotein alpha-subunit	Short-chain fatty acid metabolism
ucsf_hc.01_1.G217B.01869	1/3, 1/3	N	Y	MdhA , Malate dehydrogenase	Sugar metabolism
ucsf_hc.01_1.G217B.06371	1/3, 2/3	N	Y	Fructose 1,6-biphosphate aldolase	Sugar metabolism
ucsf_hc.01_1.G217B.05368	2/3, 1/3	N	Y	Malate dehydrogenase	Sugar metabolism
ucsf_hc.01_1.G217B.07435	0/3, 2/3	N	Y	Triosephosphate isomerase	Sugar metabolism
ucsf_hc.01_1.G217B.07860	2/3, 1/3	N	Y	TAL1, transaldolase	Sugar metabolism
ucsf_hc.01_1.G217B.11344	0/3, 1/3	N	N	Sulfate transporter	Transporter
ucsf_hc.01_1.G217B.04416	1/3, 0/3	N	N	Unknown protein	Unknown function
ucsf_hc.01_1.G217B.06694	1/3, 1/3	N	N	SH3 domain-containing protein	Unknown function
ucsf_hc.01_1.G217B.07179	1/3, 0/3	N	N	Unknown protein	Unknown function
ucsf_hc.01_1.G217B.12254	0/3, 1/3	N	N	Unknown protein	Unknown function
ucsf_hc.01_1.G217B.04391	1/3, 0/3	N	N	Tetratricopeptide repeat (TPR) domain-containing protein	Unknown function
ucsf_hc.01_1.G217B.06606	0/3, 1/3	N	N	Conserved protein	Unknown function

Amongst the *Hc* proteins identified in the host cytosol there were metabolic enzymes, translation regulators, transcription factors, kinases, GTPases, and several proteins of unknown function (Table 3.1). It would be interesting to determine if any of the proteins typically found inside of the yeast cell cytosol could be moonlighting and affecting the function of the host proteins as well.

Hc Secreted Cysteine-rich Protein-1 (Scp1) is required for optimal macrophage lysis

To determine if any of macrophage cytosol localized proteins are contributing to macrophage cell death caused by *Hc* we narrowed our focus to proteins that resemble the effectors of phytopathogenic fungi; signal-peptide containing, cysteine-rich, small proteins. Both Cbp1 and Yps-3 fit that mold, and additionally a third protein of interest emerged as a candidate, which contains a putative cerato-platanin (CP) domain. The founding member of the CP family was identified as a phytotoxin produced by the Ascomycete *Ceratocystis platani* that causes

canker stain on plants (de Oliveira et al., 2011; Pazzagli et al., 1999). The CP family of proteins tends to be hydrophobic and cell wall associated, Additional orthologs have been discovered in human fungal pathogens as well, such as the *Aspergillus fumigatus* allergen Asp F13 which causes an allergic response (Basu et al., 2018; Kurup et al., 2000) and *Coccidioides immitis* specific antigen AgCS which is a serine protease (Cole et al., 1989; Hung et al., 2000; Pan & Cole, 1995; Resnick et al., 1987; Resnick et al., 1990). We called this protein Secreted Cysteine-rich Protein-1 (Scp1)

Hc expresses the SCP1 transcript in both the mycelial and yeast phases but it is more prominent in the yeast phase (Figure 3.3). According to ribosomal profiling data, the transcript is equally translated by both life phases of *Hc* (Gilmore et al., 2015). We first confirmed that Scp1 is localized to the cytosolic fraction by overexpressing Scp1-3XFLAG in a wildtype background. Using an episomally expressed CRISPR-Cas9 system with 2 sgRNAs, we deleted the Scp1 locus in the G217B *Hc* genome and confirmed the deletion of the locus with PCR analysis of the genomic locus (Figure 3.3). When we tested the Scp1 mutant in macrophage infection, we found that it had a partial lysis defect, suggesting that this CP-containing protein is necessary for optimal lysis of macrophages (Figure 3.3).

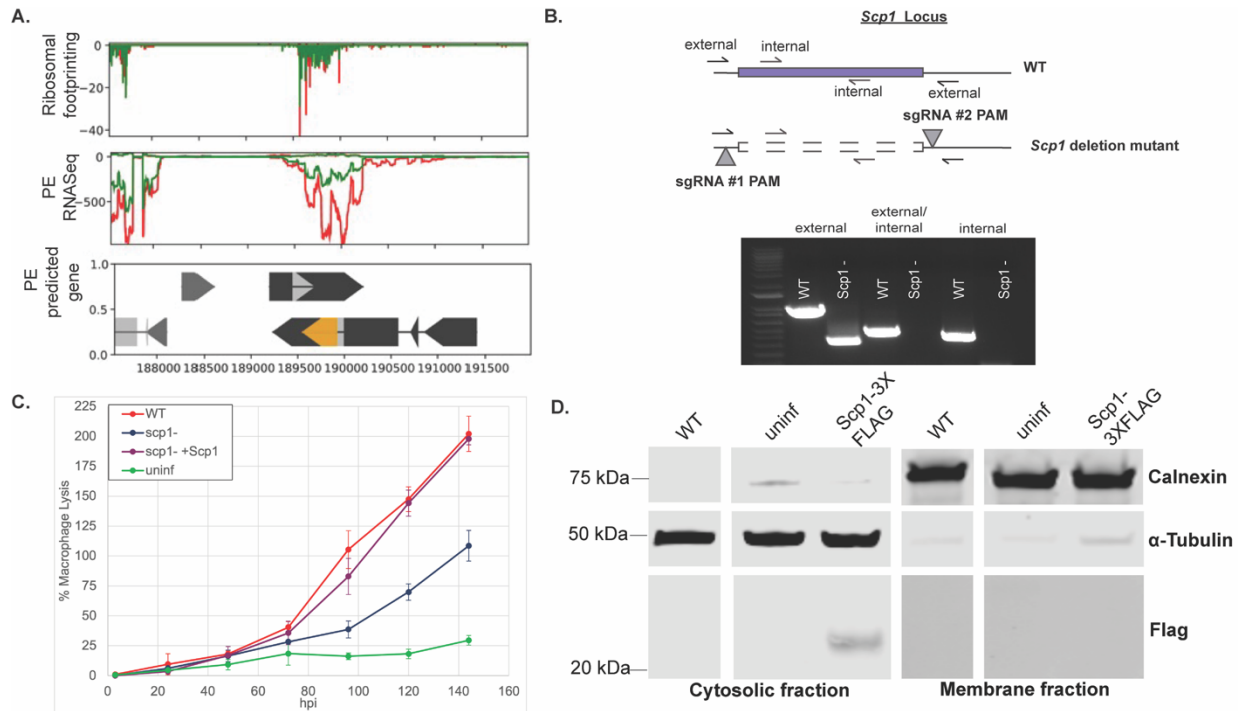


Figure 3.3: *Scp1* is a yeast expressed protein that is necessary for optimal lysis of macrophages during infection.

(A) Ribosomal and transcript profile of the *Scp1* locus both in the yeast phase (Zamith-Miranda et al.) and the mycelial phase (Kurup et al.) show that this protein is expressed by both phases but more so in the yeast phase.

(B) Schematic of episomally expressed CRISPR-Cas9 2-sgRNA deletion of *Scp1* and PCR analysis of deletion mutant monitoring for the presence of the edited locus.

(C) Lactate dehydrogenase release assay of *Scp1* mutant- infected macrophages (MOI of 1) shows a partial lysis defect.

(D) Western blot of BMDM lysates infected with Hc expressing *Scp1*-3XFLAG fractionated into cytosolic and membrane fractions and probed for a cytosolic marker alpha-tubulin and a membrane marker calnexin. *Scp1* is probed for with an anti-FLAG antibody.

The Hc-containing phagosome is not permeabilized

Many intracellular bacterial pathogens are able to create pores in the enveloping phagosomal compartment they reside in to gain access to the cytosolic space (Flieger et al., 2018; Mitchell et al., 2016). One of the most famous examples is the *Listeria monocytogenes* virulence determinant Listeriolysin O (LLO), a toxin that is capable of perforating the bacteria-containing phagosome thus freeing up the bacteria to spread to other cells and propagating the infection (Nguyen et al., 2019). Since many *Hc* proteins are detectable in the host macrophage cytosol we

wanted to test the hypothesis that the phagosome is permeable, making it possible for these effectors to passively enter the cytosol through a leaky membrane.

To ascertain membrane permeability, we used the CCF4-AM assay (Thermo Fisher Scientific K1095 LiveBLAzer™ FRET-B/G Loading Kit with CCF4-AM) which has been well established as a measurement of vacuolar rupture caused by bacterial pathogens like *Shigella flexneri* and *Mycobacterium tuberculosis* (Keller et al., 2013). CCF4-AM is a FRET probe consisting of two fluorophores attached by a Beta-Lactam linkage. When this probe is preloaded into the host cell cytosol and is uncleaved, FRET causes the probe to emit green fluorescence. When this probe encounters Beta-Lactamase, an enzyme typically secreted by bacteria to cleave B-lactam antibiotics, the probe is cleaved in half and the FRET is disrupted, leaving the probe to emit blue fluorescence. To use this assay during a *Hc* infection we engineered G217B *Hc* to express a strep-tagged version of secreted Beta-Lactamase under the control of the H2AB promoter. We selected isolates of *Hc* that secrete strep-Beta-lactamase extracellularly into culture supernatants and monitored for whether these secreted versions were functional by using a colorimetric assay with Nitrocefin which changes color depending on the presence of active Beta-Lactamase (Figure 3.4). As a positive control for this assay, we used *Legionella pneumophila* (*Lp*), a bacterial pathogen that has previously been reported to permeabilize the Legionella-containing vacuole using its Type IV Secretion System known as Icm/Dot (Chauhan & Shames, 2021; Isaac & Isberg, 2014). To determine if the *Hc*-containing phagosome is permeabilized we loaded the CCF4-AM dye into macrophages that were either (1) uninfected, (2) infected with WT *Lp*, (3) infected with a dotA mutant of *Lp*, (4) infected with WT *Hc*, or (5) infected with *Hc* secreting strep-Beta-lactamase. Using flow cytometry, we monitored how many of the cells had a shift from green to blue in the cytosol suggesting the probe was cleaved by Beta-lactamase. While the macrophage cytosol from cells that were infected with WT *Lp* displayed a significant shift to blue, the cytosol from uninfected macrophages, dotA *Lp*-infected and the Beta-lactamase expressing *Hc*-infected macrophages remained green, suggesting that the secreted Beta-lactamase was

unable to enter the macrophage cytosol and that the *Hc*-containing phagosome is not permeable (Figure 3.4).

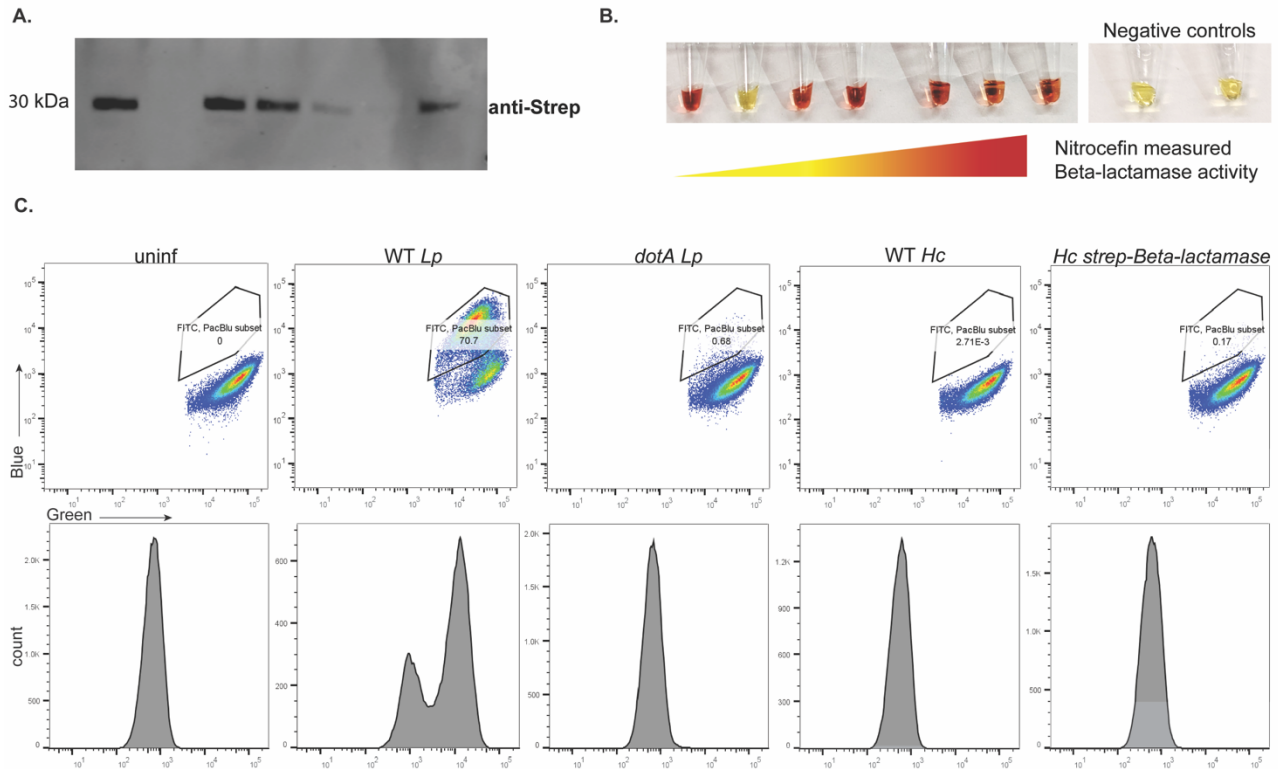


Figure 3.4: The *Hc*-containing phagosome is not permeable to the CCF4-AM probe. (A) Western blot of concentrated culture supernatants of *Hc* expressing a secreted strep-tagged version of Beta-lactamase. (B) Colorimetric assay that shows the functionality of Beta-lactamase found in the concentrated *Hc* supernatants using the compound Nitrocefin. (C) Flow cytometry assay measuring the shift from green to blue in the macrophage cytosols using the CCF4-AM FRET. Macrophages infected with WT *Lp* were used as a positive control for the assay. Uninfected macrophages, *dotA* mutant *Lp*, and WT-*Hc* infected were used as negative controls.

Discussion and future directions

Hc, like many other intracellular pathogens, employs the strategy of using secreted protein effectors to cope with its surroundings. Being a thermal dimorph, *Hc* has two different forms which are specialized to deal with the drastically different environments of the soil and the animal host. In both phases, the expression of signal peptide-containing proteins is enriched, showcasing how *Hc* could be delivering proteins into its immediate local environment to ameliorate whatever stresses it could be encountering (Figure 3.1).

A common theme amongst fungal virulence factors, especially of the phytopathogenic fungi, are that they are cysteine-rich. These cysteines are usually found as a part of disulfide bridges that provide extra stability and prevent unfolding in the face of harsh environmental conditions. *Hc* yeast seem to rely on cysteine-rich proteins as virulence factors to survive in an intracellular compartment and presumably the disulfide bridges in the cysteine-rich proteins allow them to carry out their roles and not be immediately destroyed (Figure 3.1). By searching for the characteristics of being cysteine-rich, secreted, and small, we were able to generate a candidate list of protein effectors that could play a role during macrophage infection (Figure 3.2).

An experimental approach we used to identify protein effectors was to analyze by mass spectrometry all the *Hc* proteins that are found in the cytosol of the host macrophage cell (Table 3.1). In addition to finding proteins that do fit those criteria of being small, secreted, and cysteine rich (identified in figure 3.2), we identified many proteins that would be typically found in the *Hc* cytosol and would play a role keeping the yeast alive and functional. This list included proteins that did not have any signal peptide and hence would not be expected to be found extracellularly. This hints that *Hc* could be delivering proteins into the environment by non-canonical means, possibly including extracellular vesicles (EVs). The literature points to a role of fungal EVs in virulence (Albuquerque et al., 2008; Nosanchuk et al., 2008; Rodrigues et al., 2008; Zamith-Miranda et al., 2021). *Hc* could be using both strategies of direct secretion and EVs to deliver effectors that modulate the host response and eventually cause macrophage cell death.

Among the proteins identified in the host cytosol, one was the *Hc* ortholog of Asp F13, whose homologs are known to be virulence factors in two human fungal pathogens: *Aspergillus fumigatus* and *Coccidioides immitis*. When we deleted this gene from the genome, we discovered that *Hc* yeast had a partial lysis defect when infecting macrophages, indicating that it does function as a virulence factor. In the future it would be interesting to delve further and explore how this Asp F13 ortholog is contributing to lysis by figuring out its host targets, its localization during infection, its molecular structure, and whether it has a phenotype during an *in vivo* murine lung infection. It

would also be interesting to determine if any of the other candidates identified in the cytosol could be functioning as virulence factors. In particular, it would be extremely interesting to see if any of the proteins that already have a normal role in *Hc* viability could affect host macrophage cell processes as well, or moonlight in a completely novel fashion.

The presence of *Hc* proteins in the host cytosol raised the question of how these effectors are delivered to that space. Are they being transported directly through a pore in a permeabilized phagosome or are they finding alternative ways like fusion of vesicles with the phagosome membrane that then delivers proteins into the host cytosol? We tested the model of a permeabilized *Hc*-containing phagosome using a CCF4-AM assay and Beta-lactamase expressing *Hc* strain and found no evidence of permeabilization. This suggests that either the phagosomal membrane is selectively permeable to small-sized *Hc* effectors, or that effectors could be specifically transported across the phagosomal membrane. Alternatively, effectors could be released through the fusion of vesicles or multi-vesicular bodies (MVBs) with the phagosome. It would be interesting to study a *Hc* canonical secretion mutant, such as a *sec6* Δ mutant, to determine whether the mutation abrogates the presence of all *Hc* proteins in the cytosol or if EVs could compensate for this loss of canonical secretion.

Chapter 4: *Histoplasma* species have an expanded family of putative cystine-knot genes which contain a virulence factor, Knot-1

KNOTTIN Finder

The first set of identified knottins already indicated that *Hc* had expanded this protein family (Gilmore et al., 2015, 2021). To identify more knottins in the *Hc* genome, we wrote an unbiased and naïve algorithm called KNOTTIN finder that could identify any putative knottins in the *Hc* genome based on the size of the predicted protein and the specific cysteine spacing found in the fungi1 family (Figure 4.1). The algorithm functions in the following sequential steps: (1) Translate a *Hc* contig into all 6 possible reading frames (2) segment all the reading frames by stop codons (3) find all the cysteines in one reading frame on each segment and find all the segments that have at least 6 cysteines (4) determine if the cysteines are spaced like the fungi1 knottins and (5) determine if the ORF is 250 amino acids or less. This KNOTTIN finder algorithm identifies the previous 12 putative knottin genes and additionally locates 14 highly yeast-enriched putative knottins. Notably, KNOTTIN finder is even able to detect previously unannotated genes in areas of the genome that have no predicted genes but which nonetheless have ribosomal occupancy signal (Figure 4.1). The full list of the 26 putative knottin genes is listed in Table 4.1. For the vast majority of the putative knottin hits the gene structure consisted of 2 exons and 1 intron, with the 6 cysteine knottin domain at the end of the gene in the second exon (Figure 4.1). The knottin hits are distributed across the entirety of the *Hc* G217B chromosomes and are not preferentially at the ends or middle of chromosomes. Since they are not clustered in any one particular location, they are probably not a part of regulatory cluster (Figure 4.1).

To check if this expansion in fungi1 family knottins was specific to the *Hc* genome or whether this occurs in other closely fungal genomes as well, we ran the KNOTTIN Finder algorithm over all 623 fungal genomes in the ENSEMBL database along with several other fungal genomes of interest from GenBank such as the *Cladosporium fulvum* genome that includes

AVR9, the founding member of the fungi1 knottins (Benson et al., 2013; Howe et al., 2020). We found that this expansion of knottins is specific to *Hc* and other closely related thermally dimorphic species, but the number of knottin genes steeply drops off in other fungal genomes (Figure 4.2). Figure 4.2 is a simplified heatmap that indicates the number of total knottins in each genome compared to a species tree based on the left. The knottins are grouped into 15 clades based on the *Hc* G217B genome. Most fungi have between 0 to 5 knottins per genome including hits in the basal phyla of Mucormycota and order Chytridiomycota suggesting the ancient origin of this fungi1 family. Amongst the Onygenales order, which contains both the Onygenaceae and Ajellomycetaceae families of thermally dimorphic fungal pathogens, the Onygenaceae (including *Coccidioides* species) only have 0-2 knottins per genome. In contrast when we look at Ajellomycetaceae genomes we note a rapid expansion of knottins. Per genome *Blastomyces* have 2-3, *Paracoccidioides* have 4-6, *Emergomyces* have 10-17, and *Histoplasma* genomes have 22-27 knottins. It seems that the rapid expansion of fungi1 knottins is specific to *Hc* genomes and other closely related thermal dimorphic species, which raises the question of whether these proteins are useful for *Hc* as virulence factors and hence their rapid expansion.

Table 4.1: List of putative knottin hits generated by the KNOTTIN Finder algorithm in the *Hc* G217B genome. For each hit the predicted transcript name is listed, if only one is associated with the given locus, and the predicted length of the protein is listed. Additionally, it is indicated whether this list was a part of the original 12 published *Hc* knottin genes (Gilmore et al., 2015) or a brand new hit identified by KNOTTIN Finder.

Transcript	Genomic locus and strand	Published in (Gilmore et al., 2015)	Predicted length (amino acids)
ucsf_hc.01_1.G217B.02070	HISTO_DF.Contig537:487498..487836 (+)	Y	134
ucsf_hc.01_1.G217B.08731	HISTO_ZL.Contig1131:409719..410183 (-)	Y	177
ucsf_hc.01_1.G217B.08018	HISTO_LJ.Contig29:4234..4500 (+)	Y	99
ucsf_hc.01_1.G217B.00356	HISTO_AS.Contig189:18688..19155 (-)	Y	177
ucsf_hc.01_1.G217B.02027	HISTO_DF.Contig537:301453..301641 (-)	Y	84
ucsf_hc.01_1.G217B.08494	HISTO_ZH.Contig107:315720..315998 (+)	Y	95
ucsf_hc.01_1.G217B.05476	HISTO_GY.Contig460:314162..314434 (-)	Y	110
ucsf_hc.01_1.G217B.05219	HISTO_GX.Contig297:258609..258860 (+)	Y	69
ucsf_hc.01_1.G217B.05263	HISTO_GX.Contig297:365303..365794 (+)	Y	117
ucsf_hc.01_1.G217B.01232	HISTO_BP.Contig459:386502..387035 (+)	Y	208
ucsf_hc.01_1.G217B.05774	HISTO_GY.Contig471:176183..176641 (+)	Y	175
ucsf_hc.01_1.G217B.10526	HISTO_ZT.Contig174:56914..57396 (+)	Y	192
unannotated	HISTO_ZU.Contig65:1032473..1032958 (+)	N	162
unannotated	HISTO_ZU.Contig65:1270872..1271444 (+)	N	191
ucsf_hc.01_1.G217B.11056	HISTO_ZU.Contig65:71018..71218 (-)	N	81

Transcript	Genomic locus and strand	Published in (Gilmore et al., 2015)	Predicted length (amino acids)
unannotated	HISTO_ZL.Contig1117:15644..16192 (-)	N	183
unannotated	HISTO_FE.Contig19:302861..303076 (+)	N	72
unannotated	HISTO_ZL.Contig25:50367..50636 (+)	N	90
unannotated	HISTO_GL.Contig285:23503..23961 (+)	N	177
unannotated	HISTO_FJ.Contig643:121716..122057 (-)	N	135
ucsf_hc.01_1.G217B.07201	HISTO_KK.Contig134:5007..5354 (+)	N	116
ucsf_hc.01_1.G217B.08080	HISTO_LS.Contig117:2136..2636 (-)	N	67
ucsf_hc.01_1.G217B.04958	HISTO_GL.Contig296:344809..345279 (+)	N	182
ucsf_hc.01_1.G217B.00750	HISTO_BM.Contig14:19642..20142 (-)	N	181
ucsf_hc.01_1.G217B.06783	HISTO_KF.Contig470:13747..13902 (+)	N	124
ucsf_hc.01_1.G217B.04359	HISTO_FX.Contig167:324768..325250 (+)	N	178



Figure 4.1: KNOTTIN Finder is a naïve algorithm to search for fungi1-like putative knottins in genomes.

(A) Schematic of the key sequential steps in the KNOTTIN algorithm.

(B) Two examples of newly discovered knottins displayed in a genome browser. The top block represents a previously annotated gene that is a KNOTTIN finder hit whereas the bottom block represents a previously unannotated ORF that was identified by KNOTTIN finder that does show ribosomal occupancy in the yeast phase.

(C) Distribution of putative knottin genes across the *Hc* G217B chromosomes assembled from Nanopore reads. The knottins are marked with red dashes below each chromosome. The blue/green tracks indicate transposons whereas the black markers indicate rRNA. The names of genes of interest are marked above their chromosomal locations.

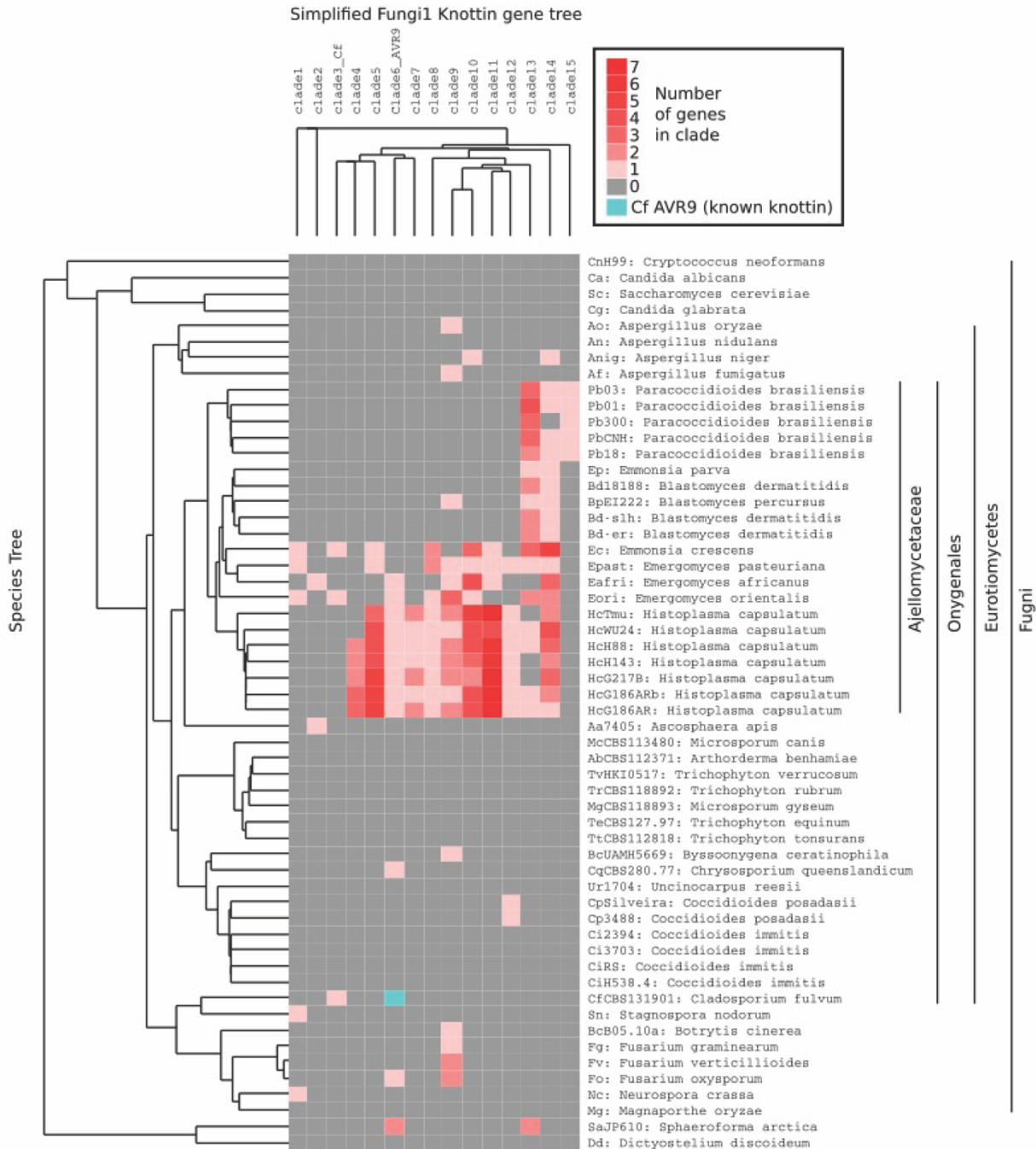


Figure 4.2: Heatmap showing the number of knottins in the genomes of selected fungi. The knottin families discovered in *Hc* G217B are classified into 15 clades (Schwartz et al.) and are compared to a species tree (right) based on GCD10. The intensity of the red indicates how many knottins of each clade were found in that genome. Teal represents the original AVR9 knottin from *C. fulvum*, the founding member of the fungi1 knottin family. Branch lengths in both trees are not to scale. Unannotated genomes and those with no knottin hits are omitted for clarity.

Deletion of Knot1 generates a lysis defective mutant

Amongst the list of knottins identified by KNOTTIN Finder there were 4 proteins of interest that stood out as candidate virulence factors because of previous studies completed in our lab. For ease, I will refer to them by their internal lab names: Rockstar1, Rockstar6, Rockstar10, and the *Hc* AVR9 homolog. The Rockstar candidates were previously identified as putative virulence factors because they were the targets of the Required for Yeast (RYP) transcription factors (Beyhan et al., 2013; Nguyen & Sil, 2008; Webster & Sil, 2008) and were highly enriched in the yeast phase. Rockstar10 was a particularly interesting candidate because it was previously identified in an *Agrobacterium*-mediated screen for Lysis Defective Mutants (LDFs) (Isaac et al., 2015) as a gene that was required for optimal lysis of macrophages (mutant UA35-G3).

When dissecting the clades to which Rockstar1, Rockstar6, Rockstar10, and *Hc* AVR9 belong, we found that Rockstar1 and Rockstar6 have clear paralogs whereas AVR9 and Rockstar10 do not (Figure 4.3). The 6-cysteine pattern that makes up the knottin domain is represented with lines across the clades. The red dot marks the putative cleavage site where the knottin domain is typically cleaved to form the mature peptide. The fact that Rockstar1 and Rockstar6 have paralogs in *Hc G217B* could preclude us from determining its role during infection because of functional redundancy. Using an episomally expressed CRISPR-Cas9 system we either (1) used a single-guide system to disrupt each of the putative knottins by inserting or cutting a single bp, leading to a truncated allele of the knottin or (2) used a double-guide system to cut twice immediately around the knottin CDS and generate a clean deletion mutant (Figure 4.4) (Kujoth et al., 2020). For the single-guide disruption mutants we used TIDE (Tracking of Indels by Decomposition) (Brinkman et al., 2014) to determine where a single base pair was inserted or deleted whereas for the double-guide deletion mutants we would use PCR of genomic DNA to

determine the size of the locus with external and internal primer pairs. Table 4.2 lists the single- and double-guide protospacer and PAM sequence used to generate the CRISPR mutants.

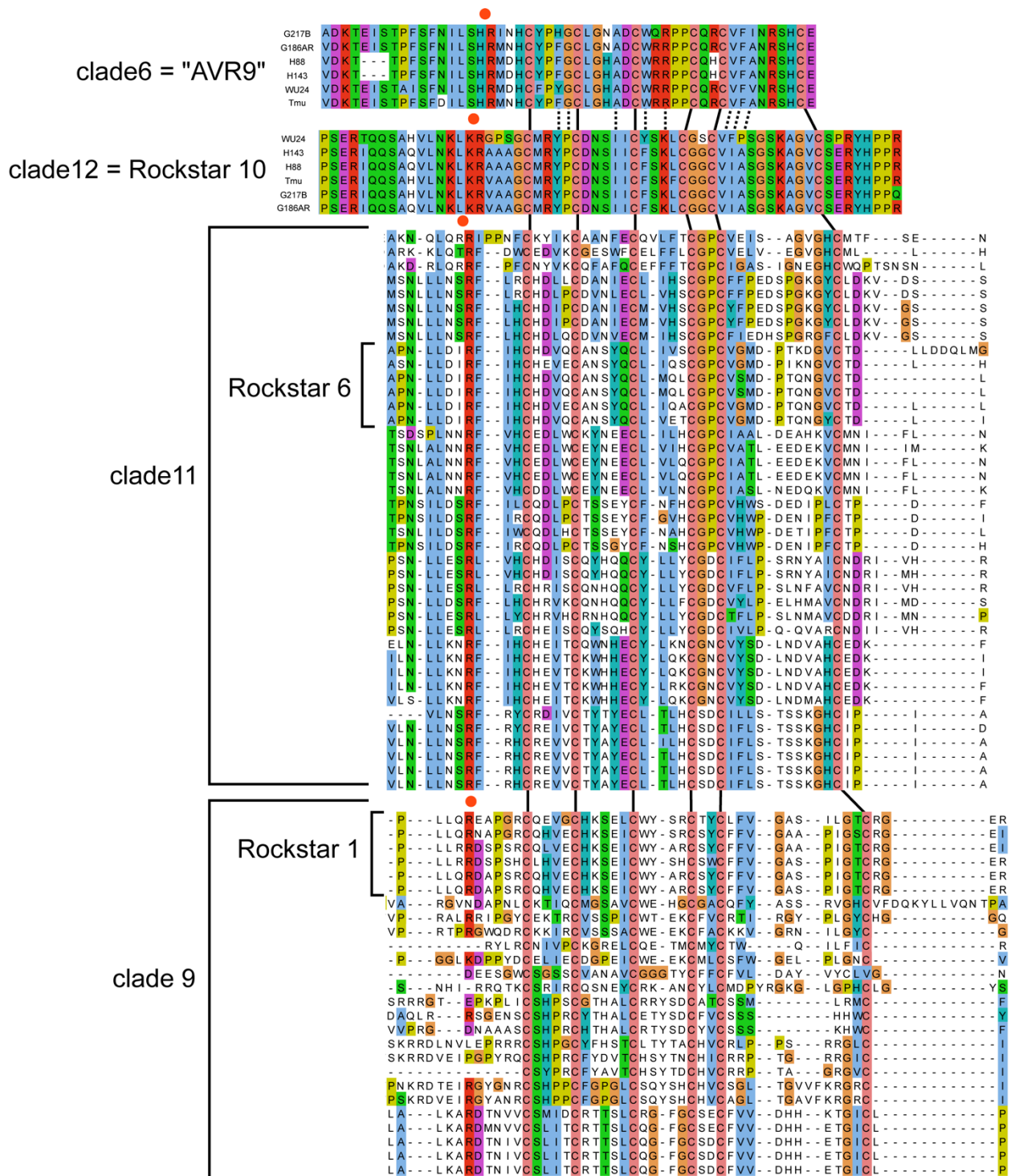


Figure 4.3: Probcons alignments (Do et al., 2005) of Rockstar1, Rockstar6, Rockstar10, and *Hc* AVR9 homolog clades. Rockstar6 and Rockstar1 have multiple paralogs in the *Hc* G217B genome, denoted by the brackets in each clade, whereas AVR9 and Rockstar10 do not. Lines

between the clades indicate the positioning of the 6-cysteine knottin spacing. The red dot indicates a putative cleavage site to generate the mature knottin peptide.

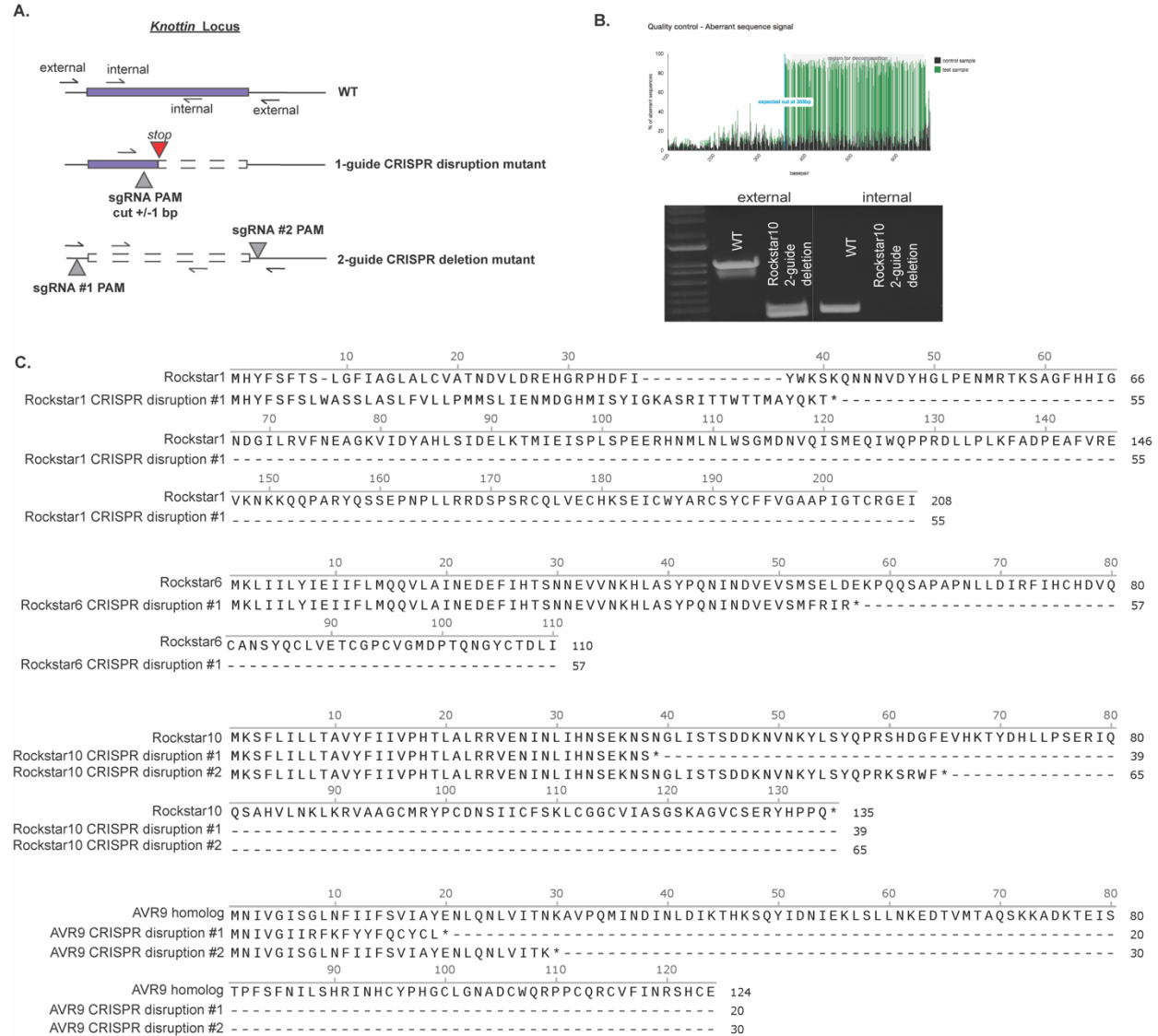


Figure 4.4: Generation of knottin disruption and deletion mutant alleles using CRISPR-Cas9. (A) Illustration of screening methods used to find single-guide disruption mutants or double-guide deletion mutants. (B) Example of a Rockstar10 single-guide deletion mutant confirmed with TIDE analysis and a double-guide mutant confirmed with PCR analysis of Rockstar10 locus from isolated genomic DNA. (C) Alignments of WT knottin protein sequences with the single-guide disruption alleles which lead to truncated alleles.

Table 4.2: List of sgRNA protospacers and their corresponding PAM sites used to generate knottin CRISPR mutants in *Hc* G217B.

Knottin gene	1-guide vs. 2-guide	Protospacer sequence	PAM sequence
Rockstar1	1-guide	GATGAAGCCCAGAGACGTAA	AGG
Rockstar1	2-guide	TCTATCTGGCGAAACATTG	GGG
Rockstar1	2-guide	TTCGTCGGCGCCGCTCCAAT	CGG
Rockstar6	1-guide	TTTCTCATCTAATTCTGACA	TGG
Rockstar6	2-guide	ACAACATAATTCCGATTGA	AGG
Rockstar6	2-guide	ACGTGACCGTTTAGATCACG	TGG
Rockstar10	1-guide	AACTCAGAGAAAAATTCTAA	TGG
Rockstar10	1-guide	TCAAACCATCGTGACTCCG	AGG
Rockstar10	2-guide	ATCAACCGATATATAAGACT	TGG
Rockstar10	2-guide	TGCGCTATATTGTAATTAGA	CGG
AVR9	1-guide	ATGAATATTGTTGGAATATC	AGG
AVR9	1-guide	AAATCTAGTTATCACGAATA	AGG
AVR9	2-guide	TCCAATATGATAAAAGTGGA	AGG
AVR9	2-guide	TTGAATTCTATATCAATCGC	TGG

Rockstar1, Rockstar6, and the *Hc* AVR9 homolog disruption mutants did not have any defects in macrophage lysis, but Rockstar10 did have a partial lysis defect (Figure 4.5). This partial lysis defect was not the result of a lack of intracellular growth as shown by intracellular CFU analysis. Despite the Rockstar10 gene being disrupted with an early stop codon in both disruption mutants, the transcript is still generated. We considered the possibility that the intracellular lysis defect is due to a defect in intracellular fungal replication that is secondary to deleterious effects of the premature stop codon-containing transcript (Chang et al., 2007). We tested the Rockstar10 double-guide deletion mutant which expresses no detectable Rockstar10 transcript side by side with the disruption mutants and found that despite the macrophage lysis defect being less prominent, *Hc* is able to grow intracellularly in a more robust manner (Figure 4.5). Additionally, we were also able to complement the lysis defect phenotype by expressing wildtype Rockstar10 in the Rockstar10 double-guide deletion mutant (Figure 4.5).

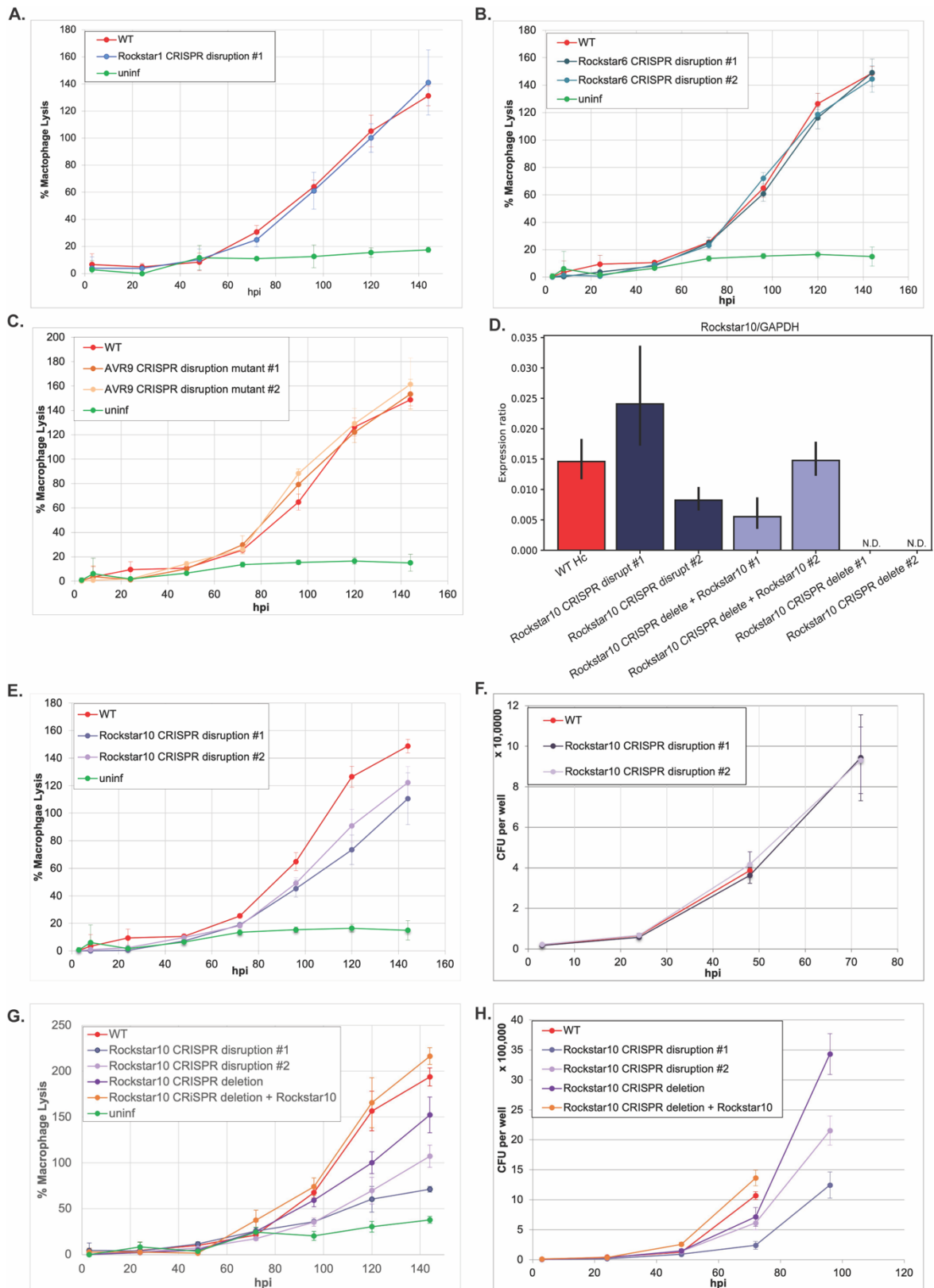


Figure 4.5: The knottin Rockstar10, but not Rockstar1, Rockstar6, or the AVR9 homolog, disruption and deletion mutants have a defect in macrophage lysis.

- (A) LDH analysis of macrophages infected with a Rockstar1 CRISPR disruption mutant at an MOI of 0.5.
- (B) LDH analysis of macrophages infected with a Rockstar6 CRISPR disruption mutant at an MOI of 0.5.
- (C) LDH analysis of macrophages infected with the *Hc* AVR9 CRISPR disruption mutants at an MOI of 0.5.
- (D) Quantitative PCR analysis monitoring for the presence of Rockstar10 transcript in the *Hc* CRISPR mutants.
- (E) LDH analysis of macrophages infected with the Rockstar10 CRISPR disruption mutants at an MOI of 0.5.
- (F) Intracellular CFU analysis of macrophages infected with the Rockstar10 CRISPR disruption mutants.
- (G) LDH analysis of macrophages infected with the Rockstar10 CRISPR disruption mutants, the Rockstar10 double-guide deletion mutant, and the Rockstar10 complemented strain at an MOI of 0.5.
- (H) Intracellular CFU analysis of macrophages infected with the Rockstar10 CRISPR disruption mutants, the Rockstar10 double-guide deletion mutant, and the Rockstar10 complemented strain at an MOI of 0.5

Rockstar10 does not contribute to the Integrated Stress Response in macrophages

To determine if Rockstar10 is directly contributing to macrophage lysis or whether this resulting phenotype is an indirect result of the *Hc* yeast not being able to carry out some other function, we transformed a 3XFLAG-tagged allele of Rockstar10 into the single-guide disruption mutant and monitored whether the tagged form was secreted extracellularly. We found that Rockstar10-3XFLAG was secreted into culture supernatants and that the secretion of other known virulence factors such as Cbp1 and Yps-3 into the culture supernatants was not affected (Figure 4.6). Like the other effectors mentioned in this dissertation, Rockstar10-3XFLAG can also be found only in the cytosolic fraction and not the membrane fraction when infected macrophage lysates are fractionated. Since Rockstar10 can be found in the cytosol of the host macrophage during infection and contributes to optimal lysis, we wanted to determine if there is a reduction in the Integrated Stress Response as that is a key step on the way to *Hc*-mediated macrophage death (Chang et al., 2007). Using quantitative PCR analysis we monitored for the induction of CHOP and TRIB3 transcripts in macrophages that are infected with either WT, the Rockstar10 deletion mutant, the complemented strain, treated with Tunicamycin, or uninfected (Figure 4.6). We found that there was no significant reduction in the induction of CHOP or TRIB3 transcripts

when macrophages were infected with the Rockstar10 deletion mutant, suggesting that under normal infection conditions Rockstar10 must be contributing to cell death in a parallel ISR-independent pathway.

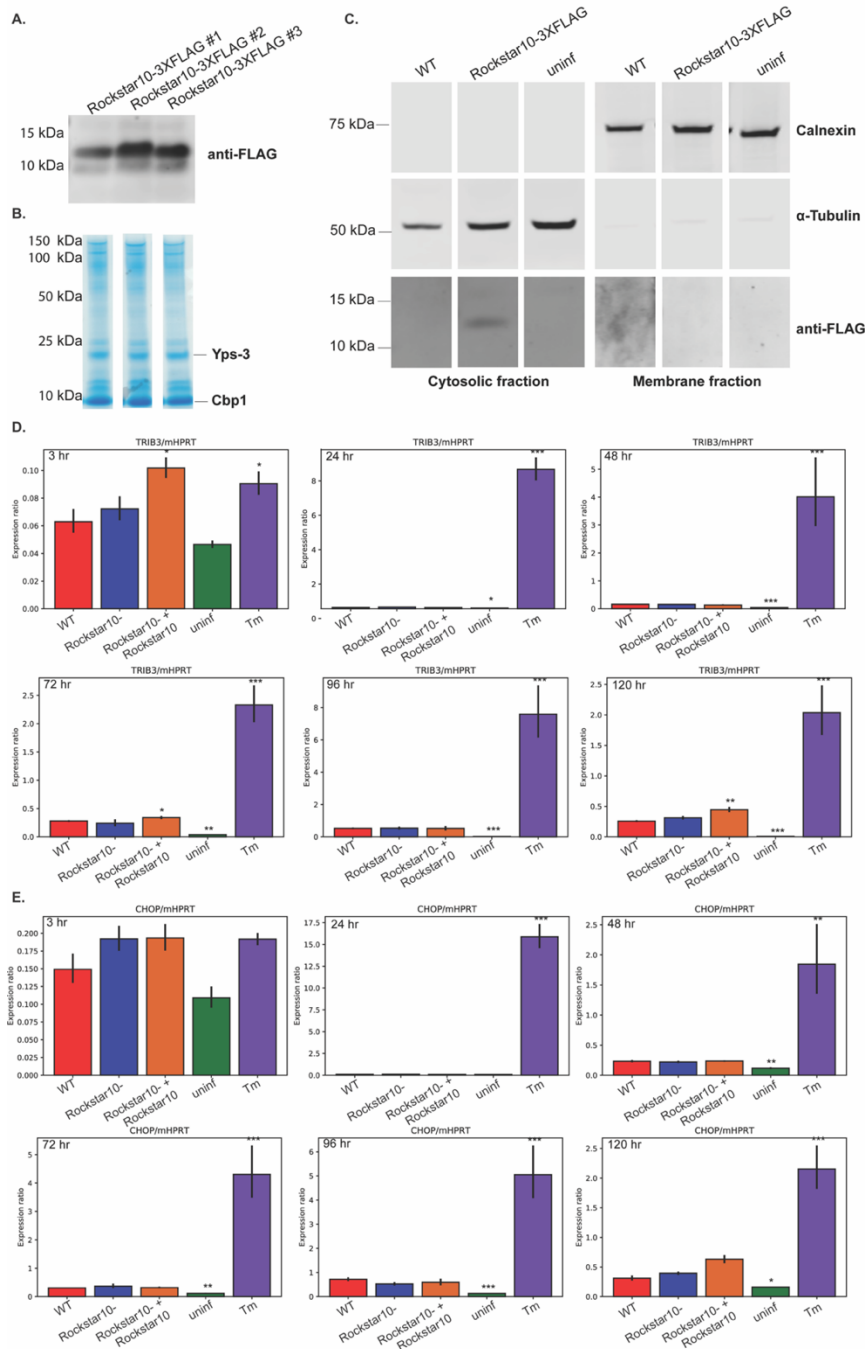


Figure 4.6: Rockstar10 is able to enter the macrophage cytosol during infection but does not contribute to the induction of the Integrated Stress Response.

(A) Western Blot of concentrated culture supernatants of three independent *Hc* isolates that express and secrete Rockstar10-3XFLAG in the background of the Rockstar10 CRISPR disruption mutant #1.

(B) InstantBlue stained SDS-PAGE gel of concentrated supernatants of the same three isolates that express Rockstar10-3XFLAG.

€ Western Blot of fractionated macrophage lysates of WT *Hc*, Rockstar10 single-guide disruption mutant #1+ Rockstar10-3XFLAG, and uninfected samples probed with anti-alpha-tubulin (cytosolic marker), calnexin (membrane marker) and anti-FLAG.

(D) qPCR analysis of TRIB3 transcript induction in macrophages infected with WT, Rockstar10 deletion mutant, and Rockstar10 complemented *Hc* strains as well as uninfected macrophages and Tunicamycin treated (2.5 ug/mL) over the course of 0-120 hpi and an MOI of 0.5.

€ qPCR analysis of CHOP transcript induction in macrophages infected with WT, Rockstar10 deletion mutant, and Rockstar10 complemented *Hc* strains as well as uninfected macrophages and Tunicamycin treated (2.5 ug/mL) over the course of 0-120 hpi and an MOI of 0.5.

Discussion and future directions

The cystine knot is a highly stable and versatile fold that is found all across nature. We find that *Hc* and other closely related fungal pathogen members of the Ajellomycetaceae family have drastically expanded the fungi1 family of knottins in their genomes whereas most other fungi have 0-2 knottins of the fungi1 family. Fungi1 is not the only fungal family of knottins in the KNOTTIN database. There is a second annotated family known as fungi2 which has a different cysteine spacing altogether and it would be interesting to determine if any of the *Hc* genes fit that model or any other cysteine knot model that has been previously uncharacterized in *Hc*.

Of the first four fungi1 knottin candidates we have identified and disrupted in the *Hc* G217B genome, only one, Rockstar10, had a partial lysis defect in macrophages. We disrupted Rockstar10 by either generating truncated alleles with a single-guide CRISPR disruption strategy or a clean double-guide CRISPR strategy that completely excises out the Rockstar10 CDS. We found that both had a macrophage lysis defect but that the disruption mutants could not reach the same intracellular fungal burdens and had a more severe lysis defect than the clean deletion mutant. The truncated alleles generated with single-guide CRISPR strategy were still making the Rockstar10 transcript which probably would be undergoing Nonsense mediated decay because of the early stop codon. This might burden the cells translational machinery and make the cells sicker, indirectly exacerbating the macrophage lysis defect.

Like the other virulence factors, we have explored in this work, Rockstar10 is also secreted, cysteine-rich, and small. We find that it also accesses the cytosol directly as measured by fractionation but curiously does not contribute to the induction of the ISR cytosolic cascade. We have previously speculated the ISR is not the only macrophage stress response that is triggered during *Hc* infection since infection of CHOP or TRIB3 mutant macrophages still undergo some lysis (English et al., 2017). Perhaps understanding the mechanism of how Rockstar10 contributes to macrophage cell death would shed further light on this process.

The future steps to this project are to understand the targets of Rockstar10 in the macrophage cytosol as well as to determine if it interacts with any *Hc* proteins. Additionally, it would be interesting to determine the macrophage transcriptional response to wild-type *Hc* vs the Rockstar10 mutant. A key experiment would be to determine the structure of the Rockstar10 protein and confirm whether the disulfide bridges do interweave to form a knottin fold as predicted. Finally, it would be interesting to determine if Rockstar10 has a role in the murine lung infection model of histoplasmosis.

Chapter 5: Materials and Methods

Determining the conservation of Cbp1 in Ajellomycetaceae genomes and generating protein alignments

The Cbp1 protein alignment from Fig S3 of (English et al., 2017) was extended as follows: First, we used HMMer 3.1b2 (Eddy, 2011) to build an HMM from the previous alignment and used it to search for homologs in the following annotated protein sets, downloaded from Genbank: *Emergomyces africanus* (GCA_001660665.1), *Emergomyces pasteuriana* (GCA_001883825.1), *Emmonsia parva* (GCA_001014755.1), *Blastomyces percursus* (GCA_001883805.1), *Paracoccidioides venezuelensis* Pb300 (GCA_001713645.1) and *Paracoccidioides restrepiensis* PbCNH (GCA_001713695.1). This yielded single homologs in *E. africanus*, *Pb300*, and *PbCNH*, two homologs in *E. pasteuriana*, and no homologs in *Ep parva* or *B. percursus*, which is consistent with loss of *CBP1* in genus *Blastomyces*. The exon annotations of the five new homologs were refined based on the previous protein alignment. Four of the new homologs are syntenic to the previously known Cbp1s and share the conserved two intron structure. The remaining homolog, from *E. pasteuriana*, is in a distinct genomic location and has three introns. TBLASTN from NCBI BLAST 2.6.0 (Altschul et al., 1997) was then used to search the full set of Cbp1 protein sequences against the unannotated *Emergomyces orientalis* genome (GCA_002110485.1), yielding one hit orthologous to the conserved two intron Cbp1 sequence and one hit orthologous to the three intron *E. pasteuriana* paralog. Exons were annotated for both *E. orientalis* homologs based on the existing protein alignment, as above. All sequences were then aligned with PROBCONS 1.12 (Do et al., 2005) to yield the final alignment.

Species Tree generation

Full length midasin sequences were inferred by using NCBI TBLASTN 2.6.0 (Altschul et al., 1997) to search the G217B predicted sequence HISTO_DA.Contig93.FgenesH_Aspergillus.103.final_new against each genome of interest, retaining the top non-redundant hits spanning the

full protein. An HMM was built from the initial TBLASTN alignments with hmmbuild (HMMer 3.1b2)(Eddy, 2011), all hits were realigned to the HMM with hmalign (HMMer 3.1b2), and the resulting multiple alignment was refined with PROBCONS 1.12 (Do et al., 2005). A phylogenetic tree was inferred from the ungapped positions of the PROBCONS multiple alignment with IQTREE 1.5.3 (Nguyen et al., 2015).

BMDM Culture conditions

Bone marrow derived macrophages (BMDMs) were isolated from the tibias and femurs of 6-8 week old C57BL/6J (Jackson Laboratories stock no. 000664) mice and differentiated in BMM (bone marrow derived macrophage media) which consists of Dulbecco's Modified Eagle Medium, D-MEM High Glucose (UCSF Cell Culture Facility), 20% Fetal Bovine Serum (Atlanta Cat #: S11150, Lot #: D18043), 10% v/v CMG supernatant (the source of CSF-1), 2 mM glutamine (UCSF Cell Culture Facility), 110 µg/mL sodium pyruvate (UCSF Cell Culture Facility), penicillin and streptomycin (UCSF Cell Culture Facility) with 20% Fetal Bovine Serum (Atlanta Cat #: S11150, Lot #: D18043). Undifferentiated monocytes were plated in BMM that contains BMM for 7 days at 37°C and 5% CO₂. Adherent cells were then scraped and frozen down in 40% FBS and 10% DMSO until further use. *Hc* cultures were grown in liquid *Histoplasma* macrophage media (HMM) using an orbital shaker or on HMM agarose plates [cite].

Generation of Hc strains

H. capsulatum strain G217B *ura5*Δ (WU15) was a kind gift from the lab of William Goldman (University of North Carolina, Chapel Hill). For all studies involving the *cbp1* and *yps-3* mutants, “wildtype” refers to G217B *ura5*Δ transformed with a *URA5*-containing episomal vector (pLH211), *cbp1* refers to G127Bura5 Δ*cbp1*::*T-DNA* as previously described [cite Isaacs DT] transformed with the same *URA5*-containing episomal vector, and “complemented” strain refers to G217Bura5Δ*cbp1*::*T-DNA* transformed with the *URA5*-containing plasmid bearing the wild-type CBP1 gene (pDTI22) as previously described [cite Isaacs, DT et al]. The *Emergomyces* CBP1 coding sequences (*E. africanus*, *E. orientalis*, *E. crescens*, *E. pasteuriana_1*, *E. pasteuriana_2*)

and *E. crescens*> *G217B* or *E.crescens*>*Pb03* chimeric constructs (N-terminal helix residues, C-terminal loop residues, both C-terminal and N-terminal residues, 1st helix swap) constructs were synthesized as gBlocks™ by Integrated DNA Technologies and cloned into pDTI22, replacing the *G217B CBP1* coding sequence but maintaining the flanking sequences. *P. americana* strain *Pb03* Cbp1 gene construct includes the *Hc G217B Cbp1* signal peptide fused to the mature *Pb03* protein coding sequence flanked by the same regulatory sequences of pDTI22 as previously described (English et al., 2017). All tagged Cbp1 expressing strains including 1xstrep-*Hc G217B Cbp1*, 2xstrep-*Pb03 Cbp1*, 3XFLAG-*Hc G217B Cbp1*, 3XFLAG-*Hc Pb03 Cbp1*, were N-terminally tagged with the tag situated between the *G217B Cbp1* signal peptide and the mature protein sequence and were flanked by the same regulatory sequences in pDTI22 and introduced into the *Hc G217B cbp1* mutant strain. The *yps3* mutant was generated from the *G217B ura5Δ* parental strain transformed with the episomal plasmid pDAZ021 which contains a bidirectional H2Ab promoter driving Cas9 and two sgRNA cassettes targeting the sequences on both sides of the *G217B Yps-3* gene (Joehnk, in preparation). Single colony isolates for PCR screened in the *yps-3* genomic locus to look for excisions in the colony population and the isolates with the most likely edited band were struck out for further single colony isolation until an isolate with a clean excision between the two sgRNA target sites was detected. pBJ219 was subsequently lost from the mutant by growing the *Hc* yeast in the presence of exogenous uracil and then screening for plasmid loss. Subsequently, the *G217B ura5Δ yps3Δ* was transformed with the *URA5*-containing episomal plasmid (pLH211). The overexpression strains used to detect and purify Yps-3 were generated by transforming *G217B ura5Δ* parental strain with an episomal plasmid with each of the C-terminally tagged Yps-3 alleles (Yps-3-6xHistidine, Yps-3-2xstrep, Yps-3-3XFLAG) flanked by the Cbp1 promoter and CatB terminator. The control for the StrepTactin pulldowns was an N-terminally Twinstrep™ (Iba Lifesciences) tagged enhanced GFP (eGFP) that was fused to the *G217B Cbp1* signal peptide and cloned into the same episomal plasmid (pDTI22) as all the other Cbp1 constructs. For all Cbp1, Yps3, eGFP, and CRISPR construct plasmids, approximately 50

ng of PacI-linearized DNA was electroporated into the appropriate parental strain (G217B *ura5Δ*, G217B *ura5Δ cbp1::T-DNA*, or G217B *ura5Δ yps3Δ*) as previously described [Isaacs DT et al]. The plasmid pLH211 was used as a vector control. Transformants were selected on HMM agarose plates.

Hc secreted protein detection in culture supernatants

To detect *Hc* secreted proteins (tagged Cbp1 alleles and Cbp1 homologs, tagged Yps-3 homologs, tagged 2xstrep-eGFP) in culture supernatants, 4-5 day *Hc* cultures were grown in liquid HMM and yeast were pelleted by centrifugation. The supernatants were subjected to filtration using 0.22 μm filters, and the resultant filtrates were concentrated using Amicon Ultra Centrifugal Filter Units with a 3 kDa cutoff (EMD Millipore). Protein concentration was quantified using the Bio-Rad protein assay (Bio-Rad Laboratories). Equal amounts of protein were separated by SDS-PAGE, and proteins were visualized by staining the gel with InstantBlue™ Coomassie Protein Stain (ISB1L – abcam 119211)

Macrophage Infections

Macrophage infections with G217B *Hc* strains were performed as described previously (Hwang et al., 2008). Briefly, the day before infection, macrophages were seeded in tissue culture-treated dishes. On the day of infection, yeast cells from logarithmic-phase *Hc* cultures ($OD_{600} = 5-7$) were collected, resuspended in BMM, sonicated for 3 seconds on setting 2 using a Fisher Scientific Sonic Dismembrator Model 100, and counted using a hemacytometer at 40X magnification. Depending on the multiplicity of infection (MOI), the appropriate number of yeast cells was then added to the macrophages. After a 2-hour phagocytosis period, the macrophages were washed once with d-PBS to remove extracellular yeast and then fresh media was added. For infections lasting longer than 2 days, fresh media was added to the cells at approximately 48 hpi.

Fractionation of Hc-infected macrophage lysates

2.5×10^7 BMDMs were plated on a TC-treated 15-cm plates and allowed to adhere for at least 24 hrs. The BMDMs were then infected with *Hc* at an MOI = 5 and the infection was allowed to

proceed for 24 hours. At 24 hours post infection, cells were collected by scraping without washing and spun down at 2500 rpm for 5 min to pellet the intact cells. The cell pellet was then resuspended in 500 μ L of d-PBS, transferred to a 1.5 mL tube, and spun at 1000 rpm for 2 min. The cell pellet was then resuspended in 300 μ L of homogenization buffer (150 mM KCl, 20 mM HEPES pH 7.4, 2 mM EDTA, cOmplete Mini Protease Inhibitor Cocktail tablet-Roche 04693124001). For the unfractionated sample, the cell pellet was resuspended in homogenization buffer with 1% TritonX-100. For the fractionated samples, the cell lysate was then gently passaged through a 27-gauge needle to disrupt only the plasma membrane and not any internal membranous compartments. The lysate was then spun at 3000 rpm for 5 minutes to pellet *Hc* cells and macrophage nuclei. The remaining lysate was then further clarified by centrifuging twice at 3000 rpm with removal of 275 μ L and 250 μ L respectively to avoid contamination of the lysate with *Hc*. After the final low speed spin, 225 μ L was placed in ultracentrifuge tubes (Beckman Coulter 349622), weighed, and loaded into a Beckman Coulter Fixed Angle Rotor TLA100.3. The samples were then spun at 45,000 rpm for 2 hours in a TL-100 tabletop ultracentrifuge to pellet the membranes. After the spin, 175 μ L of supernatant, representing the cytosolic fraction, was transferred into a separate 1.5 mL tube. The remaining supernatant was discarded to prevent cross-contamination between the cytosolic and membrane fractions. The pellet, representing the membrane fraction, was resuspended in 225 μ L of homogenization buffer with 1% TritonX-100. All samples were flash frozen in liquid nitrogen and stored at -80°C.

Lactate dehydrogenase release assay

To quantify macrophage lysis, BMDMs were seeded (7.5×10^4 cells per well of a 48-well plate) and infected as described above. At the indicated time points, the amount of LDH in the supernatant was measured as described previously [cite]. BMDM lysis was calculated as the percentage of total LDH from supernatant of the uninfected wells with uninfected macrophages lysed in 1% Triton-X at the time of infection. Due to continued replication of BMDMs over the

course of the experiment, the total LDH at later time points is greater than the total LDH from the initial time point, resulting in an apparent lysis that is greater than 100%

Intracellular replication

BMDMs were seeded (7.5×10^4 cells per well of a 48-well plate) and infected in triplicate as described above. At the indicated timepoints, culture supernatants were removed and 500 μ l of ddH₂O was added. After incubating at 37°C for 15 min, the macrophages were mechanically lysed by vigorous pipetting. The lysate was collected, sonicated to disperse any clumps, counted, and plated on HMM agarose in appropriate dilutions. After incubation at 37°C with 5% CO₂ for 12–14 days, CFUs were enumerated. To prevent any extracellular replication from confounding the results, intracellular replication was not monitored after the onset of macrophage lysis.

Purification, crystallization and structural determination of Cbp1

2-3 L of G217B *Hc* expressing each different *cbp1* allele were grown at 37°C with 5% CO₂ for 5 days. Culture medium was concentrated using an amicon cell outfitted with a 5kDa molecular weight cutoff membrane. Concentrated medium was diluted 1:50 in MonoA buffer (20 mM Tris-HCl pH 7.5, 20 mM NaCl) and run through a HiTrapQ ion exchange column. Protein generally eluted at a 24% MonoB buffer concentration (20 mM Tris-HCl pH 7.5, 1 M NaCl). Eluted fractions were pooled and concentrated using a 3 kDa molecular cutoff spin concentrator. The final product was separated from remaining contaminants using a size exclusion approach with a Superdex 75 10/300 column run with SEC buffer (50 mM Tris-HCl pH 7.5, 150 mM NaCl). Purity of the final elution was verified by SDS-PAGE and concentrated using a 3 kDa MWCO spin concentrator. Pb03 Cbp1 was concentrated to 6 mg/mL and H88 Cbp1 was concentrated to 14 mg/mL. Crystallization trays were set up in sitting drop vapor diffusion trays at room temperature using 2 μ L + 2 μ L drops of protein and crystallization solution. Crystals of Pb03 Cbp1 formed in 0.05 M HEPES pH 6.5, 35% PEG 6000, and were seen after 24 hours and allowed to grow for 48 hours to reach full size. H88 Cbp1 crystallized in 0.02 M CoCl₂, 0.2 M MES pH 6.5, 2 M Ammonium sulfate using the same setup as for Pb03 Cbp1, crystals were seen after 48 hours and reached

full size in 1 week. To provide phase information, full sized Pb03 Cbp1 crystals were soaked for 2 hours in 10 mM potassium tetrachloroplatinate (II) from the Hampton Heavy Atom kit screen. Derivatized and native Pb03 Cbp1 crystals were cryoprotected using ethylene glycol. H88 Cbp1 crystals were cryoprotected using glycerol. All diffraction data were collected at ALS BL 8.3.1 on a Pilatus3 S 6M detector. Data processing and refinement was conducted in the CCP4 and Phenix programming suites. Datasets were processed using XDS and sailed using AIMLESS in the CCP4 suite. The structures were solved using Phaser in the Phenix crystallography suite. Beamline 8.3.1 at the Advanced Light Source is operated by the University of California Office of the President, Multicampus Research Programs and Initiatives grant MR-15-328599, NIH (R01 GM124149 and P30 GM 124169), Plexxikon Inc., and the Integrated Diffraction Analysis Technologies program of the US Department of Energy Office of Biological and environmental Research. The Advanced Light Source (Berkeley, CA) is a national user facility operated by Lawrence Berkeley National Laboratory on behalf of the US Department of Energy under contract number DE-AC02-05CH11231, Office of Basic Energy Sciences. We would like to thank James Holton and George Meigs for their help at the beamline. We thank the X-ray Crystallography Facility at University of California, San Francisco. We would like to thank Liam McKay for his coordination of the remote data collection.

BMDM infection with *Emergomyces africanus* yeast

Emergomyces africanus (clinical isolate CBS 136260 (Schwartz et al., 2018; Staff, 2018)), was grown in brain-heart infusion broth (BHI) (Cat No. 110493, Merck, USA), at 37 °C, 180 rpm, for 5 days. Yeasts were then sub-cultured for a further 3 days by 1:20 dilution into fresh BHI, until reaching an optical density of 3-4. BMDMs were seeded in 8-well μ -Slide imaging slides (Cat. No. 80826, ibidi, Germany) at a density of 7.5×10^4 cells/well in 0.375 ml BMM (DMEM, high glucose, GlutaMAX™ supplement, pyruvate (Thermo Fisher, Cat no. 10569010), 20% FBS (Thermo Fisher, Cat. no. 10270106), Penicillin-streptomycin (50 units/ml) (Thermo Fisher, Cat. no. 15140148), 20 ng/ml mCSF (R&D Systems, Cat no. 416-ML)), and incubated at 37 °C, 5% CO₂

for 24 h. Yeast cells used for infection were washed twice by centrifugation and resuspension in PBS, counted using a haemocytometer, then the appropriate volume of yeast suspension was added to BMM. On day 0, BMDMs were infected by replacing the media with 0.375 ml yeast suspension in BMM, with a total of 7.5×10^4 yeasts/well (MOI=1). The BMDMs were fed on day 2 by removing 200 μ l spent media from wells and replacing it with 200 μ l BMM.

LDH assay sample collection of BMDMs infected with E. africanus

BMDMs were seeded in 48-well tissue culture plates at a density of 1×10^5 cells/well in 0.5 ml BMM, and incubated at 37 °C, 5% CO₂ for 24 h. Yeast cells used for infection were washed twice by centrifugation and resuspension in PBS, counted using a haemocytometer, then the appropriate volume of yeast suspension was added to BMM. On day 0, BMDMs were infected by replacing the media with 0.5 ml yeast suspension in BMM, with a total of 1×10^5 yeasts/well (MOI=1). Media was replaced with 0.5 ml fresh BMM for wells containing uninfected BMDMs. Uninfected BMDMs were lysed on day 0 by removing the media and replacing it with 0.5 ml 0.2 % Tween-20 in distilled water, and the lysate was collected and stored in 1.5 ml microcentrifuge tubes at 4 °C. The BMDMs were fed on day 2 by adding 200 μ l BMM. On days 0, 1, 3, 5 and 7, spent media (175 μ l) was collected from wells in and stored in 1.5 ml microcentrifuge tubes at 4 °C for later analysis in the LDH assay.

Imaging of E. africanus infected BMDMS

On imaging days, the media was removed and replaced with 250 μ l pre-warmed 4% PFA for 30 min. The PFA was then removed and replaced with PBS. The slides were imaged using a Zeiss Axiovert 200M inverted fluorescence microscope with a Zeiss AxioCam HSc camera.

Immunofluorescence of FLAG-Pb03 Cbp1 during macrophage infection

1.5×10^5 BMDMs were plated on 12 mm circular coverslips (Fisher Scientific 12-545-80) in a 24-well plate and infected as described above with the following *Hc* strains at an MOI of 3; cbp1 mutant with wildtype G217B Cbp1 and 3XFLAG-Pb03 Cbp1. At 24 and 48 hours post infection

cells were fixed with 4% Paraformaldehyde for 15 minutes at room temperature and washed 3 times with d-PBS to remove residual paraformaldehyde. Fixed cells were permeabilized and nonspecific binding sites were blocked with a filter-sterilized Saponin Block solution (0.2 % Saponin from Quillaja Bark (Sigma-Aldrich S7900), 2% heat inactivated FBS (Atlanta Cat #: S11150, Lot #: D18043)) for 1 hour at room temperature. Cells were stained a monoclonal primary mouse anti-FLAG M2 antibody (Millipore Sigma F3165) at a dilution of 1:250 and incubated in a light-blocking incubation chamber overnight with 4°C. Coverslips were washed 3 times with block for 5 min to wash off any remaining primary antibody. Coverslips were incubated with a polyclonal IgG (H+L) Highly Cross-Adsorbed Goat anti-Mouse, Alexa Fluor™ 488 (Fisher Scientific A11029) secondary at a dilution of 1 drop into 500 µL of block for 1 hour at room temperature in a light-blocking incubation chamber. Coverslips were then washed 3 times with d-PBS for 5 minutes and then briefly dunked into double distilled water and the excess liquid is absorbed by the corner of a kimwipe. Coverslips are mounted on glass slides with a drop of Vectashield Mounting media with DAPI that has 1:100 Calcofluor White (1 mg/mL). Coverslips are sealed to the glass slide with clear nail polish. Images were taken on a Nikon CSU-X1 spinning disk confocal microscope

Affinity purification of 1x/2xstrep- tagged secreted proteins

1xstrep/2xstrep-tagged proteins (2xstrep-eGFP, 1xstrep G217B *Hc* Cbp1, 2xstrep *Pb03* Cbp1, and *Yps-3-1x/2xstrep*) were purified from either *Hc* culture supernatants or from *Hc*-infected macrophage lysates. In the case of *Hc* culture supernatants, 25 mL of *Hc* culture was grown for 4 days at 37°C with 5% CO₂ and passed through a 0.22 µm syringe filter. Roche cOmplete Mini Protease Inhibitor Cocktail tablet (Roche 04693124001) was added to the filtered supernatant which was then concentrated down in a 3000 MWCO Amicon 15 mL centrifugal filters (Millipore Sigma UFC900324) to approximately 500 µL and then diluted back to 1 mL total with d-PBS. To generate *Hc*-infected macrophage lysates, 4 plates of BMDMs seeded at a density of 2.25x10⁷ were infected with *Hc* at an MOI = 5. At 24 hours post infection, the adherent cells were scraped

in 10 mL of cold d-PBS and pelleted at 1500 rpm for 10 min at 4°C. After decanting the d-PBS, the cell pellet was suspended in 1 mL of cold lysis buffer (50 mM TRIS-HCl pH 7.5, 150 mM NaCl, 1 mM EDTA, 0.5% NP-40, 1 tablet of Roche cOmplete Protease inhibitor Cocktail, and 1 tablet of Millipore Sigma PhosStop 4906845001). The lysate was sonicated 2 times for 5 seconds at setting 2 using a Fisher Scientific Sonic Dismembrator Model 100 with 1 min on ice in between. The cells were further lysed for 1 hr at 4°C with a rotisserie revolver and the lysate was clarified with a 20 min spin at 13,000 rpm at 4°C. Both the *Hc* supernatant and macrophage lysates were applied to pre-washed Magstrep “type3” XT beads (Iba Life Sciences 2-4090-002) and allowed to bind overnight at 4°C on a rotisserie revolver. The Magstrep beads with bound strep-tagged proteins were then washed three times with wash buffer Buffer W (Iba Lifesciences 2-1003-100) and eluted with Buffer BXT (Iba Lifesciences 2-1042-025).

Yps3-6xHis purification

3 Liters of G217B *Hc* expressing Yps3-6xHis were grown at 37°C with 5% CO₂ for 5 days. The supernatant was sterile filtered through a 0.22 µm 0.5 or 1L vacuum filter and concentrated using the Amicon® 200 mL Stirred Cell (UFSC20001) with a 3 kDa NMW Ultrafiltration Disc (Millipore PLBC06210) and Amicon® Ultra 15 mL Centrifugal Filters with a 3kDa NMW (Millipore UFC9003). The concentrated supernatant was applied to a cobalt resin to achieve a His-tag pulldown using the HisPur™ Cobalt Purification Kit (ThermoScientific™ 90092). The elutions were then applied to a cation exchange column to purify Yps3-6xhis. The majority of the Yps-3-6xhis emerged with Cbp1 in the flow-through.

Yps3-6xhis and Cbp1 protein interaction assays

Concentrated supernatant was diluted 1:50 in Mono A buffer (20mM Tris-HCl pH 7.0, 20 mM NaCl). The sample was applied to a HitrapS cation exchange column and eluted with 25% MonoB buffer (20 mM Tris-HCL pH 7.0, 1 M NaCl). The flow-through fractions contained both Cbp1 and Yps3-6xHis, as a complex of these proteins would retain a negative charge at the buffered pH. The complex was validated by passage through a Superdex75 Size Exclusion column using 50

mM Tris pH 7.0, 150 mM NaCl. Both Cbp1 and Yps-3-6xHis eluted in a monodispersed peak. To determine at what molar ratios this complex of Yps-3 and Cbp1 forms at pure Yps-3-6xHis and G217B Cbp1, were mixed in different molar ratios and pulled down with NiNTA resin. For the Yps3-6xhis pulldown, the SEC flowthrough that contained both Cbp1 and Yps3-6xhis was incubated with 20 uL of washed 50% NiNTA bead slurry for 30 minutes at room temperature with shaking and then the beads were washed with 20 column volumes of NiNTA wash buffer (50 mM Tris-HCl pH 7, 150 mM NaCl, and 30 mM of Imidazole). The complex was eluted with 6 column volumes of NiNTA elution buffer (50 mM Tris-HCl pH 7, 150 mM NaCl, 500 mM of Imidazole). We verified the identity of the proteins in the complex by western blot using native antibody for Cbp1 and anti-his for Yps3.

Mass Spectrometry

This work used the Vincent J. Proteomics/Mass Spectrometry Laboratory at UC Berkeley, supported in part by NIH S10 Instrumentation Grant S10RR025622. For gel band, 1D, and 2D MUDPIT Mass spectrometric analysis, trypsin or chymotrypsin were used to digest protein into peptides according to Facility protocols. We would like to thank Lori Kohlstaedt, the facility director, for helpful advice and work done on this project.

SDS-PAGE Protein Gel and Western Blot analysis

Protein samples were mixed with 4X Protein Loading Buffer (Li-COR 926-31097) and 1:20 DTT (1M DTT) and denatured at 95°C for 5 minutes. Proteins were separated by SDS-PAGE on NOVEX-NuPAGE 4-12% BIS-TRIS gels with MES Running Buffer and Precision Plus Dual Xtra Protein Standards (Bio-Rad161-0377) were used to estimate the molecular weight of proteins. For Western blots, the SDS-PAGE separated proteins were transferred to nitrocellulose membranes. Non-specific binding to the membrane was blocked with Odyssey® PBS Blocking Buffer (Fisher Scientific NC9877369) and probed with the antibodies listed below. Blots were imaged on an Odyssey CLx and analyzed using ImageStudio2.1 (Li-COR). The following primary antibodies were used: monoclonal mouse anti-FLAG M2 (Millipore Sigma F3165), monoclonal

mouse anti-strep (StreMab Classic iba LifeSciences 2-1507-001), custom generated Rabbit anti-Cbp1 (Rb83), custom generated Rabbit anti-RYP1, mouse anti-LAMP1 (cell signaling D401S), mouse anti-alpha-tubulin (Novus biological DM1A), Rabbit anti-calnexin (abcam 22595), mouse anti-His (ABclonal AE003).

CCF4-AM Assay

Protocol was adapted from correspondence with Dr. Sunny Shin from University of Pennsylvania, Perelman School of Medicine. The functionality of strep-Beta-Lactamase expressed by *Hc* was determined by using concentrated culture supernatants with 0.25 mg/mL of Nitrocefin (Toku-E N005) and incubated for 30 minutes at room temperature and the colorimetric change was monitored. 1×10^7 BMDMs were plated in non-TC treated 10 cm plates and infected with the following strains at an MOI of 5 for 24 hours; “WT” G217B *ura5⁻* with URA5 gene on an episomal plasmid, G217B *ura5⁻* with strep-Beta Lactamase driven by the *cbp1* promoter on an episomal plasmid. BMDMs were also spin infected with the following *Legionella pneumophila* strains at an MOI of 100 for 4 hours; “WT” *flaA*, *BlaM-RalF*, and “dotA” *dotA*, *BlaM-RalF*. Cells were scraped and washed with cold Flow Buffer (PBS with 2% FBS, 2 mM EDTA) with Probenecid (Life Technologies P36400). Washed cells were incubated with the LiveBLazer FRET-B/G Loading Kit with CCF4-AM dye (Life Technologies K1095) for 90 minutes at room temperature in a light protected environment. Dyed cells were analyzed by flow cytometry on FACS Aria Fusion “Jabba the Hutt” in UCSF Parnassus Flow Core with the following lasers; AmCyan (515/20 VioletE), PacBlu (450/50 Violet F), and FITC (515/20 Blue B). Data was analyzed with FlowJo V10.7

RNA isolation and RT-PCR

For RNA isolation from *Hc* yeast cells, 10 mL of *Hc* yeast culture is washed and resuspended in 1 mL of Qiazol (Qiagen) and bead-beaten in a Mini-BeadBeater-96 (BioSpec 1001) for 2 minutes in a 2 mL screw cap tube with approximately 1/3 of the volume filled with zirconia beads. 200 μ L of chloroform was added to the lysate, vortexed for 15 seconds, and centrifuged at 12,000xg for

20 minutes at 4°C. The organic phase was saved for further downstream RNA purification. For RNA isolation from cultured cells, BMDMs were seeded (1×10^6 cells per well of a 6-well plate) and infected in triplicate as describe. Triplicate wells of infected macrophages were lysed in 1mL total of QIAzol (Qiagen). For both *Hc* and BMDMs RNA, total RNA was isolated from the aqueous phase using Econo-spin columns (Epoch Life Science) and then subjected to on-column PureLink DNase (Invitrogen) digestion. To generate cDNA, 2-4 μ g total RNA was reverse transcribed using Maxima Reverse Transcriptase (Thermo Scientific), an oligo-dT primer, and pdN9 primers following manufacturer's instructions. Quantitative PCR was performed on 1:10 to 1:50 dilutions of cDNA template using FastStart SYBR Green MasterMix with Rox (Roche). Reactions were run on an Mx3000P machine (Stratagene) and analyzed using MxPro software (Stratagene). Cycling parameters were as follows: 95°C for 10 min, followed by 40 cycles of 95°C (30 s), 55°C (60 s), and 72°C (30 s), followed by dissociation curve analysis. Abundances of CHOP and TRIB3 were normalized to HPRT levels. Rockstar10 levels were normalized to *Hc* ACT1 levels.

Table 5.1: Primers used for the studies in this work.

Primer name	Sequence
DAZ061_F_Rock1_proto3	GGACGAAACGAGTAAGCTCGTC GATGAAGCCCAGAGACGTAA GTTTTAGAGCTAGAAATAGCAAG
DAZ062_R_Rock1_proto3	GACGAGCTTACTCGTTTCGTCCTCACGGACTCATCAGGATGAACGG TGATGTCTGCTCAAGC
DAZ026_F_rock10_proto1	GGACGAAACGAGTAAGCTCGTC AACTCAGAGAAAAATTCTAA GTTTTAGAGCTAGAAATAGCAAG
DAZ027_R_rock10_proto1	GACGAGCTTACTCGTTTCGTCCTCACGGACTCATCAGAACTCACGGT GATGTCTGCTCAAGC
DAZ028_F_rock10_proto2	GGACGAAACGAGTAAGCTCGTC TCAAACCATCGTGACTCCG GTTTTAGAGCTAGAAATAGCAAG
DAZ029_R_rock10_proto2	GACGAGCTTACTCGTTTCGTCCTCACGGACTCATCAGTCAAACGGT GATGTCTGCTCAAGC
DAZ030_F_avr9_proto1	GGACGAAACGAGTAAGCTCGTC ATGAATATTGTTGGAATATC GTTTTAGAGCTAGAAATAGCAAG
DAZ031_R_avr9_proto1	GACGAGCTTACTCGTTTCGTCCTCACGGACTCATCAGCATGAATGGT GATGTCTGCTCAAGC
DAZ032_F_avr9_proto2	GACGAGCTTACTCGTTTCGTCCTCACGGACTCATCAGATGAATCGGT GATGTCTGCTCAAGC

Primer name	Sequence
DAZ033_R_avr9_proto3	GACGAGCTTACTCGTTTCGTCCTCACGGACTCATCAGAAATCTCGGT GATGTCTGCTCAAGC
DAZ043_F_Rock1_5'	CAATACCGCCATGGAGCTAGATATTCAA
DAZ044_R_Rock1_3'	GGCTGACTTAGTCCTCATGTTTTCTGG
DAZ045_F_Rock6_proto1_5'	AAAGGTCAACCAAGTCCTTACAGTTGTAT
DAZ046_R_Rock6_proto1_3'	ATAATGTAAAAGTGTGGTGGTCAACCTG
DAZ047_F_Rock6_proto2_5'	CATAAAGGACACATGACTCGCGTTC
DAZ048_R_Rock6_proto2_3'	CAACAACAATAACAGTAATCAGGTTAATCACCATC
DAZ049_F_Rock10_5'	GCAATAAATTCAGCAGCTCTCACCT
DAZ050_R_Rock10_3'	CCACTTAGCGCAGTTAAGACTATAAATTTTCC
DAZ051_F_AVR9_5'	CTGCGCCCCGCTAAATACTTACAATG
DAZ052_R_AVR9_3'	CCAAGACATCCATGAGGATAACAGTG
DAZ065_Gibson_insert_Hc_1XFLAG_F	CTTCTAAGCGTGATTATAAGGATGATGACGATAAGGATCA
DAZ066_Gibson_insert_Hc_R	TTCTAAGCTTAATTTTACCACAAGCAGCCCTTG
DAZ067_Gibson_vector_1XFLAG_R	TCATCCTTATAATCACGCTTAGAAGCATTCTCAGG
DAZ068_Gibson_vector_Hc_F	GCTTGTGGTAAAATTAAGCTTAGAATCAAACAATTC
DAZ069_Gibson_insert_3XFLAG_F	GCTTCTAAGCGTGATTATAAGGATCATGATGGCGA
DAZ070_Gibson_vector_3XFLAG_R	GATCCTTATAATCACGCTTAGAAGCATTCTCAGGC
DAZ071_Gibson_insert_Pb03_1XFLAG_R	CTTCTAAGCGTGATTATAAGGATGATGACGATAAGGCTCAAC
DAZ072_Gibson_vector_Pb03_F	GGCTGCTTCTAAAATTAAGCTTAGAATCAAACAAT
DAZ073_Gibson_insert_Pb03_R	TTCTAAGCTTAATTTTAGAAGCAGCCTTCGCAGCC
DAZ074_Gibson_FLAG_seq_F	AGAGAAAACCCAGCGAAAATCACCC
DAZ075_Gibson_FLAG_seq_R	GAAGAACAAAGGATAACAGGGCGGA
DAZ092_rock10_gateway_attb1_5'_F	GGGG ACA AGT TTG TAC AAA AAA GCA GGC TGC CATCGAGCGCCTCGTGC

Primer name	Sequence
DAZ093_rock10_gateway_attb2_3'_R	GGGG AC CAC TTT GTA CAA GAA AGC TGG GTC TCTCTATGCGGTACCGGGCT
DAZ093_rock10_gateway_attb2_3'_R	GGGG AC CAC TTT GTA CAA GAA AGC TGG GTC TCTCTATGCGGTACCGGGCT
DAZ094_rock10_seq_F	CAGACCAATGATGAGAGCGCGC
DAZ095_rock10_seq_F	CATCATAGATTTTATATGGAAAATCGCGGGC
DAZ096_rock10_seq_F	GTACAGTACATACCTCGTATGCAGGCA
DAZ097_rock10_seq_F	GAAGATATTTGTGAGCGGATCGATCAGA
DAZ098_rock10_seq_F	GAAGGGTTCCACAATGTTGTGAG
DAZ100_rock10_seq_F	CTTTGATGGCTGGGCATTCAATCT
DAZ101_rock10_seq_F	GATACGCGATGTTGACCTAGCG
DAZ114_GA_yps3strep_insert_R	GATCCAGTCGACTCACTTCTCGAACTGTGGGTGTGACCATCCGCCAC CCCCTCCGCCTGC
DAZ115_GA_yps3strep_vector_F	CTGCGAGGCAGGCGGAGGGGGTGGCGGATGGTCACACCCACAGTT CGAGAAGTGAGTCGA
DAZ116_GA_yps3strep_insert_F	ATTTCCAGAACAACCACTTCGTCATTCAAATGCTGAACATCAAATC GATCTCAACCCTC
DAZ117_GA_yps3strep_vector_R	GGGTTGAGATCGATTTGATGTTTCAGCATTTTGAATGACGAAGTGGT TGTTCTGGAAATGA
DAZ149_Gibson_yps3_2xstrep_vector_F	GCGGCGGCGGCAGCGGCGGCAGCGCGTGGAGCCATCCGCAGTTTG AAAAATGAGTCGACTGGATCCGCGG
DAZ150_Gibson_yps3_2xstrep_insert_R	CCGCCGCTGCCGCCGCCGCTGCCGCCGCTTTTTCAAATGCGGATG GCTCCATCCGCCACCCCTCCGCCTGCC
DAZ151_Gibson_yps3_3xflag_insert_R	CTTATCGTCATCCTTATAATCGATATCATGATCCTTATAATCGCCATC ATGATCCTTATAATCTCCGCCACCCCTCCGCCTGCCTCGCA
DAZ152_Gibson_yps3_3XFLAG_vector_F	TATCGATTATAAGGATGACGATAAGTGAGTCGACTGGATCCGCGGC TCGA
DAZ153_Gibson_yps3_vector_R	TTGAGATCGATTTGATGTTTCAGCATTTTGAATGACGAAGTGGTTGTT CTG
DAZ158_Gibson_yps3_3xflag_vector_F	GATATCGATTATAAGGATGACGATAAGAATTAAGCTTAGAATCAAA CAAT
DAZ159_Gibson_yps3_insert_R	TCTAAGAATTGTTTATTCTAAGCTTAATTCTTATCGTCATCCTTATA AT
DAZ160_Gibson_yps3_2xstrep_vector_F	CGCAGTTTGAAAAAATTAAGCTTAGAATCAAACAATTCTTAGACA GTGG
DAZ161_Gibson_insert_2xstrep_R	TTGTTTATTCTAAGCTTAATTTTTTTCAAATGCGGATGGCTCCACG CGCTGCCGCCGC
DAZ162_Gibson_yps3_1xstrep_vector_F	CACAGTTCGAGAAGAATTAAGCTTAGAATCAAACAATTCTTAGACA GTGG
DAZ163_Gibson_yps3_1xstrep_insert_R	AATTGTTTATTCTAAGCTTAATTCTTCTCGAACTGTGGGTGTGACC ATC

Primer name	Sequence
DAZ168_Cbp1prom_seq_BAS707_F	GGACGAGTAGGCATTCTCCACACG
DAZ170_GA_Scp1_2xstrep_vector_F	GATTGTGGGATGGGCGGAGGGGGTGGCGGATGGAGCCATCCGCA GTTTGAAAAAGGCGGC
DAZ171_GA_Scp1_3xha_vector_F	GATTGTGGGATGGGCGGAGGGGGTGGCGGAAACATCTTTTACCCA TACGATGTTCTGAC
DAZ172_GA_Scp1_3xflag_vector_F	GATTGTGGGATGGGCGGAGGGGGTGGCGGAGATTATAAGGATCA TGATGGCGATTATAAG
DAZ173_GA_Scp1_6xhis_vector_F	TACTTCCAGGCGCATCACCACCATCATCACTGAGTCGACTGGATCCG CGGCTCGAGTTAA
DAZ180_GA_SCP1_2xstrep_vector_F	AGGCGGCGGCAGCGGCGGCGGCAGCGGCGGCAGCGCGTGGAGCC ATCCGCAGTTTGAAAAATGAGTCGACTGGATCCGCGGCTCGAGTTA
DAZ181_GA_SCP1_2xstrep_insert_R	CCGCCGCCGCTGCCGCCCTTTTTCAAAGTGGCTCCATCC GCCACCCCTCCGCCATCCCACAATCCCCGGCACCGCCTCA
DAZ184_GA_SCP1_3XFLAG_vector_F	ATGATGGCGATTATAAGGATCATGATATCGATTATAAGGATGACGA TAAGTGAGTCGACTGGATCCGCGG
DAZ185_GA_SCP1_3XFLAG_insert_R	GATATCATGATCCTTATAATCGCCATCATGATCCTTATAATCTCCGCC ACCCCTCCGCCATCCCACAATCCCCGGCA
DAZ194_Cbp1_BAS707_vector_R	ACGCTTAGAAGCATTCTCAGGCG
DAZ206_rock10_5'_proto1	GGACGAAACGAGTAAGCTCGTC ATCAACCGATATATAAGACT GTTTTAGAGCTAGAAATAGCAAG
DAZ207_rock10_3'_proto1	GACGAGCTTACTCGTTTCGTCCTCACGGACTCATCAGATCAACCGGT GATGTCTGCTCAAGC
DAZ208_rock6_5'_proto1	GGACGAAACGAGTAAGCTCGTC ACAACTAATATTCCGATTGA GTTTTAGAGCTAGAAATAGCAAG
DAZ209_rock6_3'_proto1	GACGAGCTTACTCGTTTCGTCCTCACGGACTCATCAG ACAACT CGGTGATGTCTGCTCAAGC
DAZ210_rock1_5'_proto1	GGACGAAACGAGTAAGCTCGTC ATCTATCTGGCGAAACATTG GTTTTAGAGCTAGAAATAGCAAG
DAZ211_rock1_3'_proto1	GACGAGCTTACTCGTTTCGTCCTCACGGACTCATCAG ATCTAT CGGTGATGTCTGCTCAAGC
DAZ212_avr9_5'_proto1	GGACGAAACGAGTAAGCTCGTC TCCAATATGATAAAAGTGGA GTTTTAGAGCTAGAAATAGCAAG
DAZ213_avr9_3'_proto1	GACGAGCTTACTCGTTTCGTCCTCACGGACTCATCAG TCCAAT CGGTGATGTCTGCTCAAGC
DAZ214_SCP1_5'_proto1	GGACGAAACGAGTAAGCTCGTC GGCAGTTCAGTGATCGGGTA GTTTTAGAGCTAGAAATAGCAAG
DAZ215_Scp1_3'_proto1	GACGAGCTTACTCGTTTCGTCCTCACGGACTCATCAG GGCAGT CGGTGATGTCTGCTCAAGC

Primer name	Sequence
DAZ216_yps3_5'_proto1	GGACGAAACGAGTAAGCTCGTC TATTGAGCTGCGATTA GTTTTAGAGCTAGAAATAGCAAG
DAZ217_yps3_3'_proto1	GACGAGCTTACTCGTTTCGTCCTCACGGACTCATCAG TATTGA CGGTGATGTCTGCTCAAGC
DAZ218_rock10_5'_proto2	GGACGAAACGAGTAAGCTCGTCTGCGCTATATTGTAATTAGAGTTT TAGAGCTAGAAATAGCAAG
DAZ219_rock10_3'_proto2	GACGAGCTTACTCGTTTCGTCCTCACGGACTCATCAGTGC GCTCGGTGATGTCTGCTCAAGC
DAZ220_rock6_5'_proto2	GGACGAAACGAGTAAGCTCGTCACGTGACCGTTTAGATCACGGTTT TAGAGCTAGAAATAGCAAG
DAZ221_rock6_3'_proto2	GACGAGCTTACTCGTTTCGTCCTCACGGACTCATCAGACGTGACGGT GATGTCTGCTCAAGC
DAZ222_rock1_5'_proto2	GGACGAAACGAGTAAGCTCGTC TTCGTCGGCGCCGCTCCAAT GTTTTAGAGCTAGAAATAGCAAG
DAZ223_rock1_3'_proto2	GACGAGCTTACTCGTTTCGTCCTCACGGACTCATCAG TTCGTC CGGTGATGTCTGCTCAAGC
DAZ224_avr9_5'_proto2	GGACGAAACGAGTAAGCTCGTCTTGAATTCTATATCAATCGCGTTTT AGAGCTAGAAATAGCAAG
DAZ225_avr9_3'_proto2	GACGAGCTTACTCGTTTCGTCCTCACGGACTCATCAGTTGAATCGGT GATGTCTGCTCAAGC
DAZ226_Scp1_5'_proto2	GGACGAAACGAGTAAGCTCGTCACCATATCATGGCAGGCCAGTTT TAGAGCTAGAAATAGCAAG
DAZ227_Scp1_3'_proto2	GACGAGCTTACTCGTTTCGTCCTCACGGACTCATCAGACCATACGGT GATGTCTGCTCAAGC
DAZ228_yps3_5'_proto2	GGACGAAACGAGTAAGCTCGTCGAGAGTTAGTTGGGACAGCGGTT TTAGAGCTAGAAATAGCAAG
DAZ229_yps3_3'_proto2	GACGAGCTTACTCGTTTCGTCCTCACGGACTCATCAGGAGAGTCGG TGATGTCTGCTCAAGC
DAZ230_GA_vector_Cbp1_F	TAAAAGGCAGCGATTATAGCGCCC
DAZ231_GA_Hc_Cbp1_Nterm_insert_R	TGGGCGCTATAATCGCTGCCTTTTAATTCGCCGCGGAAGAAAGCC
DAZ232_GA_Hc_Cbp1_Cterm_insert_R	TGGGCGCTATAATCGCTGCCTTTTACCACAAGCAGCCCTTGCATG
DAZ233_GA_Pb03_Cbp1_Nterm_insert_R	AGTGGGCGCTATAATCGCTGCCTTTTAGGAAGCAGCAGCGGTAGC
DAZ234_GA_Pb03_Cbp1_Cterm_insert_R	AGTGGGCGCTATAATCGCTGCCTTTTAGAAGCAGCCTTCGCAGCC
DAZ235_GA_2xstrep_insert_F	GCCTGAGAATGCTTCTAAGCGTTGGAGCCATCCGCAGTTTGAAAAA GGCGGCGGCAGCGG

Primer name	Sequence
DAZ236_GA_Cbp1_3XFLAG_insert_F	GCGCCTGAGAATGCTTCTAAGCGTGACTACAAAGACCATGACGGTG ATTATAAAGATCAT
DAZ237_GA_Eafri_Cbp1_full_insert_F	TCCAGAACAACCACTTCGTCATTCAAATGCATTTCTCCAAGGTCGT CGG
DAZ238_GA_BAS707_emmonsia_vector_R	TTTGAATGACGAAGTGGTTGTTCTGGAAAAG
DAZ239_GA_Eafri_Cbp1_full_insert_R	GCGCTATAATCGCTGCCTTTTATTAACATCCCTGGCATGCTGCG
DAZ240_Epast1_cbp1_full_insert_F	GAACAACCACTTCGTCATTCAAATGTATTTCTCCAAGGTTGCTGCT CCT
DAZ241_GA_Epast1_cbp1_full_insert_R	GCGCTATAATCGCTGCCTTTTATTACCAAAGCATTGTCTGCATTCT TCGG
DAZ242_GA_BAS707_SP_vector_R	ACGCTTAGAAGCATTCTCAGGCG
DAZ243_GA_Epast2_insert_R	TGGGCGCTATAATCGCTGCCTTTTATTACGGGCATCCGCCACAAG
DAZ244_GA_Epast2_Cbp1_full_insert_F	GAACAACCACTTCGTCATTCAAATGAAGCTCTCCACCACCATCG
DAZ246_GA_Eori_Cbp1_insert_R	GCGCTATAATCGCTGCCTTTTATTACAAGCACCCGGAACAGCC
DAZ247_GA_Eori_Cbp1_full_insert_F	AGAACAACCACTTCGTCATTCAAATGCATTTCTCCAAGGTCATTGC TCC
DAZ249_GA_EcEUMH_Cbp1_insert_R	CGCTATAATCGCTGCCTTTTATTAAGCATCCATTGCACTGCTCAGT AG
DAZ250_GA_EcEUMH3008_cbp1_full_insert_F	ACAACCACTTCGTCATTCAAATGTATTTCTCCAAGGTCATCGCTACT GC
DAZ267_R10_qPCR_R	TTCTACTCTCCGTAGTGCTAATG
DAZ268_R10_qPCR_F	ATTCAGAATAACTGCAACCGTT
DAZ269_GA_yps3_6xhis_ins_R	ATGGTGGTGTGCGCCTGGAAGTACAGTTTTCTGCCTCGCAGTGT TTATAAAGCGGAAC
DAZ270_GA_yps3_6xhis_vec_F	CAGGCGCATCACCACCATCATCACTAAAAGGCAGCGATTATAGCGC CCAC
DAZ281_GA_ins_2xstrep_eGFP_R	CAGTGGGCGCTATAATCGCTGCCTTTTACTTGTACAGCTCGTCCATG CCG
DAZ282_GA_ins_2xstrep_eGFP_F	GCCATCCGCAGTTTGAAAAATGGTGAGCAAGGGCGAGGA
DAZ283_GA_vec_2xstrep_R	TTTTTCAAACGCGGATGGCTCCACG
DAZ284_2guide_screening_F	TTACCAATGCGGATCACGGTAT

Primer name	Sequence
DAZ285_2guide_CRISPR_screen_R	TATATACAACACCTTCAAAAAGGATCATCG
DAZ286_rock1_2guide_seq_F	GTACTTCAGATGGTCAGGACGGCT
DAZ287_rock1_2guide_seq_R	AGATAGATAGGCAGGTAGGCAGGC
DAZ288_rock6_2guide_seq_F	GAGGTGATGAGTTGAGAACCTTGGGAG
DAZ289_rock6_2guide_seq_R	GGTAGTAGAGGGGACGAACCAATCCAAAC
DAZ290_rock10_2guide_seq_F	GTGCTAGCACATGAGTGGGGAT
DAZ291_rock10_2guide_seq_R	TCCCCCACCAGAGCTTCG
DAZ292_avr9_2guide_seq_F	TTAAGCAATGGTACGCCCGCT
DAZ293_avr9_2guide_seq_R	CTGCTAGGAATTATGTCAAGAACTGCATG
DAZ294_Scp1_2guide_seq_F	TCCCTACGTTTCTCGCATAAATCTATCGG
DAZ295_Scp1_2guide_seq_R	CGTATGCATTCCGTGATGCAACAC
DAZ296_yps3_2guide_seq_F	AGCACCCAGTCGTTTCGTTTC
DAZ297_yps3_2guide_seq_R	GCACACAAGATGTTCCCTATGTCCG
DAZ312_R10_int_F	TGCGTTATTGCAAGTGGTAGTAAGGC
DAZ313_R1_int_F	TTTGTCCGGGAGGTGAAGAATAAAAAACAACAACCAG
DAZ314_R6_int_F	AGCGCCTAACTTATTGGATATTCGGTTTATTC
DAZ315_AVR9_int_F	TATCCCATCGAATAAATCACTGTTATCCTCATGGA
DAZ316_SCP1_int_F	TTAGCAAAGGCAGCAATGAATGAGCTGACA
DAZ317_yps3_int_F	ACAACACTACGACATCTACAAGCAATTCCGT
DAZ325_Ec_Cterm_all_insert_R	CGCTATAATCGCTGCCTTTTATTAAAAGCATCCCTTGCACTGCTCAGTAG
DAZ326_Pb_SP_GA_vec_R	AACAGCTGGTTGAGCACGCTTAGAAGCATTCTCAGGCG
DAZ327_Hc_SP_GA_vec_R	AACAGTGGGTTGATCACGCTTAGAAGCATTCTCAGGCG
DAZ328_SCP1_internal_R	TGTCAGCTCATTATTGCTGCCTTTGCTAAG
DAZ329_r6_2g_screen_F	ATCGTTATTCTAGAATGAGGGCCTGAACCAT
DAZ330_r6_2g_screen_R	AATTTAAATCACATCCACCCATTACAAATTTTCGATATGCTGGC
DAZ335_R1_2g_CRISPR_int_F	TCGCTCTTTGTGTTGCTACCAATGATGTC

Primer name	Sequence
DAZ336_R1_2g_CRISPR_int_R	CCAGAGGTTGAGCATATTATGTCTTTCCTCTGG
DAZ337_R6_2g_CRISPR_int_F	GGTGTCTGTTCATCACGTGATCATAAAGGA
DAZ338_R6_2g_CRISPR_int_R	TGAATAAACCGAATATCCAATAAGTTAGGCGCTG
DAZ339_AVR9_2g_CRISPR_int_F	TCAGTGTTATTGCTTATGAAAACCTGGTGAGTAGTATCT
DAZ340_AVR9_2g_CRISPR_int_R	TCCATGAGGATAACAGTGATTTATTCGATGGGATAA
DAZ341_R10_2g_CRISPR_int_F	GGAGAGTAGAAAACATAAACCTCATTCACTCAGAGA
DAZ342_R10_2g_CRISPR_int_R	AACATACACCAGCCTTACTACCACTTGC
DAZ343_SCP1_2g_CRISPR_int_F	TGAAATCGTCCATCATCTCTACGATCGC
DAZ344_SCP1_2g_CRISPR_int_R	CAGTAACAGTCATATCAGTCCTTCCGATCTCG
DAZ345_Yps3_2g_CRISPR_int_F	AAATCGATCTCAACCTCCTCCTCCTT
DAZ346_Yps3_2g_CRISPR_int_R	CAGTGTTTATAAAGCGGAACCTCTGGCA
DAZ356_SCP1_complementation_F_atb1	GGGACAAGTTTGTACAAAAAAGCAGGCTGCAAAGGAGGAGATGC CAATTCCTCCACA
DAZ357_SCP1_complementation_R_atb2	GGGACCACTTTGTACAAGAAAGCTGGGTCGAGAGCAAGAATATG TATCTGGCAAGTCAA
DAZ358_SCP1_comp_seq_F	GTAGGCGTAAAATCCCCTTCTAGATAGATAGATAATCAG
DAZ359_SCP1_comp_seq_F	AGTTCAGCTCCAAAAGAAGTTCGGGA
DAZ360_SCP1_comp_seq_F	GTTCTCAAATAACCAGCTACTCAATGCGTTC
DAZ361_SCP1_comp_seq_F	GATCAATCTTTGAGATAAATACTGCCAGTTGAGTGAC
DAZ362_SCP1_comp_seq_F	GGCACTTGGAGTTAAGAAATGGCTGGA
DAZ363_SCP1_comp_seq_F	AATCTATCGGCTTATACCCCTTGTGACTG
DAZ364_SCP1_comp_seq_F	AATTGAAATTCGAGGAGACTGGCGTG
DAZ365_SCP1_comp_seq_F	GTGTTGCATCACGGAATGCATACGTA

DAZ366_SCP1_comp_seq_F	ACAAGGAGGGTGGAAAATTCAATTTATGCTATGAA
DAZ367_Yps3_complement_F_attb1	GGGGACAAGTTTGTACAAAAAAGCAGGCTGCCATGAAAGAATTATTAGAGACTATATAAGTATGAAGCACAGAGTGG
DAZ368_Yps3_complement_R_attb2	GGGGACCACTTTGTACAAGAAAGCTGGGTC TTGATATCCATGATCTCCAGCTTCAGCG
DAZ373_Eafri_Cterm_GA_insert_R	GGGCGCTATAATCGCTGCCTTTTAAACATCCCTGGCATGCTGCG
DAZ374_Eori_Cterm_GA_insert_R	GGGCGCTATAATCGCTGCCTTTTACAAGCACCCGGAACAGCC
DAZ375_Ec_Cterm_GA_insert_R	CGCTATAATCGCTGCCTTTTAAAAGCATCCATTGCACTGCTCAGTAG
DAZ376_Epast1_Cterm_GA_insert_R	GGCGCTATAATCGCTGCCTTTTACCAAAGCATTGTCTGCATTCTTCGG
DAZ377_Epast2_Cterm_GA_insert	GTGGGCGCTATAATCGCTGCCTTTTACGGGCATCCGCCACAAG
DAZ378_yps3_comp_F	GATCCGCCTGAAGATACTAAGTTCACAACC
DAZ379_yps3_comp_F	ATAGTGTTGAACATTGCTCCACCCTG
DAZ380_yps3_comp_F	GATTGAATTGATTAGACTGACCATGTGATCATGCAT
DAZ381_yps3_comp_F	GTGTGAATTTTCATCAAGATTTATAGTGCTGTCTAGTTGT
DAZ382_yps3_comp_F	GCAAGAGCTCCACTTTCTTCATCATCGAA
DAZ383_yps3_comp_F	GATTCATAGATGTTTCGATAAGTCAAGTTGCAGC
DAZ384_yps3_comp_F	CTTCCATCATTCCAATCGACTTGCAAGTATATCAAAA
DAZ385_yps3_comp_F	GGAAAGCTTCATCTATGTGCTCCAAATAGGG
DAZ386_yps3_comp_F	TGTCTTTCAACACAACGTAGGCGC
DAZ387_yps3_comp_F	CAAGCCAGTGTACATGGATTTGTGAATGATG
DAZ388_yps3_comp_R	TCTTGATATCCATGATCTCCAGCTTCAGCG
OAS 5390_mCHOP_F	CTGGAAGCCTGGTATGAGGAT
OAS 5391_mCHOP_R	CAGGGTCAAGAGTAGTGAAGGT
OAS 2778_mTRIB3_F	TGCAGGAAGAAACCGTTGGAG
OAS 2779_mTRIB3_R	CTCAGGCTCATCTCTCACTCG
OAS 2768_mHPRT_F	AGGTTGCAAGCTTGCTGGT
OAS 2769_mHPRT_R	TGAAGTACTCATTATAGTCAAGGGCA
OAS 1337_Hc_ACT1_F	CTGGCATCACACCTTCTACA
OAS 1338_Hc_ACT1_R	GAGAAATAGCGTGCGGAAGA

References

- Abidi, F. E., Roh, H., & Keath, E. J. (1998). Identification and characterization of a phase-specific, nuclear DNA binding protein from the dimorphic pathogenic fungus *Histoplasma capsulatum*. *Infect Immun*, 66(8), 3867-3873. <https://doi.org/10.1128/IAI.66.8.3867-3873.1998>
- Ackerman, S. E., Currier, N. V., Bergen, J. M., & Cochran, J. R. (2014). Cystine-knot peptides: emerging tools for cancer imaging and therapy. *Expert Rev Proteomics*, 11(5), 561-572. <https://doi.org/10.1586/14789450.2014.932251>
- Albuquerque, P. C., Nakayasu, E. S., Rodrigues, M. L., Frases, S., Casadevall, A., Zancoppe-Oliveira, R. M., Almeida, I. C., & Nosanchuk, J. D. (2008). Vesicular transport in *Histoplasma capsulatum*: an effective mechanism for trans-cell wall transfer of proteins and lipids in ascomycetes. *Cell Microbiol*, 10(8), 1695-1710. <https://doi.org/10.1111/j.1462-5822.2008.01160.x>
- Alto, N. M., & Orth, K. (2012). Subversion of cell signaling by pathogens. *Cold Spring Harb Perspect Biol*, 4(9), a006114. <https://doi.org/10.1101/cshperspect.a006114>
- Altschul, S. F., Madden, T. L., Schaffer, A. A., Zhang, J., Zhang, Z., Miller, W., & Lipman, D. J. (1997). Gapped BLAST and PSI-BLAST: a new generation of protein database search programs. *Nucleic Acids Res*, 25(17), 3389-3402. <https://doi.org/10.1093/nar/25.17.3389>
- Alves, L. R., Peres da Silva, R., Sanchez, D. A., Zamith-Miranda, D., Rodrigues, M. L., Goldenberg, S., Puccia, R., & Nosanchuk, J. D. (2019). Extracellular Vesicle-Mediated RNA Release in *Histoplasma capsulatum*. *mSphere*, 4(2). <https://doi.org/10.1128/mSphere.00176-19>
- Arauz, A. B., & Papineni, P. (2021). Histoplasmosis. *Infect Dis Clin North Am*, 35(2), 471-491. <https://doi.org/10.1016/j.idc.2021.03.011>

- Asrat, S., de Jesus, D. A., Hempstead, A. D., Ramabhadran, V., & Isberg, R. R. (2014). Bacterial pathogen manipulation of host membrane trafficking. *Annu Rev Cell Dev Biol*, 30, 79-109. <https://doi.org/10.1146/annurev-cellbio-100913-013439>
- Avery, S. V., Singleton, I., Magan, N., & Goldman, G. H. (2019). The fungal threat to global food security. *Fungal Biol*, 123(8), 555-557. <https://doi.org/10.1016/j.funbio.2019.03.006>
- Baker, N. A., Sept, D., Joseph, S., Holst, M. J., & McCammon, J. A. (2001). Electrostatics of nanosystems: application to microtubules and the ribosome. *Proc Natl Acad Sci U S A*, 98(18), 10037-10041. <https://doi.org/10.1073/pnas.181342398>
- Baltazar, L. M., Zamith-Miranda, D., Burnet, M. C., Choi, H., Nimrichter, L., Nakayasu, E. S., & Nosanchuk, J. D. (2018). Concentration-dependent protein loading of extracellular vesicles released by *Histoplasma capsulatum* after antibody treatment and its modulatory action upon macrophages. *Sci Rep*, 8(1), 8065. <https://doi.org/10.1038/s41598-018-25665-5>
- Basu, T., Seyedmousavi, S., Sugui, J. A., Balenga, N., Zhao, M., Kwon Chung, K. J., Biardel, S., Laviolette, M., & Druey, K. M. (2018). *Aspergillus fumigatus* alkaline protease 1 (Alp1/Aspf13) in the airways correlates with asthma severity. *J Allergy Clin Immunol*, 141(1), 423-425 e427. <https://doi.org/10.1016/j.jaci.2017.07.034>
- Batanghari, J. W., Deepe, G. S., Jr., Di Cera, E., & Goldman, W. E. (1998). *Histoplasma* acquisition of calcium and expression of CBP1 during intracellular parasitism. *Mol Microbiol*, 27(3), 531-539. <https://doi.org/10.1046/j.1365-2958.1998.00697.x>
- Batanghari, J. W., & Goldman, W. E. (1997). Calcium dependence and binding in cultures of *Histoplasma capsulatum*. *Infect Immun*, 65(12), 5257-5261. <https://doi.org/10.1128/IAI.65.12.5257-5261.1997>
- Beaussart, A., Brandhorst, T., Dufrene, Y. F., & Klein, B. S. (2015). Blastomyces Virulence Adhesin-1 Protein Binding to Glycosaminoglycans Is Enhanced by Protein Disulfide Isomerase. *mBio*, 6(5), e01403-01415. <https://doi.org/10.1128/mBio.01403-15>

- Beck, M. R., Dekoster, G. T., Cistola, D. P., & Goldman, W. E. (2009). NMR structure of a fungal virulence factor reveals structural homology with mammalian saposin B. *Mol Microbiol*, 72(2), 344-353. <https://doi.org/10.1111/j.1365-2958.2009.06647.x>
- Beck, M. R., DeKoster, G. T., Hambly, D. M., Gross, M. L., Cistola, D. P., & Goldman, W. E. (2008). Structural features responsible for the biological stability of Histoplasma's virulence factor CBP. *Biochemistry*, 47(15), 4427-4438. <https://doi.org/10.1021/bi701495v>
- Benedict, K., & Mody, R. K. (2016). Epidemiology of Histoplasmosis Outbreaks, United States, 1938-2013. *Emerg Infect Dis*, 22(3), 370-378. <https://doi.org/10.3201/eid2203.151117>
- Benson, D. A., Cavanaugh, M., Clark, K., Karsch-Mizrachi, I., Lipman, D. J., Ostell, J., & Sayers, E. W. (2013). GenBank. *Nucleic Acids Res*, 41(Database issue), D36-42. <https://doi.org/10.1093/nar/gks1195>
- Beyhan, S., Gutierrez, M., Voorhies, M., & Sil, A. (2013). A temperature-responsive network links cell shape and virulence traits in a primary fungal pathogen. *PLoS Biol*, 11(7), e1001614. <https://doi.org/10.1371/journal.pbio.1001614>
- Beyhan, S., & Sil, A. (2019). Sensing the heat and the host: Virulence determinants of *Histoplasma capsulatum*. *Virulence*, 10(1), 793-800. <https://doi.org/10.1080/21505594.2019.1663596>
- Bohse, M. L., & Woods, J. P. (2005). Surface localization of the Yps3p protein of *Histoplasma capsulatum*. *Eukaryot Cell*, 4(4), 685-693. <https://doi.org/10.1128/EC.4.4.685-693.2005>
- Bohse, M. L., & Woods, J. P. (2007a). Expression and interstrain variability of the YPS3 gene of *Histoplasma capsulatum*. *Eukaryot Cell*, 6(4), 609-615. <https://doi.org/10.1128/EC.00010-07>
- Bohse, M. L., & Woods, J. P. (2007b). RNA interference-mediated silencing of the YPS3 gene of *Histoplasma capsulatum* reveals virulence defects. *Infect Immun*, 75(6), 2811-2817. <https://doi.org/10.1128/IAI.00304-07>

- Brandhorst, T., Wuthrich, M., Finkel-Jimenez, B., & Klein, B. (2003). A C-terminal EGF-like domain governs BAD1 localization to the yeast surface and fungal adherence to phagocytes, but is dispensable in immune modulation and pathogenicity of *Blastomyces dermatitidis*. *Mol Microbiol*, 48(1), 53-65. <https://doi.org/10.1046/j.1365-2958.2003.03415.x>
- Brinkman, E. K., Chen, T., Amendola, M., & van Steensel, B. (2014). Easy quantitative assessment of genome editing by sequence trace decomposition. *Nucleic Acids Res*, 42(22), e168. <https://doi.org/10.1093/nar/gku936>
- Brown, G. D., Denning, D. W., Gow, N. A., Levitz, S. M., Netea, M. G., & White, T. C. (2012). Hidden killers: human fungal infections. *Sci Transl Med*, 4(165), 165rv113. <https://doi.org/10.1126/scitranslmed.3004404>
- Brown, G. D., Denning, D. W., & Levitz, S. M. (2012). Tackling human fungal infections. *Science*, 336(6082), 647. <https://doi.org/10.1126/science.1222236>
- Burt, W. R., Underwood, A. L., & Appleton, G. L. (1981). Hydroxamic acid from *Histoplasma capsulatum* that displays growth factor activity. *Appl Environ Microbiol*, 42(3), 560-563. <https://doi.org/10.1128/aem.42.3.560-563.1981>
- Chang, Y. F., Imam, J. S., & Wilkinson, M. F. (2007). The nonsense-mediated decay RNA surveillance pathway. *Annu Rev Biochem*, 76, 51-74. <https://doi.org/10.1146/annurev.biochem.76.050106.093909>
- Chauhan, D., & Shames, S. R. (2021). Pathogenicity and Virulence of *Legionella*: Intracellular replication and host response. *Virulence*, 12(1), 1122-1144. <https://doi.org/10.1080/21505594.2021.1903199>
- Cheek, S., Krishna, S. S., & Grishin, N. V. (2006). Structural classification of small, disulfide-rich protein domains. *J Mol Biol*, 359(1), 215-237. <https://doi.org/10.1016/j.jmb.2006.03.017>

- Chu, J. H., Feudtner, C., Heydon, K., Walsh, T. J., & Zaoutis, T. E. (2006). Hospitalizations for endemic mycoses: a population-based national study. *Clin Infect Dis*, 42(6), 822-825. <https://doi.org/10.1086/500405>
- Cole, G. T., Zhu, S. W., Pan, S. C., Yuan, L., Kruse, D., & Sun, S. H. (1989). Isolation of antigens with proteolytic activity from *Coccidioides immitis*. *Infect Immun*, 57(5), 1524-1534. <https://doi.org/10.1128/IAI.57.5.1524-1534.1989>
- da Silva, T. A., Roque-Barreira, M. C., Casadevall, A., & Almeida, F. (2016). Extracellular vesicles from *Paracoccidioides brasiliensis* induced M1 polarization in vitro. *Sci Rep*, 6, 35867. <https://doi.org/10.1038/srep35867>
- Dade, J., DuBois, J. C., Pasula, R., Donnell, A. M., Caruso, J. A., Smulian, A. G., & Deepe, G. S., Jr. (2016). HcZrt2, a zinc responsive gene, is indispensable for the survival of *Histoplasma capsulatum* in vivo. *Med Mycol*, 54(8), 865-875. <https://doi.org/10.1093/mmy/myw045>
- de Guillen, K., Lorrain, C., Tsan, P., Barthe, P., Petre, B., Saveleva, N., Rouhier, N., Duplessis, S., Padilla, A., & Hecker, A. (2019). Structural genomics applied to the rust fungus *Melampsora larici-populina* reveals two candidate effector proteins adopting cystine knot and NTF2-like protein folds. *Sci Rep*, 9(1), 18084. <https://doi.org/10.1038/s41598-019-53816-9>
- de Oliveira, A. L., Gallo, M., Pazzagli, L., Benedetti, C. E., Cappugi, G., Scala, A., Pantera, B., Spisni, A., Pertinhez, T. A., & Cicero, D. O. (2011). The structure of the elicitor Ceratoplatenin (CP), the first member of the CP fungal protein family, reveals a double psibeta-barrel fold and carbohydrate binding. *J Biol Chem*, 286(20), 17560-17568. <https://doi.org/10.1074/jbc.M111.223644>
- Do, C. B., Mahabhashyam, M. S., Brudno, M., & Batzoglou, S. (2005). ProbCons: Probabilistic consistency-based multiple sequence alignment. *Genome Res*, 15(2), 330-340. <https://doi.org/10.1101/gr.2821705>

- Dodds, P. N., & Rathjen, J. P. (2010). Plant immunity: towards an integrated view of plant-pathogen interactions. *Nat Rev Genet*, 11(8), 539-548. <https://doi.org/10.1038/nrg2812>
- Dolinsky, T. J., Nielsen, J. E., McCammon, J. A., & Baker, N. A. (2004). PDB2PQR: an automated pipeline for the setup of Poisson-Boltzmann electrostatics calculations. *Nucleic Acids Res*, 32(Web Server issue), W665-667. <https://doi.org/10.1093/nar/gkh381>
- Du, H., Bing, J., Hu, T., Ennis, C. L., Nobile, C. J., & Huang, G. (2020). *Candida auris*: Epidemiology, biology, antifungal resistance, and virulence. *PLoS Pathog*, 16(10), e1008921. <https://doi.org/10.1371/journal.ppat.1008921>
- Dukik, K., Munoz, J. F., Jiang, Y., Feng, P., Sigler, L., Stielow, J. B., Freeke, J., Jamalain, A., Gerrits van den Ende, B., McEwen, J. G., Clay, O. K., Schwartz, I. S., Govender, N. P., Maphanga, T. G., Cuomo, C. A., Moreno, L. F., Kenyon, C., Borman, A. M., & de Hoog, S. (2017). Novel taxa of thermally dimorphic systemic pathogens in the Ajellomycetaceae (Onygenales). *Mycoses*, 60(5), 296-309. <https://doi.org/10.1111/myc.12601>
- Eddy, S. R. (2011). Accelerated Profile HMM Searches. *PLoS Comput Biol*, 7(10), e1002195. <https://doi.org/10.1371/journal.pcbi.1002195>
- Eissenberg, L. G., Goldman, W. E., & Schlesinger, P. H. (1993). *Histoplasma capsulatum* modulates the acidification of phagolysosomes. *J Exp Med*, 177(6), 1605-1611. <https://doi.org/10.1084/jem.177.6.1605>
- English, B. C., Van Prooyen, N., Ord, T., Ord, T., & Sil, A. (2017). The transcription factor CHOP, an effector of the integrated stress response, is required for host sensitivity to the fungal intracellular pathogen *Histoplasma capsulatum*. *PLoS Pathog*, 13(9), e1006589. <https://doi.org/10.1371/journal.ppat.1006589>
- Finkel-Jimenez, B., Wuthrich, M., & Klein, B. S. (2002). BAD1, an essential virulence factor of *Blastomyces dermatitidis*, suppresses host TNF-alpha production through TGF-beta-dependent and -independent mechanisms. *J Immunol*, 168(11), 5746-5755. <https://doi.org/10.4049/jimmunol.168.11.5746>

- Flieger, A., Frischknecht, F., Hacker, G., Hornef, M. W., & Pradel, G. (2018). Pathways of host cell exit by intracellular pathogens. *Microb Cell*, 5(12), 525-544. <https://doi.org/10.15698/mic2018.12.659>
- Fredlund, J., & Enninga, J. (2014). Cytoplasmic access by intracellular bacterial pathogens. *Trends Microbiol*, 22(3), 128-137. <https://doi.org/10.1016/j.tim.2014.01.003>
- Garfoot, A. L., Dearing, K. L., VanSchoiack, A. D., Wysocki, V. H., & Rappleye, C. A. (2017). Eng1 and Exg8 Are the Major beta-Glucanases Secreted by the Fungal Pathogen *Histoplasma capsulatum*. *J Biol Chem*, 292(12), 4801-4810. <https://doi.org/10.1074/jbc.M116.762104>
- Garfoot, A. L., & Rappleye, C. A. (2016). *Histoplasma capsulatum* surmounts obstacles to intracellular pathogenesis. *FEBS J*, 283(4), 619-633. <https://doi.org/10.1111/febs.13389>
- Garfoot, A. L., Zemska, O., & Rappleye, C. A. (2014). *Histoplasma capsulatum* depends on de novo vitamin biosynthesis for intraphagosomal proliferation. *Infect Immun*, 82(1), 393-404. <https://doi.org/10.1128/IAI.00824-13>
- Gilmore, S. A., Voorhies, M., Gebhart, D., & Sil, A. (2015). Genome-Wide Reprogramming of Transcript Architecture by Temperature Specifies the Developmental States of the Human Pathogen *Histoplasma*. *PLoS Genet*, 11(7), e1005395. <https://doi.org/10.1371/journal.pgen.1005395>
- Gilmore, S. A., Voorhies, M., Gebhart, D., & Sil, A. (2021). Correction: Genome-Wide Reprogramming of Transcript Architecture by Temperature Specifies the Developmental States of the Human Pathogen *Histoplasma*. *PLoS Genet*, 17(4), e1009509. <https://doi.org/10.1371/journal.pgen.1009509>
- Govender, N. P., & Grayson, W. (2019). Emergomycosis (*Emergomycetes africanus*) in Advanced HIV Disease. *Dermatopathology (Basel)*, 6(2), 63-69. <https://doi.org/10.1159/000495405>
- Hakimi, M. A., & Bougdour, A. (2015). *Toxoplasma's* ways of manipulating the host transcriptome via secreted effectors. *Curr Opin Microbiol*, 26, 24-31. <https://doi.org/10.1016/j.mib.2015.04.003>

- Ham, H., Sreelatha, A., & Orth, K. (2011). Manipulation of host membranes by bacterial effectors. *Nat Rev Microbiol*, 9(9), 635-646. <https://doi.org/10.1038/nrmicro2602>
- He, Q., McLellan, H., Boevink, P. C., & Birch, P. R. J. (2020). All Roads Lead to Susceptibility: The Many Modes of Action of Fungal and Oomycete Intracellular Effectors. *Plant Commun*, 1(4), 100050. <https://doi.org/10.1016/j.xplc.2020.100050>
- Holbrook, E. D., Edwards, J. A., Youseff, B. H., & Rappleye, C. A. (2011). Definition of the extracellular proteome of pathogenic-phase *Histoplasma capsulatum*. *J Proteome Res*, 10(4), 1929-1943. <https://doi.org/10.1021/pr1011697>
- Holbrook, E. D., & Rappleye, C. A. (2008). *Histoplasma capsulatum* pathogenesis: making a lifestyle switch. *Curr Opin Microbiol*, 11(4), 318-324. <https://doi.org/10.1016/j.mib.2008.05.010>
- Holbrook, E. D., Smolnycki, K. A., Youseff, B. H., & Rappleye, C. A. (2013). Redundant catalases detoxify phagocyte reactive oxygen and facilitate *Histoplasma capsulatum* pathogenesis. *Infect Immun*, 81(7), 2334-2346. <https://doi.org/10.1128/IAI.00173-13>
- Holm, L. (2020). DALI and the persistence of protein shape. *Protein Sci*, 29(1), 128-140. <https://doi.org/10.1002/pro.3749>
- Howard, D. H. (1964). Intracellular Behavior of *Histoplasma Capsulatum*. *J Bacteriol*, 87, 33-38. <https://doi.org/10.1128/jb.87.1.33-38.1964>
- Howard, D. H. (1965). Intracellular Growth of *Histoplasma Capsulatum*. *J Bacteriol*, 89, 518-523. <https://doi.org/10.1128/jb.89.2.518-523.1965>
- Howard, D. H., Rafie, R., Tiwari, A., & Faull, K. F. (2000). Hydroxamate siderophores of *Histoplasma capsulatum*. *Infect Immun*, 68(4), 2338-2343. <https://doi.org/10.1128/IAI.68.4.2338-2343.2000>
- Howe, K. L., Contreras-Moreira, B., De Silva, N., Maslen, G., Akanni, W., Allen, J., Alvarez-Jarreta, J., Barba, M., Bolser, D. M., Cambell, L., Carbajo, M., Chakiachvili, M., Christensen, M., Cummins, C., Cuzick, A., Davis, P., Fexova, S., Gall, A., George, N., Gil,

- L., Gupta, P., Hammond-Kosack, K. E., Haskell, E., Hunt, S. E., Jaiswal, P., Janacek, S. H., Kersey, P. J., Langridge, N., Maheswari, U., Maurel, T., McDowall, M. D., Moore, B., Muffato, M., Naamati, G., Naithani, S., Olson, A., Papatheodorou, I., Patricio, M., Paulini, M., Pedro, H., Perry, E., Preece, J., Rosello, M., Russell, M., Sitnik, V., Staines, D. M., Stein, J., Tello-Ruiz, M. K., Trevanion, S. J., Urban, M., Wei, S., Ware, D., Williams, G., Yates, A. D., & Flicek, P. (2020). Ensembl Genomes 2020-enabling non-vertebrate genomic research. *Nucleic Acids Res*, 48(D1), D689-D695. <https://doi.org/10.1093/nar/gkz890>
- Hung, C. Y., Ampel, N. M., Christian, L., Seshan, K. R., & Cole, G. T. (2000). A major cell surface antigen of *Coccidioides immitis* which elicits both humoral and cellular immune responses. *Infect Immun*, 68(2), 584-593. <https://doi.org/10.1128/iai.68.2.584-593.2000>
- Hwang, L. H., Mayfield, J. A., Rine, J., & Sil, A. (2008). Histoplasma requires SID1, a member of an iron-regulated siderophore gene cluster, for host colonization. *PLoS Pathog*, 4(4), e1000044. <https://doi.org/10.1371/journal.ppat.1000044>
- Isaac, D. T., Berkes, C. A., English, B. C., Murray, D. H., Lee, Y. N., Coady, A., & Sil, A. (2015). Macrophage cell death and transcriptional response are actively triggered by the fungal virulence factor Cbp1 during *H. capsulatum* infection. *Mol Microbiol*, 98(5), 910-929. <https://doi.org/10.1111/mmi.13168>
- Isaac, D. T., & Isberg, R. (2014). Master manipulators: an update on *Legionella pneumophila* Icm/Dot translocated substrates and their host targets. *Future Microbiol*, 9(3), 343-359. <https://doi.org/10.2217/fmb.13.162>
- Joehnk, B., Voorhies, M., Walcott, K., Sil, A. (in preparation). Recyclable CRISPR/Cas9 mediated gene disruption and deletions in *Histoplasma*, manuscript in preparation. In.
- Kall, L., Krogh, A., & Sonnhammer, E. L. (2007). Advantages of combined transmembrane topology and signal peptide prediction--the Phobius web server. *Nucleic Acids Res*, 35(Web Server issue), W429-432. <https://doi.org/10.1093/nar/gkm256>

- Kauffman, C. A. (2007). Histoplasmosis: a clinical and laboratory update. *Clin Microbiol Rev*, 20(1), 115-132. <https://doi.org/10.1128/CMR.00027-06>
- Keath, E. J., & Abidi, F. E. (1994). Molecular cloning and sequence analysis of yps-3, a yeast-phase-specific gene in the dimorphic fungal pathogen *Histoplasma capsulatum*. *Microbiology (Reading)*, 140 (Pt 4), 759-767. <https://doi.org/10.1099/00221287-140-4-759>
- Keller, C., Mellouk, N., Danckaert, A., Simeone, R., Brosch, R., Enninga, J., & Bobard, A. (2013). Single cell measurements of vacuolar rupture caused by intracellular pathogens. *J Vis Exp*(76), e50116. <https://doi.org/10.3791/50116>
- Kugler, S., Young, B., Miller, V. L., & Goldman, W. E. (2000). Monitoring phase-specific gene expression in *Histoplasma capsulatum* with telomeric GFP fusion plasmids. *Cell Microbiol*, 2(6), 537-547. <https://doi.org/10.1046/j.1462-5822.2000.00078.x>
- Kujoth, G. C., Sullivan, T. D., & Klein, B. S. (2020). Gene Editing in Dimorphic Fungi Using CRISPR/Cas9. *Curr Protoc Microbiol*, 59(1), e132. <https://doi.org/10.1002/cpmc.132>
- Kurup, V. P., Banerjee, B., Hemmann, S., Greenberger, P. A., Blaser, K., & Cramer, R. (2000). Selected recombinant *Aspergillus fumigatus* allergens bind specifically to IgE in ABPA. *Clin Exp Allergy*, 30(7), 988-993. <https://doi.org/10.1046/j.1365-2222.2000.00837.x>
- Lo Presti, L., Lanver, D., Schweizer, G., Tanaka, S., Liang, L., Tollot, M., Zuccaro, A., Reissmann, S., & Kahmann, R. (2015). Fungal effectors and plant susceptibility. *Annu Rev Plant Biol*, 66, 513-545. <https://doi.org/10.1146/annurev-arplant-043014-114623>
- Lockhart, S. R., & Guarner, J. (2019). Emerging and reemerging fungal infections. *Seminars in Diagnostic Pathology*, 36(3), 177-181. <https://doi.org/10.1053/j.semmp.2019.04.010>
- Lockhart, S. R., Toda, M., Benedict, K., Caceres, D. H., & Litvintseva, A. P. (2021). Endemic and Other Dimorphic Mycoses in The Americas. *J Fungi (Basel)*, 7(2). <https://doi.org/10.3390/jof7020151>

- Madej, T., Lanczycki, C. J., Zhang, D., Thiessen, P. A., Geer, R. C., Marchler-Bauer, A., & Bryant, S. H. (2014). MMDB and VAST+: tracking structural similarities between macromolecular complexes. *Nucleic Acids Res*, 42(Database issue), D297-303. <https://doi.org/10.1093/nar/gkt1208>
- Maiga, A. W., Deppen, S., Scaffidi, B. K., Baddley, J., Aldrich, M. C., Dittus, R. S., & Grogan, E. L. (2018). Mapping *Histoplasma capsulatum* Exposure, United States. *Emerg Infect Dis*, 24(10), 1835-1839. <https://doi.org/10.3201/eid2410.180032>
- Maresca, B., & Kobayashi, G. S. (1989). Dimorphism in *Histoplasma capsulatum*: a model for the study of cell differentiation in pathogenic fungi. *Microbiol Rev*, 53(2), 186-209. <https://doi.org/10.1128/mr.53.2.186-209.1989>
- McBride, J. A., Gauthier, G. M., & Klein, B. S. (2019). Turning on virulence: Mechanisms that underpin the morphologic transition and pathogenicity of *Blastomyces*. *Virulence*, 10(1), 801-809. <https://doi.org/10.1080/21505594.2018.1449506>
- Mitchell, G., Chen, C., & Portnoy, D. A. (2016). Strategies Used by Bacteria to Grow in Macrophages. *Microbiol Spectr*, 4(3). <https://doi.org/10.1128/microbiolspec.MCHD-0012-2015>
- Moore, S. J., & Cochran, J. R. (2012). Engineering knottins as novel binding agents. *Methods Enzymol*, 503, 223-251. <https://doi.org/10.1016/B978-0-12-396962-0.00009-4>
- Moore, S. J., Leung C. L., Cochran, J. R. . (2012). Knottins: disulfide-bonded therapeutic and diagnostic peptides. *Drug Discov Today Technol*, 9(1), e1-e70. <https://doi.org/10.1016/j.ddtec.2011.07.003>
- Newman, S. L., Bucher, C., Rhodes, J., & Bullock, W. E. (1990). Phagocytosis of *Histoplasma capsulatum* yeasts and microconidia by human cultured macrophages and alveolar macrophages. Cellular cytoskeleton requirement for attachment and ingestion. *J Clin Invest*, 85(1), 223-230. <https://doi.org/10.1172/JCI114416>

- Newman, S. L., Gootee, L., Hilty, J., & Morris, R. E. (2006). Human macrophages do not require phagosome acidification to mediate fungistatic/fungicidal activity against *Histoplasma capsulatum*. *J Immunol*, *176*(3), 1806-1813. <https://doi.org/10.4049/jimmunol.176.3.1806>
- Nguyen, B. N., Peterson, B. N., & Portnoy, D. A. (2019). Listeriolysin O: A phagosome-specific cytolysin revisited. *Cell Microbiol*, *21*(3), e12988. <https://doi.org/10.1111/cmi.12988>
- Nguyen, L. T., Schmidt, H. A., von Haeseler, A., & Minh, B. Q. (2015). IQ-TREE: a fast and effective stochastic algorithm for estimating maximum-likelihood phylogenies. *Mol Biol Evol*, *32*(1), 268-274. <https://doi.org/10.1093/molbev/msu300>
- Nguyen, V. Q., & Sil, A. (2008). Temperature-induced switch to the pathogenic yeast form of *Histoplasma capsulatum* requires Ryp1, a conserved transcriptional regulator. *Proc Natl Acad Sci U S A*, *105*(12), 4880-4885. <https://doi.org/10.1073/pnas.0710448105>
- Nosanchuk, J. D., Nimrichter, L., Casadevall, A., & Rodrigues, M. L. (2008). A role for vesicular transport of macromolecules across cell walls in fungal pathogenesis. *Commun Integr Biol*, *1*(1), 37-39. <https://doi.org/10.4161/cib.1.1.6639>
- Pan, S., & Cole, G. T. (1995). Molecular and biochemical characterization of a *Coccidioides immitis*-specific antigen. *Infect Immun*, *63*(10), 3994-4002. <https://doi.org/10.1128/IAI.63.10.3994-4002.1995>
- Pazzagli, L., Cappugi, G., Manao, G., Camici, G., Santini, A., & Scala, A. (1999). Purification, characterization, and amino acid sequence of cerato-platanin, a new phytotoxic protein from *Ceratocystis fimbriata* f. sp. *platani*. *J Biol Chem*, *274*(35), 24959-24964. <https://doi.org/10.1074/jbc.274.35.24959>
- Personnic, N., Barlocher, K., Finsel, I., & Hilbi, H. (2016). Subversion of Retrograde Trafficking by Translocated Pathogen Effectors. *Trends Microbiol*, *24*(6), 450-462. <https://doi.org/10.1016/j.tim.2016.02.003>

- Postic, G., Gracy, J., Perin, C., Chiche, L., & Gelly, J. C. (2018). KNOTTIN: the database of inhibitor cystine knot scaffold after 10 years, toward a systematic structure modeling. *Nucleic Acids Res*, 46(D1), D454-D458. <https://doi.org/10.1093/nar/gkx1084>
- Pradhan, A., Ghosh, S., Sahoo, D., & Jha, G. (2021). Fungal effectors, the double edge sword of phytopathogens. *Curr Genet*, 67(1), 27-40. <https://doi.org/10.1007/s00294-020-01118-3>
- Rappleye, C. A., Eissenberg, L. G., & Goldman, W. E. (2007). Histoplasma capsulatum alpha-(1,3)-glucan blocks innate immune recognition by the beta-glucan receptor. *Proc Natl Acad Sci U S A*, 104(4), 1366-1370. <https://doi.org/10.1073/pnas.0609848104>
- Rappleye, C. A., Engle, J. T., & Goldman, W. E. (2004). RNA interference in Histoplasma capsulatum demonstrates a role for alpha-(1,3)-glucan in virulence. *Mol Microbiol*, 53(1), 153-165. <https://doi.org/10.1111/j.1365-2958.2004.04131.x>
- Reid, G., Lynch, J. P., 3rd, Fishbein, M. C., & Clark, N. M. (2020). Mucormycosis. *Semin Respir Crit Care Med*, 41(1), 99-114. <https://doi.org/10.1055/s-0039-3401992>
- Resnick, S., Pappagianis, D., & McKerrow, J. H. (1987). Proteinase production by the parasitic cycle of the pathogenic fungus *Coccidioides immitis*. *Infect Immun*, 55(11), 2807-2815. <https://doi.org/10.1128/IAI.55.11.2807-2815.1987>
- Resnick, S., Zimmer, B., Pappagianis, D., Eakin, A., & McKerrow, J. (1990). Purification and amino-terminal sequence analysis of the complement-fixing and precipitin antigens from *Coccidioides immitis*. *J Clin Microbiol*, 28(2), 385-388. <https://doi.org/10.1128/JCM.28.2.385-388.1990>
- Rodrigues, M. L., Nimrichter, L., Oliveira, D. L., Nosanchuk, J. D., & Casadevall, A. (2008). Vesicular Trans-Cell Wall Transport in Fungi: A Mechanism for the Delivery of Virulence-Associated Macromolecules? *Lipid Insights*, 2, 27-40. <https://doi.org/10.4137/lpi.s1000>
- Rodriguez, L., Voorhies, M., Gilmore, S., Beyhan, S., Myint, A., & Sil, A. (2019). Opposing signaling pathways regulate morphology in response to temperature in the fungal

- pathogen *Histoplasma capsulatum*. *PLoS Biol*, 17(9), e3000168.
<https://doi.org/10.1371/journal.pbio.3000168>
- Rooney, P. J., & Klein, B. S. (2004). Sequence elements necessary for transcriptional activation of BAD1 in the yeast phase of *Blastomyces dermatitidis*. *Eukaryot Cell*, 3(3), 785-794.
<https://doi.org/10.1128/EC.3.3.785-794.2004>
- Samaddar, A., & Sharma, A. (2021). Emergomycosis, an Emerging Systemic Mycosis in Immunocompromised Patients: Current Trends and Future Prospects. *Front Med (Lausanne)*, 8, 670731. <https://doi.org/10.3389/fmed.2021.670731>
- Schwartz, I. S., Govender, N. P., Sigler, L., Jiang, Y., Maphanga, T. G., Toplis, B., Botha, A., Dukik, K., Hoving, J. C., Munoz, J. F., de Hoog, S., Cuomo, C. A., Colebunders, R., & Kenyon, C. (2019). Emergomycetes: The global rise of new dimorphic fungal pathogens. *PLoS Pathog*, 15(9), e1007977. <https://doi.org/10.1371/journal.ppat.1007977>
- Schwartz, I. S., McLoud, J. D., Berman, D., Botha, A., Lerm, B., Colebunders, R., Levetin, E., & Kenyon, C. (2018). Molecular detection of airborne *Emergomycetes africanus*, a thermally dimorphic fungal pathogen, in Cape Town, South Africa. *PLoS Negl Trop Dis*, 12(1), e0006174. <https://doi.org/10.1371/journal.pntd.0006174>
- Sebghati, T. S., Engle, J. T., & Goldman, W. E. (2000). Intracellular parasitism by *Histoplasma capsulatum*: fungal virulence and calcium dependence. *Science*, 290(5495), 1368-1372.
<https://doi.org/10.1126/science.290.5495.1368>
- Sepulveda, V. E., Marquez, R., Turissini, D. A., Goldman, W. E., & Matute, D. R. (2017). Genome Sequences Reveal Cryptic Speciation in the Human Pathogen *Histoplasma capsulatum*. *mBio*, 8(6). <https://doi.org/10.1128/mBio.01339-17>
- Shen, Q., Beucler, M. J., Ray, S. C., & Rappleye, C. A. (2018). Macrophage activation by IFN-gamma triggers restriction of phagosomal copper from intracellular pathogens. *PLoS Pathog*, 14(11), e1007444. <https://doi.org/10.1371/journal.ppat.1007444>

- Shen, Q., & Rappleye, C. A. (2017). Differentiation of the fungus *Histoplasma capsulatum* into a pathogen of phagocytes. *Curr Opin Microbiol*, 40, 1-7. <https://doi.org/10.1016/j.mib.2017.10.003>
- Sil, A. (2019). Molecular regulation of *Histoplasma* dimorphism. *Curr Opin Microbiol*, 52, 151-157. <https://doi.org/10.1016/j.mib.2019.10.011>
- Sil, A., & Andrianopoulos, A. (2014). Thermally Dimorphic Human Fungal Pathogens-- Polyphyletic Pathogens with a Convergent Pathogenicity Trait. *Cold Spring Harb Perspect Med*, 5(8), a019794. <https://doi.org/10.1101/cshperspect.a019794>
- Staff, P. N. T. D. (2018). Correction: Molecular detection of airborne *Emergomyces africanus*, a thermally dimorphic fungal pathogen, in Cape Town, South Africa. *PLoS Negl Trop Dis*, 12(5), e0006468. <https://doi.org/10.1371/journal.pntd.0006468>
- Stergiopoulos, I., & de Wit, P. J. (2009). Fungal effector proteins. *Annu Rev Phytopathol*, 47, 233-263. <https://doi.org/10.1146/annurev.phyto.112408.132637>
- Strasser, J. E., Newman, S. L., Ciraolo, G. M., Morris, R. E., Howell, M. L., & Dean, G. E. (1999). Regulation of the macrophage vacuolar ATPase and phagosome-lysosome fusion by *Histoplasma capsulatum*. *J Immunol*, 162(10), 6148-6154. <https://www.ncbi.nlm.nih.gov/pubmed/10229858>
- Suleyman, G., & Alangaden, G. J. (2016). Nosocomial Fungal Infections Epidemiology, Infection Control, and Prevention. *Infectious Disease Clinics of North America*, 30(4), 1023-+. <https://doi.org/10.1016/j.idc.2016.07.008>
- Taylor, M. L., Espinosa-Schoelly, M. E., Iturbe, R., Rico, B., Casasola, J., & Goodsaid, F. (1989). Evaluation of phagolysosome fusion in acridine orange stained macrophages infected with *Histoplasma capsulatum*. *Clin Exp Immunol*, 75(3), 466-470. <https://www.ncbi.nlm.nih.gov/pubmed/2702784>
- <https://www.ncbi.nlm.nih.gov/pmc/articles/PMC1541969/pdf/clinexpimmunol00090-0142.pdf>

- van den Hooven, H. W., Appelman, A. W., Zey, T., de Wit, P. J., & Vervoort, J. (1999). Folding and conformational analysis of AVR9 peptide elicitors of the fungal tomato pathogen *Cladosporium fulvum*. *Eur J Biochem*, 264(1), 9-18. <https://doi.org/10.1046/j.1432-1327.1999.00503.x>
- van den Hooven, H. W., van den Burg, H. A., Vossen, P., Boeren, S., de Wit, P. J., & Vervoort, J. (2001). Disulfide bond structure of the AVR9 elicitor of the fungal tomato pathogen *Cladosporium fulvum*: evidence for a cystine knot. *Biochemistry*, 40(12), 3458-3466. <https://doi.org/10.1021/bi0023089>
- Vervoort, J., van den Hooven, H. W., Berg, A., Vossen, P., Vogelsang, R., Joosten, M. H., & de Wit, P. J. (1997). The race-specific elicitor AVR9 of the tomato pathogen *Cladosporium fulvum*: a cystine knot protein. Sequence-specific ¹H NMR assignments, secondary structure and global fold of the protein. *FEBS Lett*, 404(2-3), 153-158. [https://doi.org/10.1016/s0014-5793\(97\)00117-8](https://doi.org/10.1016/s0014-5793(97)00117-8)
- Weaver, C. H., Sheehan, K. C., & Keath, E. J. (1996). Localization of a yeast-phase-specific gene product to the cell wall in *Histoplasma capsulatum*. *Infect Immun*, 64(8), 3048-3054. <https://doi.org/10.1128/IAI.64.8.3048-3054.1996>
- Webb, B., & Sali, A. (2016). Comparative Protein Structure Modeling Using MODELLER. *Curr Protoc Protein Sci*, 86, 29 1-29 37. <https://doi.org/10.1002/cpps.20>
- Webb, B., & Sali, A. (2021). Protein Structure Modeling with MODELLER. *Methods Mol Biol*, 2199, 239-255. https://doi.org/10.1007/978-1-0716-0892-0_14
- Webster, R. H., & Sil, A. (2008). Conserved factors Ryp2 and Ryp3 control cell morphology and infectious spore formation in the fungal pathogen *Histoplasma capsulatum*. *Proc Natl Acad Sci U S A*, 105(38), 14573-14578. <https://doi.org/10.1073/pnas.0806221105>
- Wheat, L. J., Azar, M. M., Bahr, N. C., Spec, A., Relich, R. F., & Hage, C. (2016). Histoplasmosis. *Infect Dis Clin North Am*, 30(1), 207-227. <https://doi.org/10.1016/j.idc.2015.10.009>

- Woods, J. P. (2016). Revisiting old friends: Developments in understanding *Histoplasma capsulatum* pathogenesis. *J Microbiol*, 54(3), 265-276. <https://doi.org/10.1007/s12275-016-6044-5>
- Yang, Z. (2007). PAML 4: phylogenetic analysis by maximum likelihood. *Mol Biol Evol*, 24(8), 1586-1591. <https://doi.org/10.1093/molbev/msm088>
- Youseff, B. H., Holbrook, E. D., Smolnycki, K. A., & Rappleye, C. A. (2012). Extracellular superoxide dismutase protects *Histoplasma* yeast cells from host-derived oxidative stress. *PLoS Pathog*, 8(5), e1002713. <https://doi.org/10.1371/journal.ppat.1002713>
- Zamith-Miranda, D., Peres da Silva, R., Couvillion, S. P., Bredeweg, E. L., Burnet, M. C., Coelho, C., Camacho, E., Nimrichter, L., Puccia, R., Almeida, I. C., Casadevall, A., Rodrigues, M. L., Alves, L. R., Nosanchuk, J. D., & Nakayasu, E. S. (2021). Omics Approaches for Understanding Biogenesis, Composition and Functions of Fungal Extracellular Vesicles. *Front Genet*, 12, 648524. <https://doi.org/10.3389/fgene.2021.648524>
- Zarnowski, R., Cooper, K. G., Brunold, L. S., Calaycay, J., & Woods, J. P. (2008). *Histoplasma capsulatum* secreted gamma-glutamyltransferase reduces iron by generating an efficient ferric reductant. *Mol Microbiol*, 70(2), 352-368. <https://doi.org/10.1111/j.1365-2958.2008.06410.x>

Publishing Agreement

It is the policy of the University to encourage open access and broad distribution of all theses, dissertations, and manuscripts. The Graduate Division will facilitate the distribution of UCSF theses, dissertations, and manuscripts to the UCSF Library for open access and distribution. UCSF will make such theses, dissertations, and manuscripts accessible to the public and will take reasonable steps to preserve these works in perpetuity.

I hereby grant the non-exclusive, perpetual right to The Regents of the University of California to reproduce, publicly display, distribute, preserve, and publish copies of my thesis, dissertation, or manuscript in any form or media, now existing or later derived, including access online for teaching, research, and public service purposes.



Author Signature

6/3/2021

Date